Title Page:

Title: A yeast phenomic model for the influence of Warburg metabolism on genetic buffering of doxorubicin

Authors: Sean M. Santos[1] and John L. Hartman IV[1]

1. University of Alabama at Birmingham, Department of Genetics, Birmingham, AL

Email: ssantos@uab.edu, jhartman@uab.edu

Corresponding author: jhartman@uab.edu

Abstract:

Background:

Saccharomyces cerevisiae represses respiration in the presence of adequate glucose, mimicking the Warburg effect, termed aerobic glycolysis. We conducted yeast phenomic experiments to characterize differential doxorubicin-gene interaction, in the context of respiration *vs.* glycolysis. The resulting systems level biology about doxorubicin cytotoxicity, including the influence of the Warburg effect, was integrated with cancer pharmacogenomics data to identify potentially causal correlations between differential gene expression and anti-cancer efficacy.

Methods:

Quantitative high-throughput cell array phenotyping (Q-HTCP) was used to measure cell proliferation phenotypes (CPPs) of the yeast gene knockout/knockdown library, treated with escalating doxorubicin concentrations in fermentable and non-fermentable media. Doxorubicin-gene interaction was quantified by departure of the observed and expected phenotypes for the doxorubicin-treated mutant strain, with respect to phenotypes for the untreated mutant strain and both the treated and untreated reference strain. Recursive expectation-maximization clustering (REMc) and Gene Ontology-based analyses of interactions were used to identify functional biological modules that buffer doxorubicin cytotoxicity, and to characterize their Warburg-dependence. Yeast phenomic data was applied to cancer cell line pharmacogenomics data to predict differential gene expression that causally influences the anti-tumor efficacy, and potentially the anthracycline-associated host toxicity, of doxorubicin.

Results:

Doxorubicin cytotoxicity was greater with respiration, suggesting the Warburg effect can influence therapeutic efficacy. Accordingly, doxorubicin drug-gene interaction was more

extensive with respiration, including increased buffering by cellular processes related to chromatin organization, protein folding and modification, translation reinitiation, spermine metabolism, and fatty acid beta-oxidation. Pathway enrichment was less notable for glycolysis-specific buffering. Cellular processes exerting influence relatively independently, with respect to Warburg status, included homologous recombination, sphingolipid homeostasis, telomere tethering at nuclear periphery, and actin cortical patch localization. Causality for differential gene expression associated with doxorubicin cytotoxicity in tumor cells was predicted within the biological context of the phenomic model.

Conclusions:

Warburg status influences the genetic requirements to buffer doxorubicin toxicity. Yeast phenomics provides an experimental platform to model the complexity of gene interaction networks that influence human disease phenotypes, as in this example of chemotherapy response. High-resolution, systems level yeast phenotyping is useful to predict the biological influence of functional variation on disease, offering the potential to fundamentally advance precision medicine.

Keywords:

genetic buffering, yeast phenomics, quantitative high throughput cell array phenotyping (Q-HTCP), cell proliferation parameters (CPPs), doxorubicin, Warburg metabolism, differential gene interaction networks, recursive expectation-maximization clustering (REMc), pharmacogenomics, human-like / HL yeast media

Background:

Doxorubicin is used widely in oncology to treat both hematologic cancer and solid tumors [1]. Proposed mechanisms of doxorubicin cytotoxicity include topoisomerase II poisoning, DNA adduct formation, oxidative stress, and ceramide overproduction [1-6]. Topoisomerase II is an ATP-dependent enzyme that relieves the DNA torsional stress occurring with replication or transcription by catalyzing a double-stranded DNA (**dsDNA**) break, relaxing positive and negative DNA supercoiling, and finally re-ligating the DNA [7]. Inhibiting this activity can result in irreparable DNA damage and induction of apoptosis, selectively killing rapidly dividing proliferating cells [8-10]. Doxorubicin also causes histone eviction leading to chromatin trapping and damage [2, 11-13]. In addition to its potent anti-cancer therapeutic properties, doxorubicin is known for dose-limiting cardiomyocyte toxicity, causing cardiomyopathy and heart failure years post-treatment [14]. In this regard, topoisomerase IIB is highly expressed specifically in myocardiocytes, where tissue-specific deletion suppresses cardiac toxicity in mice [15]. Clinical guidelines recommend a maximum cumulative lifetime dose of 500 mg/m^2; however, doxorubicin toxicity is variable and has a genetic basis [16]. Thus, a detailed understanding of drug-gene interaction could advance the rationale for more precisely prescribing doxorubicin (among other cytotoxic agents) and also predicting toxicity, based on the unique genetic context of each patient's tumor genetic profile as well as germline functional variation.

This work establishes a yeast phenomic model to understand genetic pathways that buffer doxorubicin toxicity [17-23], and how the Warburg effect influences the doxorubicin-gene interaction network. Warburg won the Nobel Prize in 1931, yet there remains lack of consensus about how cancer cells undergo the Warburg transition and how aerobic glycolysis contributes to cancer [24-27]. In humans, aerobic glycolysis is considered a tumor-specific metabolic transition; however, yeast normally repress

respiration in the presence of adequate glucose [28-30]. Thus, we wondered whether doxorubicin-gene interaction manifests differentially under glycolytic vs. respiratory conditions in yeast and if genetic insights from this model could lead to better understanding its variable anti-tumor efficacy between different patients [17]. We observed increased toxicity of doxorubicin in non-fermentable media, where yeast must respire to proliferate, suggesting the Warburg transition could confer resistance of tumor cells to doxorubicin, and perhaps help explain the dose-limiting toxicity observed in cardiomyocytes, which have respiratory rates among the highest of all cell types [31].

We conducted yeast phenomic analysis of doxorubicin-gene interaction, consisting of quantitative high throughput cell array phenotyping (**Q-HTCP**) of the yeast knockout and knockdown (**YKO/KD**) libraries, using multiple growth inhibitory concentrations of doxorubicin in either dextrose- (**HLD**) or ethanol/glycerol-based (**HLEG**) media. Q-HTCP provided cell proliferation parameters (**CPPs**) with which to quantify doxorubicin-gene interaction and determine its dependence on respiratory *vs.* glycolytic metabolism [32-34]. The yeast phenomic model was used to predict causality underlying correlations between doxorubicin sensitivity and increased or decreased expression of the homologous human gene in pharmacogenomics data from cancer cell lines. Thus, the work details genetic pathways for buffering doxorubicin toxicity in yeast and applies the information to predict interactions between doxorubicin and functional genetic variation manifest in cancers from different, individual patients.

Methods:

Strains and media

The yeast gene knockout strain library (**YKO**) was obtained from Research Genetics (Huntsville, AL, USA). The knockdown (**KD**) collection, also known as the

Decreased Abundance of mRNA Production (**DAmP**) library, was obtained from Open Biosystems (Huntsville, AL, USA). The genetic background for the YKO library was BY4741 (S288C MAT**a** *ura3-Δ0 his3-Δ1 leu2-Δ0 met17-Δ0*). Additional information and lists of strains can be obtained at https://dharmacon.horizondiscovery.com/cdnas-and-orfs/non-mammalian-cdnas-and-orfs/yeast/#all. Some mutants appear multiple times in the library and they are treated independently in our analysis. HL yeast media, a modified synthetic complete media [20], was used with either 2% dextrose (HLD) or 3% ethanol and 3% glycerol (HLEG) as the carbon source.

Quantitative high throughput cell array phenotyping (Q-HTCP)

Phenomic data was obtained by Q-HTCP, a custom, automated method of collecting growth curve phenotypes for the YKO/KD library arrayed onto agar media [34]. A Caliper Sciclone 3000 liquid handling robot was used for cell array printing, integrated with a custom imaging robot (Hartman laboratory) and Cytomat 6001 (Thermo Fisher Scientific, Asheville, NC, USA) incubator. 384-culture array images were obtained approximately every 2 hours and analyzed as previously described [21, 34]. To obtain CPPs, image data were fit to the logistic equation, $G(t) = K/(1 + e^{-r(t-l)})$, assuming $G(0) < K$, where $G(t)$ is the image intensity of a spotted culture vs. time, K is the carrying capacity, r is the maximum specific growth rate, and l is the moment of maximal absolute growth rate, occurring when $G(t) = K/2$ (the time to reach half of carrying capacity) [32]. The resulting CPPs were used as phenotypes to measure doxorubicin-gene interaction.

Quantification of doxorubicin-gene interaction

Gene interaction was defined by departure of the corresponding YKO/KD strain from its expected phenotypic response to doxorubicin. The expected phenotype was

determined by cell proliferation phenotypes of the mutant without doxorubicin, together with those of the reference strain with and without doxorubicin [17-19, 21]. The concentrations of doxorubicin (0, 2.5, 5, 7.5 and 15 ug/mL) were chosen based on phenotypic responses being functionally discriminating in the parental strain. We tested for effects of mating type or ploidy on doxorubicin growth inhibition (**Additional File 1, Fig. S1)**, and noted only small differences between the YKO/KD parental strain genotypes, BY4741 (MAT**a** *ura3-Δ0 his3-Δ1 leu2-Δ0 met17-Δ0*), BY4742 (MAT**α** *ura3-Δ0 his3-Δ1 leu2-Δ0 lys2Δ0*), BY4741R (MAT**a** *ura3-Δ0 his3-Δ1 leu2-Δ0 lys2Δ0*), BY4742R (MAT**α** *ura3-Δ0 his3-Δ1 leu2-Δ0 met17-Δ0*), and diploid strains derived from these haploids. In this regard, haploid *MET17/lys2-Δ0* was associated with a lower carrying capacity in HLD media (**Additional File 1, Fig. S1**), but genome-wide experiments were not performed in this background.

Interaction scores were calculated as previously described [21], with slight modifications, as summarized below. Variables were defined as:

D_i = concentration (dose) of doxorubicin

R_i = observed mean growth parameter for parental Reference strain at D_i

Y_i = observed growth parameter for the YKO/KD mutant strain at D_i

$K_i = Y_i – R_i$, the difference in growth parameter between the YKO/KD mutant (Y_i) and Reference (R_i) at D_i

$K_0 = Y_0 - R_0$, the effect of gene KO/KD on the observed phenotype in the absence of doxorubicin; this value is annotated as ‘shift’ and is subtracted from all K_i to obtain L_i

$L_i = K_i - K_0$, the interaction between (specific influence of) the KO/KD mutation on doxorubicin response, at D_i

For cultures not generating a growth curve, $Y_i = 0$ for K and r, and the L parameter was assigned Y_i max, defined as the maximum observed Y_i among all

cultures exhibiting a minimum carrying capacity (K) within 2 standard deviation (SD) of the parental reference strain mean at D_i. Y_i max was also assigned to outlier values (*i.e.*, if $Y_i > Y_i$ max).

Interaction was calculated by the following steps:

1) Compute the average value of the 768 reference cultures (R_i) at each dose (D_i):

2) Assign Y_i max (defined above) if growth curve is observed at D_0, but not at D_i, or if observed Y_i is greater than Y_i max.

3) Calculate $K_i = Y_i - R_i$.

4) Calculate $L_i = K_i – K_0$

5) Fit data by linear regression (least squares): $L_i = A + B*D_i$

6) Compute the interaction value 'INT' at the max dose: INT = L_i-max = $A + B*D_{max}$

7) Calculate the mean and standard deviation of interaction scores for reference strains, mean(REF_{INT}) and SD(REF_{INT}); mean(REF_{INT}) is expected to be approximately zero, but SD(REF_{INT}) is useful for standardizing against variance (**Additional Files 2-4**).

8) Calculate interaction z-scores (**Fig. 1D**):

$$\text{z-score}(YKO/KD_{INT}) = (YKO/KD_{INT} – \text{mean}(REF_{INT}))/SD(REF_{INT})$$

z-score(YKO/KD_{INT}) > 2 for L or < -2 for K are referred to as gene deletion enhancers of doxorubicin cytotoxicity, and conversely, L interaction score < -2 or K interaction scores >2 are considered gene deletion suppressors (**Fig. 1E**).

*Recursive expectation-maximization clustering (**REMc**) and heatmap generation*

REMc is a probability-based clustering method and was performed as previously described [35]. Clusters obtained by Weka 3.5, an EM-optimized Gaussian mixture-clustering module, were subjected to hierarchical clustering in R (http://www.r-project.org/) to further aid visualization with heatmaps. REMc was performed using L

and K interaction z-scores (**Fig. 1F**). The effect of gene deletion on the CPP (in the absence of drug), termed 'shift' (K_0), was not used for REMc, but was included for visualization in the final hierarchical clustering. **Additional File 5** contains REMc results in text files with associated data also displayed as heatmaps. In cases where a culture did not grow in the absence of drug, 0.0001 was assigned as the interaction score, and associated data were colored red ('NA') in the shift columns of the heatmaps.

*Gene ontology term finder (**GTF**)*

A python script was used to format REMc clusters for analysis with the command line version of the GO Term Finder (GTF) tool downloaded from http://search.cpan.org/dist/GO-TermFinder/ [36]. GTF reports on enrichment of Gene Ontology (GO) terms by comparing the ratio of genes assigned to a term within a cluster to the respective ratio involving all genes tested. **Additional File 5** contains GTF analysis of all REMc clusters. GO-enriched terms from REMc were investigated with respect to genes representing the term and literature underlying their annotations [37].

*Gene ontology term averaging (**GTA**)*

In addition to using GTF to survey functional enrichment in REMc clusters, we developed GTA as a complementary workflow, using the GO information on SGD at https://downloads.yeastgenome.org/curation/literature/ to perform the following analysis:

1. Calculate the average and SD for interaction values of all genes in a GO term.
2. Filter results to obtain terms having GTA value greater than 2 or less than -2.
3. Obtain GTA scores defined as |GTA value| - gtaSD; filter for GTA score > 2.

The GTA analysis is contained in **Additional File 6** as tables and interactive plots created using the R *plotly* package https://CRAN.R-project.org/package=plotly. GTA results were analyzed primarily using the L interaction scores, however GTA results with K interaction scores are included in **Additional File 6 (File D).**

Validation of doxorubicin-gene interaction

We retested 364 YKO/KD strains having human homologs in the P-POD database [38] and L interaction scores greater than 2 or less than -2 in at least one media type. Strains were struck to obtain four single colonies and arranged on replicate 384 well plates along with twenty reference strain controls and reanalyzed by Q-HTCP on HLD and HLEG, as in the genome-wide experiment. Results are summarized in **Fig 2S-T**, **Additional File 2 (Tables S5-S8), and Additional Files 3-4 (Files C-D).**

Prediction of human homologs that influence tumor response to doxorubicin

PharmacoDB holds pharmacogenomics data from cancer cell lines, including transcriptomics and drug sensitivity [39]. The *PharmacoGx* R/Bioconductor package [40] was used to analyze the GDSC1000 (https://pharmacodb.pmgenomics.ca/datasets/5) and gCSI (https://pharmacodb.pmgenomics.ca/datasets/4) datasets, which contained transcriptomic and doxorubicin sensitivity results. A p-value < 0.05 was used for differential gene expression and doxorubicin sensitivity. For gene expression, the sign of the standardized coefficient denotes increased (+) or decreased (-) expression. The *biomaRt* R package [41, 42] was used with the Ensembl database [43] to match yeast and human homologs from the phenomic and transcriptomic data, classifying yeast-human homology as one to one, one to many, and many to many.

Results:

Phenomic characterization of doxorubicin response genes

The workflow for analyzing doxorubicin-gene interaction and differential buffering of doxorubicin with respect to the Warburg effect is summarized in **Fig. 1**. Alternately, in a respiratory or glycolytic (HLEG or HLD media, respectively) context (**Fig. 1A**), Q-HTCP technology was used for high throughput kinetic imaging of 384-culture cell arrays plated on agar media (**Fig. 1B**), image analysis (**Fig. 1C**), and growth curve fitting (**Fig. 1D**) to obtain the CPPs, L (time to reach half carrying capacity), K (carrying capacity), and r (maximum specific rate) [21, 32, 34], which were used to measure doxorubicin-gene interaction across the entire YKO/KD library. Departure of the observed CPP from the expected doxorubicin response for each YKO/KD strain was derived using distributions from many replicate reference strain control cultures, and summarized across all doxorubicin concentrations by linear regression (**Fig. 1E**). Interaction scores with absolute value greater than two were considered as gene *deletion enhancement* (z-score_L ≥ 2 or z-score_K ≤ -2) or *deletion suppression* (z-score_L ≤ -2 or z-score_K ≥ 2) of doxorubicin cytotoxicity. Gene deletion enhancement (*e.g.*, *mms1-Δ0*) and suppression (*e.g.*, *vps54-Δ0*) reveal functions that buffer or confer doxorubicin cytotoxicity, respectively. Doxorubicin-gene interaction profiles (selected if they contained L interaction scores with absolute value greater than two, in either HLD or HLEG media) were analyzed by REMc and assessed for GO Term enrichment (**Fig. 1F**). As a complement to clustering gene interaction profiles, functional enrichment was analyzed by GTA (see methods), systematically querying all GO processes, functions, and components (**Fig. 1G and methods**) with respect to CPPs and Warburg status. Taken together, REMc and GTA reveal genetic modules that buffer doxorubicin, and how they are influenced by Warburg metabolism (**Fig. 1H**).

Doxorubicin cytotoxicity was greater in HLEG than HLD media, evidenced by the reference strain being more growth inhibited (**Fig. 2A-L, Additional File 1, Fig. S1**). The 'L' parameter was the most sensitive CPP, while K reported larger phenotypic effects (**Fig. 2M-N) (Additional File 1, Fig. S2**). We noted positive correlation between doxorubicin-gene interaction in HLEG and HLD, however interaction was media-specific and more abundant in the context of respiration, i.e., with HLEG media (**Fig. 2O**).

We compared our results with two prior studies of doxorubicin cytotoxicity in the yeast knockout collections [44, 45]. One study was conducted in SC media with the haploid (BY4741) YKO library and identified 71 deletion enhancers of cytotoxicity [44]. A second study reported on the homozygous diploid (BY4743) YKO collection in YPD media, identifying 376 enhancers [45]. Overlap between these studies and ours is shown in **Fig. 2P-2R** and in **Additional File 7 (Table S9-10)**. While many genes overlapped between the studies, differing results were also observed, possibly attributable to strain background, media conditions, as well as methods for scoring interactions [20, 46]. To assess within-study reproducibility, we sub-cloned four colonies from glycerol stocks used in the first experiment and retested doxorubicin-gene interaction, revealing higher correlation and overall reproducibility within-study than between-study (**Fig. 2S-T**).

Identification of functional gene interaction modules

Gene interaction profiles were analyzed by REMc (**Figs. 3,4**), as described previously [35]. Briefly, REMc uses an expectation-maximization algorithm to define clusters probabilistically, and is applied recursively to resolve gene interaction profile clusters. REMc terminates when a round of clustering reveals no new clusters. The cluster naming convention is "A-B.C.D-X", where 'A' = the round of clustering, 'B' = 0, and 'C.D-X' indicates the cluster pedigree. For example, 1-0-0 refers to the first cluster of

the first round, 2-0.0-3 the fourth cluster derived from 1-0-0 (in round 2 of REMc), 3-0.0.3-1 indicates the second cluster derived from 2-0.0-3 (in round 3), and so on [35].

The main effect of the gene KO or KD on cell proliferation, *i.e.*, K_i in the absence of doxorubicin (D_0) is also referred to as 'shift' (see methods). 'Shift' was not subjected to REMc, but was included for hierarchical clustering and visualization by heatmaps after REMc (**Fig. 3; Additional File 5, File B)**. K_i is termed 'shift', because this value is subtracted from the data series for each YKO/KD to obtain L_i values, which are fit by linear regression for calculating drug-gene interaction (**Fig. 1E;** see methods).

GO TermFinder [36] was used to associate enrichment of biological functions with particular patterns of doxorubicin-gene interaction identified by REMc (**Figs. 3-4; Table 1; Additional File 5, File C**). In general, the first two rounds of REMc revealed distinctive profiles of gene interaction in respiratory vs. glycolytic media (**Fig. 4**). Later round clusters exhibited greater GO term enrichment in some cases; however, GO enrichment was other times reduced by further clustering (see **Additional File 8**).

GTA score revealed 129 GO terms, 39 of which were found by REMc/GTF (**Table 2** and **Additional File 6, Files A-C**). GTA identifies functions of smaller GO terms, *e.g.*, protein complexes. GTA with K interaction scores yielded only 35 GO terms (**Additional File 6, File D)**, with only 3 being unique from GTA with L interaction; thus, we focused on L interaction for GTA analysis. Interactive scatter plots (html files in which points contain embedded information) were used to visualize significant GO terms from both REMc and GTA (**Additional File 6, File B**). GO term-specific heatmaps further aided visualization of relationships between genes and the GO terms (see **Figs. 6-11** and **Additional File 9**) by systematically displaying, for all genes attributed to a parent term and its children, uniformity *vs.* pleiotropy of interaction effects across different conditions.

In summary, we used REMc, GTA, and GO term-specific scatterplots and heatmaps to discover genetic modules that alternatively buffer (*i.e.*, deletion enhancing) or confer (*i.e.*, deletion suppressing) doxorubicin cytotoxicity, and to determine whether the Warburg-transition exerts influence on their effects (**Fig. 5)**.

Warburg transition-dependent doxorubicin gene interaction modules

Respiration-specific gene deletion enhancement

Respiration-specific deletion-enhancing clusters (see **Fig. 4**; 1-0-7 and 1-0-8) revealed GO Term enrichment for *histone modification and chromatin organization*, *respiratory chain complex III assembly*, *protein import into mitochondria, protein urmylation*, the *NatC complex*, *protein folding in endoplasmic reticulum*, *and DNA topological change* (**Figs. 6-8; Additional File 5, File C).** Additional modules were identified using GTA (**Fig. 8C and Additional File 6, File A**).

Chromatin organization and histone modification

REMc/GTF and GTA identified several chromatin-related processes that buffer doxorubicin toxicity in a respiration-specific manner, including *DNA replication-independent nucleosome assembly*, *histone exchange*, *histone deacetylation*, and *histone methylation* (**Figs. 6 and 7)**.

(i) *DNA replication-independent nucleosome assembly (HIR complex)*

REMc/GTF identified the HIR complex (*HIR1-3* and *HPC2*), which functions as a histone chaperone in chromatin assembly and disassembly, in cluster 2-0.7-2 (**Fig. 4, Table 1**) [47]. Along with Asf1 and Rtt106, the HIR complex is involved in DNA replication-independent (*i.e.*, RNA transcriptional) histone deposition, and regulates transcription of three of the four histone genes [47-49]. Furthermore, genes encoding for

HTA1/HTB1, HHT1/2, and *HHF1/2* were also respiratory-specific deletion enhancers. Asf1 and Rtt106 function in nucleosome assembly in both DNA replication and DNA replication-independent contexts. Asf1, which functions in the Rad53-dependent DNA damage response [50], enhanced doxorubicin toxicity in both respiratory and glycolytic media, like other DNA repair genes (see below). In further contrast, genes associated with *replication-dependent nucleosome assembly* (*RLF2, CAC2, MSI1*) by the chromatin assembly factor complex, CAF-1, [51] were HLD-specific suppressors (**Fig. 6A-B**).

Prior studies have reported enhanced doxorubicin cytotoxicity due to nucleosome disassembly and "chromatin trapping" by the FACT complex, referring to binding and resulting damage to disassembled chromatin in the context of doxorubicin exposure [13]. *POB3-DAmP*, the only member of the FACT complex represented in the YKO/KD library, resulted in suppression of doxorubicin cytotoxicity (**Fig. 6B**), presumably by suppressing its effect of trapping and damaging disassembled chromatin.

(ii) *Histone exchange (Swr1 complex)*

The Swr1 complex (enriched in cluster 2-0.7-2) uses ATP hydrolysis to replace the H2A nucleosome with the H2AZ variant [52]. Swr1 complex genes showing respiration-specific buffering of doxorubicin toxicity included *RVB1, SWC3, SWC5, ARP6, SWR1*, VPS71, and *VPS72* (**Fig. 6C**). Accordingly, the H2AZ variant, Htz1, which is enriched at most gene promoters in euchromatin [53-55], was also an HLEG-specific deletion enhancer. The Swr1 complex is recruited for repair of dsDNA breaks, where the H2AZ variant is incorporated [56]; however, the interaction profile of the Swr1 complex more closely resembles other respiratory specific enhancers involved in transcriptional regulation, whereas dsDNA-break repair by homologous recombination buffered doxorubicin toxicity independent of Warburg context (see cluster 1-0-6 from **Fig. 4**, **Table 1**, and descriptions below). The Swr1 complex can also inhibit subtelomeric

spread of heterochromatin by impeding SIR-dependent silencing [57]. Consistent with knockout of Swr1 promoting silencing and having a deletion enhancing effect, deletion of *SIR1*, *SIR3* or *SIR4* (which disrupts chromatin silencing) also exerted respiratory-specific suppression of doxorubicin toxicity (**Fig. 6C**).

(iii) *Histone deacetylation (Sin3-type and HDA1 complexes)*

Deletion of genes functioning in the Rpd3L and Rpd3S histone deacetylase complexes (**HDAC**) was associated with strong respiratory enhancement of doxorubicin toxicity (cluster 2-0.7-2; **Fig. 7A**); however, genes constituting the Hda1 complex exerted weaker effects, but in both respiratory and glycolytic media (**Fig. 7A**, **Table 2**). The yeast Rpd3 deacetylase histone complexes are homologous to mammalian class I Rpd3-like proteins (Hdac1-3,8), while the yeast Hda1 complex is homologous to mammalian class II Hda1-like proteins (Hdac4-5,7,9) [58]. Hda1 and Rpd3 complexes both deacetylate histones H3 and H4; however, deletion of *RPD*3 *vs. HDA1* revealed different degrees of H4 lysine 5 and K12 hyperacetylation [59], implicating this functional distinction in Warburg-differential doxorubicin response.

Histone acetylation was GO-enriched in cluster 2-0.6-1, which displayed a Warburg-independent gene interaction profile (**Fig. 4, Table 1).** GTA analysis confirmed H3K56 acetylation (*SPT10* and *RTT109*) and histone H3 acetylation (*TAF9* and *HFI1*) as media-independent, but also histone H4 acetylation (*EAF3, ESA1, NGG1,* and *ELP4*), which was relatively respiratory-specific in its deletion enhancement (**Fig. 7B**, **Table 2**). Rtt109 promotes H3K56 acetylation, which is associated with elongating RNA polymerase II [60], and can be persistent in the setting of DNA damage [61]. Warburg-independent deletion enhancement suggests its role in DNA repair becomes invoked.

The SAS acetyltransferase complex was deletion suppressing; *SAS2* and *SAS5* were HLEG-specific, and *SAS4* was HLD-specific (**Fig. 7B**). The Sas2 acetyltransferase

complex creates a barrier against spread of heterochromatin at telomeres by opposing Sir protein deacetylation via effects on histone H4K16 [62]. The deacetylating SIR proteins (*SIR1, SIR3, SIR4*) were also HLEG-specific suppressors (**Fig. 6C**), suggesting dynamic regulation of telomeric histones (not simply acetylation or deacetylation), or perhaps a function of Sas2 acetyltransferase that is independent of SIR protein functions, confers doxorubicin cytotoxicity in respiring cells.

(iv) *Histone methylation* (*Set1C/COMPASS complex)*

Histone methylation differentially influences gene transcription, depending on the histone residues modified and the number of methyl groups added [63]. The Set1C/ COMPASS complex, which catalyzes mono-, di-, and tri- methylation of H3K4 [64-67], was enriched in cluster 1-0-7 (**Fig. 4; Table 1**). All genes tested from the Set1C/ COMPASS complex (*SPP1, SDS1, SWD1, SWD3, BRE2, SHG1; SET1* not in YKO/KD) were EG-specific deletion enhancers (**Fig. 7C**). The Set1C/COMPASS complex and H3K4 trimethylation localize at transcription start sites of actively transcribed genes [68, 69]. Furthermore, the Rad6-Bre1 complex, which mono-ubiquitinates histone H2B before Set1C/COMPASS methylates histone H3K4 [70-72], shared the same interaction profile, cross-implicating the Set1C/COMPASS and Rad6-Bre1 functions (**Fig. 7C**). The Rad6-Bre1 complex is additionally involved in the DNA damage response checkpoint to activate Rad53 [73], however, its HLEG-specific enhancing profile was more closely shared with transcriptional regulation modules, indicating its latter role is better related. *JHD1* and *JHD2* are JmjC domain family histone demethylases that act on H3-K36 and H3-K4 respectively, and their deletion suppression interactions are further evidence that histone methylation buffers doxorubicin cytotoxicity, especially in a respiratory context (**Fig. 7C**).

Taken together, the data suggest transcription-associated chromatin regulation buffers doxorubicin-mediated cellular toxicity, which is alleviated by the transition from respiratory to glycolytic metabolism. In contrast, Warburg-independent buffering by histone modifiers appears to be associated with functions related to DNA repair.

Mitochondrial functions

The abundance of deletion-enhancing doxorubicin-gene interactions in HLEG media (**Figure 2O**) caused us to closely examine genes annotated to mitochondrial function. Many mitochondrial gene deletion strains grew poorly on HLEG media, with petite-like proliferation defects on HLD media, as respiration is required to reach carrying capacity. Completely respiratory-deficient mutants clustered together in 1-0-0, however, many mitochondrial mutants maintained some or all respiratory capacity. For example, the *respiratory chain complex III assembly* and *protein import into mitochondrial matrix* terms were enriched in deletion enhancing clusters, 1-0-7 and 1-0-8 (**Table 1, Figure 4**, **Additional File 1**, **Fig. S3**). Some of these strains appeared respiratory sufficient yet the genes were required to buffer doxorubicin cytotoxicity under respiratory conditions. For example, evolutionarily conserved genes functioning in complex IV assembly (*RCF1/YML030W* and *COA6*) reached carrying capacity on HLEG media, yet exerted strong deletion enhancement of doxorubicin growth inhibition (**Additional File 1, Fig. S3A**). In contrast, other HLEG-specific deletion enhancing complex IV assembly components (*COA2*, *CMC1*, *RCF2*) and complex III assembly genes (*FMP25, FMP36, QCR9, CBP4*) were either not conserved in humans or exhibited strong respiratory defects (in absence of doxorubicin) (**Additional File 1**, **Fig. S3A-B**). Interactions specific to assembly of respiratory chain complexes may be informative for studies in cardiomyocytes regarding doxorubicin inhibition, depletion of cytochrome c and

cardiolipin, reduced workload capacity, and accelerated aging [74, 75]. Functionally conserved (*TOM70*, *TIM10*, *TIM17, TIM23,* and *MGR2*) and yeast-specific (*TOM6* and *TOM7*) genes in *protein import into mitochondrial matrix* buffered doxorubicin cytotoxicity (**Additional File 1**, **Fig. S3C-E)**, possibly due to increased oxidative stress [76], which enhances doxorubicin toxicity [1, 4].

Systematic examination of the GO annotation *mitochondrion* (**Additional File 1**, **Fig. S4**) revealed several additional respiratory-competent gene-deletion strains exhibiting HLEG-specific enhancing interactions. *COX13* encodes subunit VIa of cytochrome c oxidase, which functions with Rcf1 in the formation of respirasomes (also called 'supercomplexes') [77, 78]. Others included *COX8,* encoding subunit VIII of cytochrome c oxidase [79]; *MPC1*, encoding a mitochondrial pyruvate carrier [80, 81]; *MME1*, encoding an inner mitochondrial membrane magnesium exporter [82]; *OMS1*, an inner membrane protein predicted to have methyltransferase activity [83]*; GUF1*, a matrix-localized GTPase that binds mitochondrial ribosomes and influences cytochrome oxidase assembly [84]*;* and *MIC10 (YCL057C-A),* encoding a component of the MICOS complex, functioning in inner membrane organization and membrane contact site formation [85].

Protein folding, localization, and modification pathways

Protein biogenesis and modification pathways enriched in HLEG-specific enhancement clusters included the *endoplasmic reticulum membrane complex* (**EMC**) (2-0.7-1), *protein urmylation* (2-0.2-1), and N-terminal acetylation by the *NatC complex* (2-0.8-1) (**Figure 4, Table 1**).

(i) *Protein folding in endoplasmic reticulum (ER membrane protein complex)*

The ER membrane complex (*EMC1-6,* **Fig. 8A**) functions in protein folding in the ER [86] and together with the ER-mitochondria encounter structure (**ERMES**), the EMC enables ER-mitochondria phosphatidylserine transfer and tethering [87]. The EMC physically interacts with the mitochondrial translocase of the outer membrane (e.g., *TOM5, 6, 7, 22, 70;* described above) for the process of ER-mitochondria phosphatidylserine transfer [87]. The shared respiratory-specific, deletion-enhancing profiles suggest cooperative functions of the EMC and mitochondrial outer membrane translocase (**Additional File 1, Fig. S3D**) in buffering doxorubicin cytotoxicity. In contrast to the EMC, genes involved in the ERMES complex (1-0-0; **Additional File 5, File B-C**) were essential for respiration, and thus their influence on doxorubicin cytotoxicity could not be addressed with knockout mutants in HLEG media.

(ii) *Protein urmylation, Elongator complex, and tRNA wobble uridine thiolation*

ELP2, UBA4, URM1, and *URE2* clustered together in 2-0.2-1, constituting GO-enrichment in protein urmylation, the covalent modification of lysine residues with the ubiquitin-related modifier, Urm1 [88]. Other protein urmylation genes, *ELP6*, *NCS2,* and *NCS6/YGL211W,* displayed similar interaction profiles and clustered together in 1-0-7 (**Figure 8A**). *ELP2* and *ELP6* also function in the Elongator holoenzyme complex (*IKI1, IKI3, ELP2, ELP3, ELP4,* and *ELP6*) [89-91], associated with similar interaction profiles (**Additional File 1, Fig. S5**). *URM1*, *UBA4, NCS2,* and *NCS6* further function in tRNA wobble position uridine thiolation, where Urm1 functions as a sulfur carrier. Genes uniquely annotated to these terms (*IKI1, IKI3, ELP3, ELP4, TUM1, URE2*) also displayed related profiles (**Additional File 1, Fig. S5**). Thus, protein urmylation, Elongator complex function, and tRNA wobble thiolation appear to be distinct modules, comprised of shared genes, each buffering doxorubicin toxicity in a respiratory-specific way.

(iii) *N-terminal acetylation by the NatC complex*

The NatC complex (Mak3, Mak10, and Mak31) specifically acetylates methionine-starting hydrophobic N-terminal proteins (Met-Leu, Met-Phe, Met-Ile, Met-Tyr) [92], neutralizing positive charge on the alpha-amino group and impeding turnover by ubiquitination or other modifications [93]. N-acetylation occurs on around half of the soluble yeast proteome and over 80% in humans [94]. NatC-mediated N-terminal acetylation facilitates Golgi or inner nuclear membrane localization of some [95-98], but not most proteins [99]. The three genes encoding the NatC complex clustered together (**Fig. 8A**), however, NatC substrates were not enriched among doxorubicin-gene interactions (**Additional File 7, Table S11**). Perhaps a select few NatC targets or a novel function for NatC underlie its compensatory effects.

DNA topological change

DNA topological change, which refers to remodeling the turns of a double stranded DNA helix, was enriched in cluster 2-0.8-0 (**Figure 4, Table 1**). Representative genes were *SGS1*, *TOP1*, *RFA1*, *RMI1*, *TOP3, MMS4*, and *MUS81* (**Fig. 8B**). Types I and II topoisomerases resolve supercoiling during replication and transcription [100, 101]. Top1 is a type IB topoisomerase, which relaxes positive and negative supercoils [102, 103], compared to Top3, a type IA topoisomerase that specifically acts on negative supercoiling [104]. The Mms4-Mus81 endonuclease has overlapping functions with Top3 and Sgs1 in DNA repair [105]; however, their respective influences on doxorubicin toxicity were quantitatively distinct in both respiratory and glycolytic contexts, with a greater requirement for the *MMS4/MUS81* than *SGS1, TOP3*, *RFA1*, and *RMI1*; the latter four, functioning together for decatenation and unknotting of dsDNA [106].

GTA reveals additional biological functions that buffer doxorubicin toxicity

GTA scores revealed 71 respiratory-specific deletion enhancing GO terms, 24 of which were also found by REMc/GTF (see **Additional File 6, File A**). Strong enhancing terms (GTA value > 10) with functions relatively distinct from those identified above by REMc were *tRNA (m1A) methyltransferase complex*, *MUB1-RAD6-UBR2 ubiquitin ligase complex*, *malonyl-CoA biosynthetic process*, *pyridoxal 5'-phosphate salvage*, *maintenance of transcriptional fidelity during DNA-templated transcription elongation from RNA polymerase II promoter*, *RNA polymerase II transcription corepressor activity*, *pyruvate dehydrogenase activity*, and *eukaryotic translation initiation factor 2 complex* (**Fig. 8C**). Most terms identified by GTA consisted of 2-3 genes, and did not necessarily cluster together by REMc.

<u>Respiration-specific gene deletion suppression of doxorubicin cytotoxicity</u>

REMc clusters exhibiting respiration-dependent gene deletion suppression revealed GO Term enrichment for *regulation of fatty acid beta-oxidation*, *(*cluster 2-0.3-1) and *translation reinitiation* (cluster 2-0.3-5) **(Fig. 4, Table 1**). By GTA analysis, the *EKC/KEOPS complex* and *spermine biosynthetic process* were additionally found to confer HLEG-specific deletion suppression (**Fig. 8D, Table 2**).

Regulation of fatty acid beta-oxidation

ADR1, *OAF1*, and *PIP2* were grouped together in cluster 2-0.3-1 (**Fig. 4, Table 1**), displaying HLEG-specific gene deletion suppression (**Fig. 8D**). The Pip2-Oaf1 complex binds to oleate response elements, and along with *ADR1*, regulates transcription of peroxisomal genes [107, 108]. Doxorubicin inhibits beta-oxidation of long chain fatty acids in cardiac tissues, which is reversed by supplementing with propionyl-L-carnitine,

and alleviates effects of doxorubicin cardiotoxicity [109]. Thus, the yeast model may be informative for investigating related gene networks in greater depth.

Translation reinitiation

In the respiratory-specific deletion suppressing cluster 2-0.3-5 (**Fig. 4)**, *TMA20*, *TMA22*, and *TIF34* represented enrichment for translation reinitiation, which is necessary after termination of short upstream open reading frames (**uORFs**) [110] (**Fig. 8D**). Some uORFs function in translational regulation of a downstream protein; for example *GCN4* expression is regulated in response to amino acid starvation [110]. However, using the Welsh two sample t-test we found no significant difference in means of interaction scores between the distribution of proteins regulated or not by uORFs [111] (p-value = 0.8357) (**Additional File 7, Table S12**).

Spermine biosynthetic process

Loss of spermine biosynthesis, specifically *SPE2* (S-adenosylmethionine decarboxylase) and *SPE4* (spermine synthase), suppressed doxorubicin toxicity in HLEG media (**Fig. 8D**). The pathways of polyamine metabolism and their physiologic effects on cancer are complex [112, 113], and although our data suggest spermine metabolism contributes to doxorubicin cytotoxicity, how this occurs mechanistically and specifically in respiring cells awaits further study [114].

EKC/KEOPS complex

GTA revealed the EKC/KEOPS complex (*CGI121, GON7,* and *BUD32*) as HLEG-specific deletion suppressing (**Fig. 8D**). The EKC/KEOPS complex is involved in threonyl carbamoyl adenosine (t6A) tRNA modification [115], which strengthens the A-U codon–

anticodon interaction [116]. EKC/KEOPS has also been characterized with respect to telomere maintenance [117] and transcription [118]. Deletion of *GON7, BUD32,* or to a lesser extent, *CGI121,* inhibited cell proliferation in the absence of doxorubicin treatment, indicating that translational and/or transcriptional activity of the EKC/KEOPS complex function contributes to doxorubicin sensitivity.

<u>Glycolysis-specific gene deletion enhancement of doxorubicin cytotoxicity:</u>

HLD-specific deletion enhancement of doxorubicin cytotoxicity could represent lethal vulnerabilities that emerge when a tumor undergoes the Warburg transition. In this regard, several genes, but few enriched GO terms were identified by REMc (**Fig. 4,** clusters 1-0-5, 2-0.3-0, and 2-0.2-2; **Additional File 5, File A**). *Ribonucleoprotein complex subunit organization* was suggested (**Table 1)**, however, the term-specific heatmap revealed doxorubicin-gene interaction within this cellular process to be pleiotropic (**Additional File 1, Fig. S6**).

Glycolysis-specific deletion enhancing terms identified by GTA

GTA analysis revealed HLD-specific deletion-enhancing genes encoding the Cul4-RING E3 ubiquitin ligase, the Dom34-Hbs1 complex, and the Ubp3-Bre5 deubiquitinase. *GDP-Mannose Transport* and *dTTP biosynthesis* were also revealed (**Fig. 9A; Supplemental File 6, File A**). *SOF1, HRT1,* and *PRP46* were computationally inferred to form the Cul4-RING E3 ubiquitin ligase complex [119]. Yeast Sof1 is an essential protein that is required for 40s ribosomal biogenesis, and overexpression of its human ortholog, *DCAF13/WDSOF1*, is associated with aggressive tumors and poorer survival in hepatocellular carcinoma [120]. *DOM34/PELO* and *HBS1/HBS1L* facilitate recycling of stalled ribosomes by promoting dissociation of large and small subunits through a

process called no-go decay [121-123]. Knockdown by siRNA of either *WDSOF1* or *HBS1L* was synthetic lethal in a KRAS-driven tumor model [124]. The Ubp3-Bre5 deubiquitination complex regulates anterograde and retrograde transport between the ER and Golgi [125, 126]. Vrg4 and Hvg1 transport GDP-mannose into the Golgi lumen for protein glycosylation [127, 128]. Reduced dTTP pools, evidenced by *CDC8/DTYMK* and *CDC21/TYMS*, can increase doxorubicin cytotoxicity in cancer cell lines [129]. The human homologs of *UBP3*, *CDC8*, and *CDC21* were identified in genome-wide siRNA synthetic interaction studies in cancer cell line models [130-132].

For several examples above, like *SOF1/DCAF13,* genes could be targeted as both a driver of the tumor and as a sensitizer to doxorubicin. To systematically identify all candidate vulnerabilities specific to glycolytic tumor cells (not constrained by GO enrichment), we filtered the overall data set, limiting the list to genes with human homologs and to YKO/KD strains that were growth sufficient (low shift on HLD) (**Additional File 1, Fig. S7)**. The human homologs, along with functional descriptions, are provided in **Additional File 10, Table S13**.

<u>Glycolysis-specific gene deletion suppression of doxorubicin cytotoxicity</u>

HLD-specific deletion suppression clusters (**Fig. 4**, clusters 2-0.1-0, 2-0.4-0, 2-0.4-2, and 3-0.3.3-1) had GO Term enrichment for terms related to mRNA processing and *meiotic chromosome condensation*. GTA also identified *histone deubiquitination* (**Table 2**). Deletion suppression points to genes that could potentially increase doxorubicin toxicity if overexpressed.

RNA processing

HLD-specific deletion suppression clusters (2-0.4-0, 2-0.4-2**; Fig. 4**) were enriched for mRNA processing-related terms including *mRNA 3' end processing*, *mRNA cleavage*, and *7-methylguanosine cap hypermethylation* (**Table 1**), but the term-specific heatmaps revealed pleiotropic gene interaction profiles (**Additional File 1, Fig. S8**). *SWM2/YNR004W* and *TGS1* function in 7-methylguanosine (m^7G) cap trimethylation (cluster 2-0.4-0), however, the *tgs1-Δ0* allele also exerted deletion suppression in a respiratory context (**Fig. 9B**). m^7G cap trimethylation protects small nuclear RNAs (**snRNAs**), and small nucleolar RNAs (**snoRNAs**) from degradation by exonucleases [133, 134], and promotes efficient pre-rRNA processing and ribosome biogenesis [135].

Meiotic chromosome condensation

SMC2, SMC4, YCG1, and *YCS4* constitute the nuclear condensin complex, which functions in chromosome condensation and segregation. The condensin complex associates with chromosomal sites bound by TFIIIC and the RNA Pol III transcription machinery [136], where it facilitates clustering of tRNA genes at the nucleolus [137] (**Fig. 9B**). The condensin complex has been suggested as a potential therapeutic target for cancer [138], and human homologs *YCG1/NCAPG2*, *YCS4/NCAPD2*, and *SMC4/SMC4* are synthetic lethal with the Ras oncogene [124].

Histone deubiquitination

Histone deubiquitination was identified by GTA and includes *SUS1, SGF11, SGF73, UBP8, and SEM1* (**Fig. 9B)**; all except *SEM1* are part of the DUBm complex, which mediates histone H2B deubiquitination and mRNA export [139]. Loss of histone H2B ubiquitination resulting in HLEG-specific enhancement (**Fig. 7C**) is consistent with loss

of the DUBm deubiquitinase being suppressing. Together, they implicate regulation by histone ubiquitination as a mechanism of doxorubicin response. The human homologs of *UBP8, USP22* and *USP51,* were identified in an RNAi screen for resistance to ionizing radiation [140].

Warburg transition-independent doxorubicin gene-interaction modules:

Since many tumors have both respiratory and glycolytic cell populations, targeting Warburg-independent interactions could be especially efficacious, as described below.

Deletion enhancement:

Cluster 1-0-6 (**Fig. 4**) had a strong deletion-enhancing profile in both metabolic contexts with GO Term enrichment for DNA repair (**Fig. 10**), as well as histone acetylation (discussed above, **Fig. 7B**). GTA analysis additionally revealed the Lst4-Lst7, the Cul8-RING ubiquitin ligase, and MCM complexes (**Fig. 10B**).

DNA repair

Warburg-independent, deletion-enhancing pathways included homologous recombination and break-induced replication repair (**Fig. 10A),** along with the Ino80 complex (**Fig. 10B**), the latter explained by its role of histone acetylation in recruitment of DNA repair machinery to dsDNA break sites [52]. The Ino80 complex influences doxorubicin response in fission yeast [141, 142], further suggesting evolutionary conservation of this interaction, and thus potential relevance to mammalian systems [143]. DNA repair pathways, such as those involving *RAD52* and *INO80*, are evolutionarily conserved, involved in genome instability and tumorigenesis [144], and predictive of therapeutic response in some cancers [145], thus representing potential tumor-specific biomarkers for chemotherapeutic efficacy.

Complexes identified by GTA

Warburg-independent deletion enhancing modules identified by GTA were weaker, in many cases, than the dsDNA break repair pathways found by REMc, some of which had strong K parameter interactions (**Fig. 10, Additional File 9**). GTA-identified terms included: (1) The Cul8-RING ubiquitin ligase complex, which is encoded by *RTT101, RTT107, MMS1, MMS22*, and *HRT1,* and functions in replication-associated DNA repair [146]. Cul8/Rtt101, in fact, contributes to multiple complexes that regulate DNA damage responses, including Rtt101-Mms1-Mms22, which is required for Eco1-catalyzed Smc3 acetylation for normal sister chromatid cohesion establishment during S phase [147]; (2) The Lst4-Lst7 complex, which functions in general amino acid permease (*GAP1*) trafficking [148], threonine uptake, and maintenance of deoxyribonucleotide (**dNTP**) pools [19], clustered with *thr1-Δ0* (threonine biosynthesis) in 2-0.2-1 (**Additional File 5, File B**); and (3) the mini-chromosome maintenance (**MCM**) complex, which licenses and initiates DNA replication [149], was evidenced by the *mcm2-DAmP*, *mcm3-DAmP*, and *mcm5-DAmP* YKD strains (**Fig. 10B**). Work in pea plants showed that doxorubicin inhibits the *MCM6* DNA helicase activity [150]. Prior genome-wide experiments with doxorubicin did not analyze YKD mutants, thus the MCM complex highlights the utility of the DAmP collection in drug-gene interaction studies.

Media-independent deletion suppression

Genes functioning in processes that augment doxorubicin toxicity, when lost (*e.g.*, by deletion), can result in suppression. This was suggested in both respiratory and glycolytic contexts for *sphingolipid homeostasis*, *telomere tethering at nuclear periphery*, and *actin cortical patch localization* (**Fig. 4,** clusters 2-0.4-1 and 2-0.3-3). Conversely, their overexpression in cancer could potentiate toxicity and thereby therapeutic efficacy.

Sphingolipid homeostasis and metabolism

From cluster 2-0.4-1, *VPS51, VPS52, VPS53*, and *VPS54* (**Fig. 11A**) form the Golgi-associated retrograde protein (**GARP**) complex, which is required for endosome-to-Golgi retrograde vesicular transport. GARP deficiency results in accumulation of sphingolipid synthesis intermediates [151]. Also from this cluster came fatty acid elongase activity (*FEN1/ELO2* and *SUR4/ELO3*), which when deficient leads to reduced ceramide production and phytosphingosine accumulation [152, 153].

Since the GARP genes and fatty acid elongase activity genes function together in sphingolipid metabolism, we searched all genes annotated to this term and found other media-independent suppressors to include *TSC3, LIP1, SUR1, SUR2, IPT1,* and *SKN1* (**Fig. 11A**). Doxorubicin treatment induces accumulation of ceramide [5, 6], which mediates anti-proliferative responses and apoptosis in yeast and human and appears to mechanistically underlie the influence of this gene group [154] (**Additional File 1, Fig. S9**). These findings were further supported by the deletion enhancer, *SCH9*, which negatively regulates ceramide production by inducing ceramidases and negatively regulating *ISC1* (**Fig. 11A**) [155]. Multidrug-resistant HL-60/MX2 human promyelocytic leukemia cells are sensitized to doxorubicin by N,N-Dimethyl phytosphingosine [156].

Taken together, the model provides genetic detail regarding how disruption of sphingolipid metabolism increases resistance to doxorubicin, and that this occurs in a Warburg-independent manner, seemingly by reducing apoptosis associated with doxorubicin-induced ceramide overproduction [5, 157, 158].

Telomere tethering at nuclear periphery

Enrichment for *telomere tethering at nuclear periphery* in cluster 2-0.4-1 was comprised of *NUP60, NUP170, MLP1,* and *ESC1*. Paradoxically growth deficient on

HLD media, *NUP84, NUP120,* and *NUP133* also exerted deletion suppression in HLEG (**Fig. 11B**). Nuclear pore functions include coordinating nuclear-cytoplasmic transport and localizing proteins and/or chromosomes at the nuclear periphery, which contributes to DNA repair, transcription, and chromatin silencing [159]. Thus, deletion of nuclear pore genes could influence doxorubicin resistance by multiple potential mechanisms involving altering chromatin states, transcriptional regulation, maintenance of telomeric regions, and DNA repair. Doxorubicin-gene interaction profiles for all nuclear pore-related genes are provided in **Additional File 1, Fig. S10 A**.

Actin cortical patch localization

Cluster 2-0.4-1 was enriched for *actin cortical patch localization*, including *RVS167, LSB3, RVS161*, and *VRP1* (**Fig. 11B**). Related terms (*Arp2/3 protein complex* and *actin cortical patch*) exhibited similar doxorubicin-gene interaction profiles, including *ARC15*, *ARC18*, *ARC35*, *INP52*, *INP53*, *ARP2*, *ARP3*, *GTS1*, *RSP5*, and *FKS1 (*see **Additional File 1, Fig. S10 B-C**). This result corroborates studies in mouse embryonic fibroblasts where deletion of *ROCK1* increased doxorubicin resistance by altering the actin cytoskeleton and protecting against apoptosis [160, 161]. Additional literature indicates an importance of actin-related processes for doxorubicin cytotoxicity [162-164], highlighting the utility of yeast phenomics to understand these effects in greater depth.

Respiratory-deficient doxorubicin-gene interaction modules

From cluster 1-0-0, we noted that respiratory deficient YKO/KD strains (those not generating a growth curve on HLEG) also had low K and/or increased L ‘shift’ values on HLD, as would be expected of petite strains [165]. Among strains in this category, those displaying doxorubicin-gene interaction tended to show deletion enhancement (**Fig. 4**).

Respiratory deficient deletion enhancers on HLD functioned primarily in mitochondrial processes (**Additional File 5, File C**; see GO enrichment for cluster 1-0-0 and derivative clusters), including *mitochondrial translation*, *mitochondrion-ER tethering*, *protein localization into mitochondria*, *mitochondrial genome maintenance*, *respiratory chain complex assembly*, and *proton transport*. Compromise of mitochondrial respiration leading to sensitization of cells to doxorubicin is of interest given recent findings that some glycolytic cancers are respiratory deficient [166, 167].

Phenomics-based predictions of doxorubicin-gene interaction in cancer cell lines

Differential gene expression, by itself, is a poor predictor of whether protein function affects proliferative response to a particular drug [168]. Thus, yeast phenomic data, which precisely measures enhancing and suppressing interactions with respect to growth phenotypes, could provide a systems model to prioritize candidate effectors of cancer cell line sensitivity and transcriptomic data [169, 170]. To investigate this possibility, yeast doxorubicin-gene interaction was matched by homology to differential gene expression in doxorubicin-sensitive cancer cell lines, using *PharmacoGx* [40] and *biomaRt* [41, 42]) in conjunction with the GDSC1000 [171, 172] or gCSI [173, 174] databases (**Fig. 12)**. Differential gene expression was analyzed for individual tissues and also aggregated across all tissues. Yeast gene deletion enhancers were matched to human homologs underexpressed in doxorubicin-sensitive cancer cell lines, termed '**UES**'. Conversely, yeast gene deletion suppressors were matched to human homologs overexpressed in doxorubicin sensitive cells, termed '**OES**' (**Additional File 11)**.

There was greater overlap in differential gene expression between the gCSI and GDSC databases for aggregated data (compared to data for individual tissues), of which agreement was greater for OES than UES. Among individual tissues, there was highest

agreement between hematopoietic/lymphoid and lung. Differences could be partially explained by the two studies using different platforms for measuring gene expression and cell cytotoxicity (https://pharmacodb.pmgenomics.ca/drugs/273). The gCSI database also reported more UES and OES genes than GDSC (**Additional File 11, Files B and C**). Differentially expressed genes were mined with respect to p-value and matched to homologous yeast gene interactions (**Additional File 11, Files D-I**). Warburg status was not available for the cancer cell lines, so we first matched Warburg-independent yeast gene interactions to differentially expressed genes from aggregated data in both the gCSI and GDSC datasets, predicting eight UES (*ARP4/ACTL6B, ERG13/HMGCS2, PTC1/PPM1L, SCH9/RPS6KB2, SEC11/SEC11C, SEC7/ARFGEF2, SEC7/IQSEC3,* and *SIS2/PPCDC*) and 18 OES genes (*ARP2/ACTR2, CDC3/SEPT6, CKA2/CSNK2A2, DBR1/DBR1, DOA1/PLAA, EFT2/EEF2, HTS1/HARS, KIN28/CDK7, MAP1/METAP1, RPL16B/RPL13A*, *RPL32/RPL32, RPL34A/RPL34, RPL40B/ZFAND4,* RPS6A/RPS6, *SSE1/HSPA4, STO1/NCBP1, TRZ1/ELAC2,* and *UBC4/UBE2D1*) to have causal influences on the doxorubicin sensitivity phenotype (**Fig. 12C-D)**.

As detailed in **Tables 3-4** and described below, we expanded the analysis to genes representative of GO Term enrichments revealed by the yeast phenomic model, restricting to human genes differentially expressed across all cancer tissues, but without restricting by Warburg-independence or gCSI/GDSC co-evidence. Results for individual tissues are also provided in **Additional File 11, File A**.

Deletion enhancers with UES homologs

Concordance between deletion-enhancing doxorubicin-gene interaction in yeast and UES observed for the corresponding human homologs in cancer cells suggests

synergistic targets and biomarkers to increase therapeutic efficacy for doxorubicin, as summarized in **Table 3 and Fig. 12C**, and briefly discussed below.

Doxorubicin-enhancing interactions that were UES in both gCSI and GDSC included: *ACTL6B*, identified as a candidate tumor suppressor gene in primary hepatocellular carcinoma tissue [175]; *PPM1L*, which regulates ceramide trafficking at ER-Golgi membrane contact sites [176], and exhibits reduced expression in familial adenomatous polyposis [177]; *RPS6KB2*, which was UES in breast, ovarian and bone in gCSI, while *RPS6KA1*, *A2*, *A5* and *A6* were UES in select tissues in both databases (**Additional File 11, File A);** *SEC11/SEC11C*, which is upregulated in response to hypoxia in non-small cell lung cancer tissue [178], and for which deletion enhancement was stronger in HLD media (**Additional File 1, Fig. S7**); *SEC7/ARFGEF2* (alias *BIG2)* exhibits increased gene and protein expression in pancreatic cancer [179], and shRNA knockdown of *ARFGEF2* can reduce Burkitt's lymphoma cell survival [180].

We expanded the analysis above by matching yeast gene deletion enhancers to human UES genes in either database, i.e., not requiring that genes be significant in both datasets (**Figs 12E-F**). The result highlighted chromatin-related buffering processes, including nucleosome assembly (*HTA1, HTB1, HHF1, HHF2, HHT1, HHF1)*, histone exchange (*SET2/SETBP1* and *SWR1/SRCAP)*, and histone modifiers (*BRE1, HDA1, RCO1*) (**Fig. 12E, Table 3**). Other functions predicted by the yeast model to buffer doxorubicin toxicity in cancer cells included DNA topological change (*MUS81, SGS1*), mitochondrial maintenance (*MGR2, TOM70*), protein acetylation (*MAK3*), and metabolism (*SFA1, ERG13, SOD1*).

MUS81 knockdown enhances sensitivity of colon cancer lines to cisplatin and other chemotherapy agents by activating the *CHK1* pathway [181]. *MGR2/ROMO1* is involved in protein import into the mitochondrial matrix and overexpression of *ROMO1*

has been associated with poor prognosis in colorectal [182] and non-small cell lung cancer patients [183]. *MAK3/NAA30,* a component of the NatC complex (**Fig 8A**), induces p53-dependent apoptosis when knocked down in cancer cell lines [184]. The HLD-specific deletion enhancer, *SFA1,* has seven human homologs, of which three (*ADH4, ADH1A,* and *ADH6*) were UES in gCSI data (**Additional File 1, Figure S7)**.. High expression of *ADH1A* or *ADH6* was predictive of improved prognosis for pancreatic adenocarcinoma [185] and high expression of *ADH1A* or *ADH4* had improved prognosis for non-small cell lung cancer [186]. The *ERG13* homolog, *HMGCS1*, has been suggested as a synthetic lethal target for $BRAF^{V600E}$-positive human cancers [187], and *HMGCS2* plays a role in invasion and metastasis in colorectal and oral cancer [188]. Thus, doxorubicin treatment may have anti-tumor efficacy specifically in glycolytic tumors with reduced expression of *SFA1* and *ERG13* homologs.

Deletion suppressors with OES homologs

Choosing chemotherapeutic agents for patients based on their tumors exhibiting high expression of genes known to increase sensitivity represents a targeted strategy to increase therapeutic efficacy and could be particularly effective if the sensitizing overexpressed genes happen to also be drivers [189]. Human genes that are OES, homologous to yeast genes that are deletion suppressors, are highlighted in **Table 4** and **Fig. 12D**. *ARP2/ACTR2* is a member of the Arp2/3 protein complex (see **Additional File 1, Figure S10C)**, and silencing of the Arp2/3 protein complex reduces migration of pancreatic cancer cell lines [190]. *EEF2* protein is overexpressed in multiple cancer types, where shRNA knockdown inhibits growth [191]. *CDK7* overexpression in breast [192, 193] and gastric [194] cancer is predictive of poor prognosis. *RPL34* overexpression promotes proliferation, invasion, and metastasis in pancreatic [195], non-

small cell lung [196], and squamous cell carcinoma [197], while *RPL32* was also overexpressed in a prostate cell cancer model [198]. In contrast to Rps6k family members being UES/deletion enhancing, Rps6 was OES/deletion suppressing in ovarian tissue. *RPS6* overexpression portends reduced survival for patients with renal carcinoma [199] and hyperphosphosphorylation of Rps6 confers poor prognosis in non-small cell lung cancer [200]. Overexpression of *UBE2D1* is associated with decreased survival in lung squamous cell carcinoma tissue [201], and numerous additional ubiquitin-conjugating enzyme family members were OES in analysis of individual tissues (**Additional File 11, File A**).

We expanded the analysis, similar to the way described above for the deletion enhancers, by relaxing the matching criteria in order to identify additional deletion suppressing pathways revealed by the yeast model (**Additional File 11**). The extended analysis identified yeast-human conserved functions in metabolism (*SPE2, SPE4, VPS53, ELO2, ELO4*), histone demethylation (*JHD1, JHD2*), translation reinitiation (*TMA22, TIF32*), the condensin complex (*YCG1*, *YCS4*, *SMC2*), and telomere tethering at the nuclear periphery (*NUP170*) (**Table 4, Fig. 12F)**. *SPE2/AMD1* is required for spermidine and spermine biosynthesis, and up-regulation of *AMD1* by mTORC1 rewires polyamine metabolism in prostate cancer cell lines and mouse models [202]. *VPS53*, a component of the GARP complex involved in sphingolipid homeostasis, is a tumor suppressor in hepatocellular carcinoma [203-205]. Inhibition of *ELOVL6* (homologous to yeast *ELO2* and *ELO3*) in mice reduces tumor growth and increases survival [206]. The histone demethylase, *JHD1/KDM2B*, is overexpressed in pancreatic cancer [207] and is associated with poor prognosis in glioma [208] and triple negative breast cancer [209]. A second homolog, *JHD2/JARID2*, is required for tumor initiation in bladder cancer [210]. The yeast model also predicts causality underlying OES associated with genes involved

in translation reinitiation, *TMA22/DENR* (translation machinery associated) and *TIF32/EIF31. DENR-MCT-1* regulates a class of mRNAs encoding oncogenic kinases [211-213], and its overexpression in hepatocellular carcinoma is associated with metastasis [214]. *TMA22/DENR* also exerts evolutionarily conserved influence on telomeric function and cell proliferation [215]. *YCG1/NCAPG* and *SMC2/SMC2* are components of the condensin complex, which are overexpressed in cancer [138]. *NUP170/NUP155*, which functions in telomere tethering at the nuclear periphery (**Fig. 11B**), is hyper-methylated in association with breast cancer [216, 217], where its reduced expression contributes to a signature for bone metastasis [218].

Discussion:

Many genes are implicated in tumorigenesis and in chemotherapeutic response, with varying degrees of tissue-specific influence and yeast-human homology. The ability to assess mutation, differential gene expression, and other molecular correlates of cancer and chemotherapeutic efficacy is growing, but the direct assessment of drug-gene interaction (i.e., phenotypic/cell proliferative responses) remains a challenge due to the complex genetics and tissue-specific aspects of cancer. In stark contrast, yeast is a single-cell eukaryotic organism that is uniquely amenable to precise and genome-wide measures of drug-gene interaction, for which fundamental contributions to our understanding of human disease are well established [219-223]. Thus, we wondered whether phenomic analysis, using the yeast YKO/KD resource, might be informative about the potential of the Warburg effect to influence the anti-cancer efficacy of doxorubicin, and potentially other chemotherapeutic agents [25, 224]. From this unbiased systems perspective, we observed that a less extensive genetic network is required to buffer doxorubicin in glycolytic vs. respiring cells. The HLEG-specific

doxorubicin-gene interaction network points to genetic vulnerabilities that respiratory tumors have, but that can be relieved of by the Warburg transition to glycolytic metabolism. Thus, the yeast phenomic model could be applied in the context of Warburg status and analysis of somatic mutations in an individual patient's cancer, to aid in predicting doxorubicin therapeutic efficacy (**Fig. 13, Tables 3-4**). Cells can buffer the cytotoxic effects of doxorubicin in a glycolytic context with less reliance on pathways that can go awry in cancer and that influence doxorubicin cytotoxicity more in a respiratory context; examples include pathways of chromatin regulation, protein folding and modification, mitochondrial function, and DNA topological change. The yeast model also predicts that respiring tumors can better survive doxorubicin if functions for fatty acid beta-oxidation, spermine metabolism, and translation reinitiation are compromised by mutation (**Fig. 13, Table 3**). On the other hand, cells that transition to glycolytic metabolism need dTTP biosynthesis and protein complexes including the Cul4-RING E3 ubiquitin ligase, and the Ubp3-Bre5 deubuiquitinase, as well as Dom34-Hbs1, which functions in 'no-go' mRNA decay, in order to buffer doxorubicin. However, glycolytic cells become even more resistant if losing histone deubiquitination or the nuclear condensin complex (**Fig. 13, Table 3**). The yeast model also highlighted Warburg-independent pathways for which loss of function enhanced doxorubicin cytotoxicity, such as DNA repair and histone H3-K56 acetylation, along with deletion suppressing pathways, including sphingolipid homeostasis, actin cortical patch localization, and telomere tethering at the nuclear periphery (**Fig. 13, Table 3**).

Studies in cancer cell lines, mice, and acute myeloid leukemia blast cells from patients were highlighted by the yeast phenomic model, suggesting histone eviction, increased mutation rates at active promoter sites [11, 12, 225], and accumulation of damage from chromatin trapping by the FACT complex as mechanisms of doxorubicin

toxicity [13]. Further support of the importance of chromatin regulation was suggested by transcriptional control and assembly of histones, as well as histone modifications, which are all particularly important in a respiratory context. From a precision medicine perspective, tumors that are promoted by genetic compromise in chromatin regulation [226, 227] would be potentially more susceptible to treatment, but only if they have not undergone the Warburg transition to glycolysis. Analogously, patients with germline variation resulting in functional compromise of chromatin regulation may have normal tissue (e.g., cardiac muscle) that is susceptible to doxorubicin and thus may suffer greater toxic side effects of cancer treatment.

The examples of integrating yeast phenomic data with cancer cell line pharmacogenomics data to predict therapeutic efficacy are not limited to doxorubicin and/or the Warburg phenomenon. Analogous phenomic models could be generated for many cytotoxic agents and/or metabolic states. We found the global correlation of human UES and OES with yeast deletion suppressors and enhancers to be very low, consistent with yeast studies examining this expectation [168]. However, there were many examples of differential expression of individual genes, which were potentially explained biologically by the yeast phenomic model. These observations suggest that yeast phenomic models can be helpful and may even be necessary to associate differential gene expression and sensitivity of cancer cells to chemotherapy. We hope and anticipate that future integrative studies and ultimately clinical trials can further demonstrate whether yeast phenomic studies contribute useful information for personalizing clinical guidance and increasing therapeutic efficacy for patients.

The HDAC inhibitor, Abexinostat, enhanced doxorubicin cytotoxicity in cancer cell lines [228, 229], and a phase I clinical trial combining the agents in metastatic sarcomas showed some tumor responses [230]. Enhanced doxorubicin cardiotoxicity

was observed with co-administration of HDAC inhibitors in mice [231]. The yeast phenomic model suggests it could be informative to monitor the Warburg status of cancer cells in such studies (**Fig. 7A**). The Sin3-type histone deacetylase complexes (Class I) exhibit respiration-specific deletion enhancement, however the influence of *HDA1/HDAC6* (Class II) is Warburg-independent, with *HDAC6* being UES (**Fig. 12E, Table 3**). *HDAC6* has a unique structure among histone deacetylases, increasing the ability to target it pharmacologically [232]. A clinical trial using Vorinostat in combination with paclitaxel and doxorubicin-cyclophosphamide to treat advanced breast cancer showed a positive response and reduced expression of *HDAC6* in the primary tumor [233]. Ricolinostat is a clinically safe *HDAC6*-specific inhibitor [234] that could enhance doxorubicin toxicity to cancer driven by epigenetic plasticity [226, 227], if the cancer undergoes the Warburg transition, as HDA1 complex mutants are less protected by glycolysis. Yet in a respiratory context, Sin3-type complexes exhibit stronger interaction (**Fig. 7A**). While speculative, these examples are intended to illustrate the potential power of yeast phenomic models to generate novel, testable hypotheses through integration of existing knowledge and new, unbiased experimental results.

In summary, we envision yeast phenomic drug-gene interaction models as a complement to existing cancer pharmacogenomics, providing an experimental platform to quantitatively derive drug-gene interaction network knowledge that can be integrated with DNA, RNA, protein, epigenetic, metabolite profiling, and/or cell proliferation data collected from tumors. Such predictions, applied to individual patients' tumors, could be further used in conjunction with evaluation of tumor drug response; for example, before and after treatment to understand how recurrent cancer buffers the drug's toxicities. Analyses of patient-derived tumor organoids, for example, could include predictive modeling and experimental validation for development of treatment strategies, both

initially and with recurrence [235-237]. The influence of Warburg status could also be integrated into such personalized models if monitoring its influence on responsiveness of cancer to chemotherapy proves useful for selectively killing tumors [238]. Moreover, yeast phenomic models could be tailored to individual patients to examine more complex interactions: for example, in the background of homologous recombination deficiency [145]. Yeast phenomics provides the experimental capabilities and genetic tractability to model genetic buffering networks relevant to human disease at high precision and resolution, and the biological relevance of yeast genetics to human disease is established; however, the extent to which yeast phenomics is predictive of human disease biology and complexity remains to be determined.

A major premise of precision medicine should be to systematically account for the contribution of genetic variance to phenotypes as well as influential interacting factors such as cell energy metabolism, age, drugs, or other environmental factors. However, functional genetic variation in human populations, and particularly for cancer, is essentially too abundant to resolve at a systems level with respect to drug-gene interaction. Thus, yeast phenomics, which can define gene interaction networks and genetic buffering in a highly tractable way [21, 239, 240], offers the potential to help resolve disease complexity [17, 241]. Although, the example of doxorubicin is a small sliver of biology, it exemplifies the potential of yeast phenomic modeling of human disease complexity. Lastly, doxorubicin and other cytotoxic agents are typically used in combination cocktails, and a future direction should be to develop yeast phenomic drug-gene interaction network models for buffering combination therapies.

Conclusions:

A yeast phenomic model for the influence of Warburg metabolism on doxorubicin cytotoxicity revealed that glycolysis reduces the cellular reliance on genetic buffering networks. The model reports gene deletion-enhancing and deletion-suppression pathways, and leverages yeast phenomic results to predict differentially expressed human genes that are causal in their association with doxorubicin killing from cancer cell line pharmacogenomics data. As such, this yeast model provides systems level information about gene networks that buffer doxorubicin, serving as example of how the YKO/KD enables experimental designs to quantify gene interaction globally at high resolution. In the case of doxorubicin, gene networks buffer cytotoxicity differentially with respect to Warburg metabolic status. Understanding cytotoxicity in terms of differential gene interaction networks has the potential to inform systems medicine by increasing the precision and rationale for personalizing the choice of cytotoxic agents, improving anti-tumor efficacy and thereby reducing host toxicity. Yeast phenomics is a scalable experimental platform that can, in principle, be expanded to other cytotoxic chemotherapeutic agents, singly or in combination, thus providing versatile, tractable models to map drug-gene interaction networks and understand their complex influence on cell proliferation.

List of abbreviations

CPP – Cell proliferation parameter; **DAmP** – Decreased Abundance of mRNA Production; **DE** – Deletion enhancer; **dNTP** – deoxyribonucleotide triphosphate; **DS** – Deletion suppressor; **dsDNA** – double-stranded DNA; **EMC** – Endoplasmic reticulum membrane complex; **ER** – Endoplasmic reticulum; **ERMES** – ER-mitochondria encounter structure; **GARP** - Golgi-associated retrograde protein; **GO** – Gene ontology;

GTF – Gene ontology term finder; **GTA** – Gene ontology term averaging; **GTA value** – Gene ontology term average value; **gtaSD** – standard deviation of GTA value; **GTA score** – (GTA value - gtaSD); **HDAC** – Histone deacetylase complex; **HLD** – Human-like media with dextrose; **HLEG** – Human-like media with ethanol and glycerol; **INT** – Interaction score; **m7G** - 7-methylguanosine; **MCM** – Mini-chromosome maintenance; **OES** – Overexpressed in doxorubicin sensitive cells; **Q-HTCP** – Quantitative high throughput cell array phenotyping; **Ref** – Reference; **REMc** – Recursive expectation maximization clustering; **ROS** – Reactive oxygen species; **RPA** - Replication Protein A; **SD** – Standard deviation; **SGD** – Saccharomyces cerevisiae genome database; **snoRNAs** - Small nucleolar RNA; **snRNA** - Small nuclear RNA; **t6A** - Threonyl carbamoyl adenosine; **UES** – Underexpressed in doxorubicin sensitive cells; **uORF** - Upstream open reading frames; **YKO** – Yeast knockout; **YKD** = Yeast knockdown

Declarations

Ethics approval and consent to participate

-Not Applicable

Consent for Publication

-Not Applicable

Availability of data and materials

All data generated or analyzed during this study are either included in this published article and supplementary files or will be freely supplied upon request.

Competing Interests

JLH has ownership in Spectrum PhenomX, LLC, a shell company that was formed to commercialize Q-HTCP technology. The authors declare no other competing interests.

Funding

The authors thank the following funding agencies for their support: American Cancer Society (RSG-10-066-01-TBE), Howard Hughes Medical Institute (P/S ECA 57005927), NIH/NCI (P30 CA013148), NIH/NIA (R01 AG043076), and Cystic Fibrosis Foundation (HARTMA16G0).

Author's contributions

SMS and JLH designed and conducted the experiments and analysis techniques, and wrote the manuscript.

Acknowledgements

The authors thank Jingyu Guo and Brett McKinney for development of REMc tools, John Rodgers for help with Q-HTCP analysis, and Mary-Ann Bjornsti and Alex Stepanov for helpful discussions.

Endnotes

-Not Applicable

Reference List

1. Thorn CF, Oshiro C, Marsh S, Hernandez-Boussard T, McLeod H, Klein TE, Altman RB: **Doxorubicin pathways: pharmacodynamics and adverse effects.** *Pharmacogenet Genomics* 2011, **21:**440-446.
2. Yang F, Teves SS, Kemp CJ, Henikoff S: **Doxorubicin, DNA torsion, and chromatin dynamics.** *Biochim Biophys Acta* 2014, **1845:**84-89.
3. Swift LP, Rephaeli A, Nudelman A, Phillips DR, Cutts SM: **Doxorubicin-DNA adducts induce a non-topoisomerase II-mediated form of cell death.** *Cancer Res* 2006, **66:**4863-4871.
4. Angsutararux P, Luanpitpong S, Issaragrisil S: **Chemotherapy-Induced Cardiotoxicity: Overview of the Roles of Oxidative Stress.** *Oxid Med Cell Longev* 2015, **2015:**795602.
5. Delpy E, Hatem SN, Andrieu N, de Vaumas C, Henaff M, Rucker-Martin C, Jaffrezou JP, Laurent G, Levade T, Mercadier JJ: **Doxorubicin induces slow ceramide accumulation and late apoptosis in cultured adult rat ventricular myocytes.** *Cardiovasc Res* 1999, **43:**398-407.

1076 6. Kawase M, Watanabe M, Kondo T, Yabu T, Taguchi Y, Umehara H, Uchiyama T, Mizuno
1077 K, Okazaki T: **Increase of ceramide in adriamycin-induced HL-60 cell apoptosis:**
1078 **detection by a novel anti-ceramide antibody.** *Biochim Biophys Acta* 2002, **1584:**104-
1079 114.
1080 7. Chen SH, Chan NL, Hsieh TS: **New mechanistic and functional insights into DNA**
1081 **topoisomerases.** *Annu Rev Biochem* 2013, **82:**139-170.
1082 8. Tewey KM, Rowe TC, Yang L, Halligan BD, Liu LF: **Adriamycin-induced DNA damage**
1083 **mediated by mammalian DNA topoisomerase II.** *Science* 1984, **226:**466-468.
1084 9. Nitiss JL: **Targeting DNA topoisomerase II in cancer chemotherapy.** *Nat Rev Cancer*
1085 2009, **9:**338-350.
1086 10. Coldwell KE, Cutts SM, Ognibene TJ, Henderson PT, Phillips DR: **Detection of**
1087 **Adriamycin-DNA adducts by accelerator mass spectrometry at clinically relevant**
1088 **Adriamycin concentrations.** *Nucleic Acids Res* 2008, **36:**e100.
1089 11. Pang B, Qiao X, Janssen L, Velds A, Groothuis T, Kerkhoven R, Nieuwland M, Ovaa H,
1090 Rottenberg S, van Tellingen O, et al: **Drug-induced histone eviction from open**
1091 **chromatin contributes to the chemotherapeutic effects of doxorubicin.** *Nat Commun*
1092 2013, **4:**1908.
1093 12. Yang F, Kemp CJ, Henikoff S: **Doxorubicin enhances nucleosome turnover around**
1094 **promoters.** *Curr Biol* 2013, **23:**782-787.
1095 13. Nesher E, Safina A, Aljahdali I, Portwood S, Wang ES, Koman I, Wang J, Gurova KV: **Role**
1096 **of Chromatin Damage and Chromatin Trapping of FACT in Mediating the Anticancer**
1097 **Cytotoxicity of DNA-Binding Small-Molecule Drugs.** *Cancer Res* 2018, **78:**1431-1443.
1098 14. Singal PK, Iliskovic N: **Doxorubicin-induced cardiomyopathy.** *N Engl J Med* 1998,
1099 **339:**900-905.
1100 15. Zhang S, Liu X, Bawa-Khalfe T, Lu LS, Lyu YL, Liu LF, Yeh ET: **Identification of the**
1101 **molecular basis of doxorubicin-induced cardiotoxicity.** *Nat Med* 2012, **18:**1639-1642.
1102 16. Visscher H, Ross CJ, Rassekh SR, Barhdadi A, Dube MP, Al-Saloos H, Sandor GS, Caron
1103 HN, van Dalen EC, Kremer LC, et al: **Pharmacogenomic prediction of anthracycline-**
1104 **induced cardiotoxicity in children.** *J Clin Oncol* 2012, **30:**1422-1428.
1105 17. Hartman IV JL, Garvik B, Hartwell L: **Principles for the buffering of genetic variation.**
1106 *Science* 2001, **291:**1001-1004.
1107 18. Hartman IV JL, Tippery NP: **Systematic quantification of gene interactions by**
1108 **phenotypic array analysis.** *Genome Biol* 2004, **5:**R49.
1109 19. Hartman IV JL: **Buffering of deoxyribonucleotide pool homeostasis by threonine**
1110 **metabolism.** *Proc Natl Acad Sci U S A* 2007, **104:**11700-11705.
1111 20. Hartman IV JL, Stisher C, Outlaw DA, Guo J, Shah NA, Tian D, Santos SM, Rodgers JW,
1112 White RA: **Yeast Phenomics: An Experimental Approach for Modeling Gene Interaction**
1113 **Networks that Buffer Disease.** *Genes (Basel)* 2015, **6:**24-45.
1114 21. Louie RJ, Guo J, Rodgers JW, White R, Shah N, Pagant S, Kim P, Livstone M, Dolinski K,
1115 McKinney BA, et al: **A yeast phenomic model for the gene interaction network**
1116 **modulating CFTR-ΔF508 protein biogenesis.** *Genome Med* 2012, **4:**103.
1117 22. Veit G, Oliver K, Apaja PM, Perdomo D, Bidaud-Meynard A, Lin ST, Guo J, Icyuz M,
1118 Sorscher EJ, Hartman JI, Lukacs GL: **Ribosomal Stalk Protein Silencing Partially Corrects**
1119 **the DeltaF508-CFTR Functional Expression Defect.** *PLoS Biol* 2016, **14:**e1002462.

1120 23. Hartman IV JL: **Genetic and Molecular Buffering of Phenotypes.** In *Nutritional*
1121 *Genomics: Discovering the Path to Personalized Nutrition. Volume* 1. 1 edition. Edited by
1122 Rodriguez R, Kaput J. Hoboken, NJ: John Wiley & Sons; 2006: 496
1123 24. Warburg O: **On the origin of cancer cells.** *Science* 1956, **123:**309-314.
1124 25. Liberti MV, Locasale JW: **The Warburg Effect: How Does it Benefit Cancer Cells?** *Trends*
1125 *Biochem Sci* 2016, **41:**211-218.
1126 26. Schwartz L, Supuran CT, Alfarouk KO: **The Warburg Effect and the Hallmarks of Cancer.**
1127 *Anticancer Agents Med Chem* 2017, **17:**164-170.
1128 27. Xu XD, Shao SX, Jiang HP, Cao YW, Wang YH, Yang XC, Wang YL, Wang XS, Niu HT:
1129 **Warburg effect or reverse Warburg effect? A review of cancer metabolism.** *Oncol Res*
1130 *Treat* 2015, **38:**117-122.
1131 28. Diaz-Ruiz R, Rigoulet M, Devin A: **The Warburg and Crabtree effects: On the origin of**
1132 **cancer cell energy metabolism and of yeast glucose repression.** *Biochim Biophys Acta*
1133 2011, **1807:**568-576.
1134 29. Diaz-Ruiz R, Uribe-Carvajal S, Devin A, Rigoulet M: **Tumor cell energy metabolism and**
1135 **its common features with yeast metabolism.** *Biochim Biophys Acta* 2009, **1796:**252-
1136 265.
1137 30. Takeda M: **Glucose-induced inactivation of mitochondrial enzymes in the yeast**
1138 **Saccharomyces cerevisiae.** *Biochem J* 1981, **198:**281-287.
1139 31. Ventura-Clapier R, Garnier A, Veksler V, Joubert F: **Bioenergetics of the failing heart.**
1140 *Biochim Biophys Acta* 2011, **1813:**1360-1372.
1141 32. Shah NA, Laws RJ, Wardman B, Zhao LP, Hartman IV JL: **Accurate, precise modeling of**
1142 **cell proliferation kinetics from time-lapse imaging and automated image analysis of**
1143 **agar yeast culture arrays.** *BMC Syst Biol* 2007, **1:**3.
1144 33. Mani R, St Onge RP, Hartman IV JL, Giaever G, Roth FP: **Defining genetic interaction.**
1145 *Proc Natl Acad Sci U S A* 2008, **105:**3461-3466.
1146 34. Rodgers J, Guo J, Hartman IV JL: **Phenomic assessment of genetic buffering by kinetic**
1147 **analysis of cell arrays.** *Methods Mol Biol* 2014, **1205:**187-208.
1148 35. Guo J, Tian D, McKinney BA, Hartman IV JL: **Recursive expectation-maximization**
1149 **clustering: a method for identifying buffering mechanisms composed of phenomic**
1150 **modules.** *Chaos* 2010, **20:**026103.
1151 36. Boyle EI, Weng S, Gollub J, Jin H, Botstein D, Cherry JM, Sherlock G: **GO::TermFinder--**
1152 **open source software for accessing Gene Ontology information and finding**
1153 **significantly enriched Gene Ontology terms associated with a list of genes.**
1154 *Bioinformatics* 2004, **20:**3710-3715.
1155 37. Cherry JM, Hong EL, Amundsen C, Balakrishnan R, Binkley G, Chan ET, Christie KR,
1156 Costanzo MC, Dwight SS, Engel SR, et al: **Saccharomyces Genome Database: the**
1157 **genomics resource of budding yeast.** *Nucleic Acids Res* 2012, **40:**D700-705.
1158 38. Heinicke S, Livstone MS, Lu C, Oughtred R, Kang F, Angiuoli SV, White O, Botstein D,
1159 Dolinski K: **The Princeton Protein Orthology Database (P-POD): a comparative**
1160 **genomics analysis tool for biologists.** *PLoS One* 2007, **2:**e766.
1161 39. Smirnov P, Kofia V, Maru A, Freeman M, Ho C, El-Hachem N, Adam GA, Ba-Alawi W,
1162 Safikhani Z, Haibe-Kains B: **PharmacoDB: an integrative database for mining in vitro**
1163 **anticancer drug screening studies.** *Nucleic Acids Res* 2018, **46:**D994-D1002.

1164 40. Smirnov P, Safikhani Z, El-Hachem N, Wang D, She A, Olsen C, Freeman M, Selby H,
1165 Gendoo DM, Grossmann P, et al: **PharmacoGx: an R package for analysis of large**
1166 **pharmacogenomic datasets.** *Bioinformatics* 2016, **32:**1244-1246.
1167 41. Durinck S, Moreau Y, Kasprzyk A, Davis S, De Moor B, Brazma A, Huber W: **BioMart and**
1168 **Bioconductor: a powerful link between biological databases and microarray data**
1169 **analysis.** *Bioinformatics* 2005, **21:**3439-3440.
1170 42. Durinck S, Spellman PT, Birney E, Huber W: **Mapping identifiers for the integration of**
1171 **genomic datasets with the R/Bioconductor package biomaRt.** *Nat Protoc* 2009, **4:**1184-
1172 1191.
1173 43. Zerbino DR, Achuthan P, Akanni W, Amode MR, Barrell D, Bhai J, Billis K, Cummins C,
1174 Gall A, Giron CG, et al: **Ensembl 2018.** *Nucleic Acids Res* 2018, **46:**D754-D761.
1175 44. Xia L, Jaafar L, Cashikar A, Flores-Rozas H: **Identification of genes required for**
1176 **protection from doxorubicin by a genome-wide screen in Saccharomyces cerevisiae.**
1177 *Cancer Res* 2007, **67:**11411-11418.
1178 45. Westmoreland TJ, Wickramasekara SM, Guo AY, Selim AL, Winsor TS, Greenleaf AL,
1179 Blackwell KL, Olson JA, Jr., Marks JR, Bennett CB: **Comparative genome-wide screening**
1180 **identifies a conserved doxorubicin repair network that is diploid specific in**
1181 **Saccharomyces cerevisiae.** *PLoS One* 2009, **4:**e5830.
1182 46. Smith DL, Jr., Maharrey CH, Carey CR, White RA, Hartman IV JL: **Gene-nutrient**
1183 **interaction markedly influences yeast chronological lifespan.** *Exp Gerontol* 2016,
1184 **86:**113-123.
1185 47. Amin AD, Vishnoi N, Prochasson P: **A global requirement for the HIR complex in the**
1186 **assembly of chromatin.** *Biochim Biophys Acta* 2013, **1819:**264-276.
1187 48. Green EM, Antczak AJ, Bailey AO, Franco AA, Wu KJ, Yates JR, 3rd, Kaufman PD:
1188 **Replication-independent histone deposition by the HIR complex and Asf1.** *Curr Biol*
1189 2005, **15:**2044-2049.
1190 49. Imbeault D, Gamar L, Rufiange A, Paquet E, Nourani A: **The Rtt106 histone chaperone is**
1191 **functionally linked to transcription elongation and is involved in the regulation of**
1192 **spurious transcription from cryptic promoters in yeast.** *J Biol Chem* 2008, **283:**27350-
1193 27354.
1194 50. Emili A, Schieltz DM, Yates JR, 3rd, Hartwell LH: **Dynamic interaction of DNA damage**
1195 **checkpoint protein Rad53 with chromatin assembly factor Asf1.** *Mol Cell* 2001, **7:**13-
1196 20.
1197 51. Kaufman PD, Kobayashi R, Stillman B: **Ultraviolet radiation sensitivity and reduction of**
1198 **telomeric silencing in Saccharomyces cerevisiae cells lacking chromatin assembly**
1199 **factor-I.** *Genes Dev* 1997, **11:**345-357.
1200 52. Bao Y, Shen X: **SnapShot: Chromatin remodeling: INO80 and SWR1.** *Cell* 2011, **144:**158-
1201 158 e152.
1202 53. Zhang H, Roberts DN, Cairns BR: **Genome-wide dynamics of Htz1, a histone H2A variant**
1203 **that poises repressed/basal promoters for activation through histone loss.** *Cell* 2005,
1204 **123:**219-231.
1205 54. Raisner RM, Hartley PD, Meneghini MD, Bao MZ, Liu CL, Schreiber SL, Rando OJ,
1206 Madhani HD: **Histone variant H2A.Z marks the 5' ends of both active and inactive**
1207 **genes in euchromatin.** *Cell* 2005, **123:**233-248.

1208 55. Guillemette B, Bataille AR, Gevry N, Adam M, Blanchette M, Robert F, Gaudreau L:
1209 **Variant histone H2A.Z is globally localized to the promoters of inactive yeast genes**
1210 **and regulates nucleosome positioning.** *PLoS Biol* 2005, **3:**e384.
1211 56. Seeber A, Hauer M, Gasser SM: **Nucleosome remodelers in double-strand break repair.**
1212 *Curr Opin Genet Dev* 2013, **23:**174-184.
1213 57. Meneghini MD, Wu M, Madhani HD: **Conserved histone variant H2A.Z protects**
1214 **euchromatin from the ectopic spread of silent heterochromatin.** *Cell* 2003, **112:**725-
1215 736.
1216 58. Seto E, Yoshida M: **Erasers of histone acetylation: the histone deacetylase enzymes.**
1217 *Cold Spring Harb Perspect Biol* 2014, **6:**a018713.
1218 59. Rundlett SE, Carmen AA, Kobayashi R, Bavykin S, Turner BM, Grunstein M: **HDA1 and**
1219 **RPD3 are members of distinct yeast histone deacetylase complexes that regulate**
1220 **silencing and transcription.** *Proc Natl Acad Sci U S A* 1996, **93:**14503-14508.
1221 60. Schneider J, Bajwa P, Johnson FC, Bhaumik SR, Shilatifard A: **Rtt109 is required for**
1222 **proper H3K56 acetylation: a chromatin mark associated with the elongating RNA**
1223 **polymerase II.** *J Biol Chem* 2006, **281:**37270-37274.
1224 61. Masumoto H, Hawke D, Kobayashi R, Verreault A: **A role for cell-cycle-regulated histone**
1225 **H3 lysine 56 acetylation in the DNA damage response.** *Nature* 2005, **436:**294-298.
1226 62. Gartenberg MR, Smith JS: **The Nuts and Bolts of Transcriptionally Silent Chromatin in**
1227 **Saccharomyces cerevisiae.** *Genetics* 2016, **203:**1563-1599.
1228 63. Greer EL, Shi Y: **Histone methylation: a dynamic mark in health, disease and**
1229 **inheritance.** *Nat Rev Genet* 2012, **13:**343-357.
1230 64. Miller T, Krogan NJ, Dover J, Erdjument-Bromage H, Tempst P, Johnston M, Greenblatt
1231 JF, Shilatifard A: **COMPASS: a complex of proteins associated with a trithorax-related**
1232 **SET domain protein.** *Proc Natl Acad Sci U S A* 2001, **98:**12902-12907.
1233 65. Krogan NJ, Dover J, Khorrami S, Greenblatt JF, Schneider J, Johnston M, Shilatifard A:
1234 **COMPASS, a histone H3 (Lysine 4) methyltransferase required for telomeric silencing**
1235 **of gene expression.** *J Biol Chem* 2002, **277:**10753-10755.
1236 66. Roguev A, Schaft D, Shevchenko A, Pijnappel WW, Wilm M, Aasland R, Stewart AF: **The**
1237 **Saccharomyces cerevisiae Set1 complex includes an Ash2 homologue and methylates**
1238 **histone 3 lysine 4.** *EMBO J* 2001, **20:**7137-7148.
1239 67. Shilatifard A: **The COMPASS family of histone H3K4 methylases: mechanisms of**
1240 **regulation in development and disease pathogenesis.** *Annu Rev Biochem* 2012, **81:**65-
1241 95.
1242 68. Krogan NJ, Dover J, Wood A, Schneider J, Heidt J, Boateng MA, Dean K, Ryan OW,
1243 Golshani A, Johnston M, et al: **The Paf1 complex is required for histone H3 methylation**
1244 **by COMPASS and Dot1p: linking transcriptional elongation to histone methylation.**
1245 *Mol Cell* 2003, **11:**721-729.
1246 69. Ng HH, Dole S, Struhl K: **The Rtf1 component of the Paf1 transcriptional elongation**
1247 **complex is required for ubiquitination of histone H2B.** *J Biol Chem* 2003, **278:**33625-
1248 33628.
1249 70. Dover J, Schneider J, Tawiah-Boateng MA, Wood A, Dean K, Johnston M, Shilatifard A:
1250 **Methylation of histone H3 by COMPASS requires ubiquitination of histone H2B by**
1251 **Rad6.** *J Biol Chem* 2002, **277:**28368-28371.
1252 71. Sun ZW, Allis CD: **Ubiquitination of histone H2B regulates H3 methylation and gene**
1253 **silencing in yeast.** *Nature* 2002, **418:**104-108.

1254 72. Wood A, Schneider J, Dover J, Johnston M, Shilatifard A: **The Paf1 complex is essential**
1255 **for histone monoubiquitination by the Rad6-Bre1 complex, which signals for histone**
1256 **methylation by COMPASS and Dot1p.** *J Biol Chem* 2003, **278:**34739-34742.
1257 73. Giannattasio M, Lazzaro F, Plevani P, Muzi-Falconi M: **The DNA damage checkpoint**
1258 **response requires histone H2B ubiquitination by Rad6-Bre1 and H3 methylation by**
1259 **Dot1.** *J Biol Chem* 2005, **280:**9879-9886.
1260 74. Nicolay K, de Kruijff B: **Effects of adriamycin on respiratory chain activities in**
1261 **mitochondria from rat liver, rat heart and bovine heart. Evidence for a preferential**
1262 **inhibition of complex III and IV.** *Biochim Biophys Acta* 1987, **892:**320-330.
1263 75. Pereira GC, Pereira SP, Tavares LC, Carvalho FS, Magalhaes-Novais S, Barbosa IA, Santos
1264 MS, Bjork J, Moreno AJ, Wallace KB, Oliveira PJ: **Cardiac cytochrome c and cardiolipin**
1265 **depletion during anthracycline-induced chronic depression of mitochondrial function.**
1266 *Mitochondrion* 2016, **30:**95-104.
1267 76. MacKenzie JA, Payne RM: **Mitochondrial protein import and human health and**
1268 **disease.** *Biochim Biophys Acta* 2007, **1772:**509-523.
1269 77. Taanman JW, Capaldi RA: **Subunit VIa of yeast cytochrome c oxidase is not necessary**
1270 **for assembly of the enzyme complex but modulates the enzyme activity. Isolation and**
1271 **characterization of the nuclear-coded gene.** *J Biol Chem* 1993, **268:**18754-18761.
1272 78. Vukotic M, Oeljeklaus S, Wiese S, Vogtle FN, Meisinger C, Meyer HE, Zieseniss A,
1273 Katschinski DM, Jans DC, Jakobs S, et al: **Rcf1 mediates cytochrome oxidase assembly**
1274 **and respirasome formation, revealing heterogeneity of the enzyme complex.** *Cell*
1275 *Metab* 2012, **15:**336-347.
1276 79. Patterson TE, Poyton RO: **COX8, the structural gene for yeast cytochrome c oxidase**
1277 **subunit VIII. DNA sequence and gene disruption indicate that subunit VIII is required**
1278 **for maximal levels of cellular respiration and is derived from a precursor which is**
1279 **extended at both its NH2 and COOH termini.** *J Biol Chem* 1986, **261:**17192-17197.
1280 80. Herzig S, Raemy E, Montessuit S, Veuthey JL, Zamboni N, Westermann B, Kunji ER,
1281 Martinou JC: **Identification and functional expression of the mitochondrial pyruvate**
1282 **carrier.** *Science* 2012, **337:**93-96.
1283 81. Bricker DK, Taylor EB, Schell JC, Orsak T, Boutron A, Chen YC, Cox JE, Cardon CM, Van
1284 Vranken JG, Dephoure N, et al: **A mitochondrial pyruvate carrier required for pyruvate**
1285 **uptake in yeast, Drosophila, and humans.** *Science* 2012, **337:**96-100.
1286 82. Cui Y, Zhao S, Wang J, Wang X, Gao B, Fan Q, Sun F, Zhou B: **A novel mitochondrial**
1287 **carrier protein Mme1 acts as a yeast mitochondrial magnesium exporter.** *Biochim*
1288 *Biophys Acta* 2015, **1853:**724-732.
1289 83. Lemaire C, Guibet-Grandmougin F, Angles D, Dujardin G, Bonnefoy N: **A yeast**
1290 **mitochondrial membrane methyltransferase-like protein can compensate for oxa1**
1291 **mutations.** *J Biol Chem* 2004, **279:**47464-47472.
1292 84. Bauerschmitt H, Funes S, Herrmann JM: **The membrane-bound GTPase Guf1 promotes**
1293 **mitochondrial protein synthesis under suboptimal conditions.** *J Biol Chem* 2008,
1294 **283:**17139-17146.
1295 85. Pfanner N, van der Laan M, Amati P, Capaldi RA, Caudy AA, Chacinska A, Darshi M,
1296 Deckers M, Hoppins S, Icho T, et al: **Uniform nomenclature for the mitochondrial**
1297 **contact site and cristae organizing system.** *J Cell Biol* 2014, **204:**1083-1086.
1298 86. Jonikas MC, Collins SR, Denic V, Oh E, Quan EM, Schmid V, Weibezahn J, Schwappach B,
1299 Walter P, Weissman JS, Schuldiner M: **Comprehensive characterization of genes**

1300 **required for protein folding in the endoplasmic reticulum.** *Science* 2009, **323:**1693-
1301 1697.
1302 87. Lahiri S, Chao JT, Tavassoli S, Wong AK, Choudhary V, Young BP, Loewen CJ, Prinz WA: **A**
1303 **conserved endoplasmic reticulum membrane protein complex (EMC) facilitates**
1304 **phospholipid transfer from the ER to mitochondria.** *PLoS Biol* 2014, **12:**e1001969.
1305 88. van der Veen AG, Ploegh HL: **Ubiquitin-like proteins.** *Annu Rev Biochem* 2012, **81:**323-
1306 357.
1307 89. Judes A, Bruch A, Klassen R, Helm M, Schaffrath R: **Sulfur transfer and activation by**
1308 **ubiquitin-like modifier system Uba4*Urm1 link protein urmylation and tRNA**
1309 **thiolation in yeast.** *Microb Cell* 2016, **3:**554-564.
1310 90. Nakai Y, Nakai M, Hayashi H: **Thio-modification of yeast cytosolic tRNA requires a**
1311 **ubiquitin-related system that resembles bacterial sulfur transfer systems.** *J Biol Chem*
1312 2008, **283:**27469-27476.
1313 91. Noma A, Sakaguchi Y, Suzuki T: **Mechanistic characterization of the sulfur-relay system**
1314 **for eukaryotic 2-thiouridine biogenesis at tRNA wobble positions.** *Nucleic Acids Res*
1315 2009, **37:**1335-1352.
1316 92. Polevoda B, Norbeck J, Takakura H, Blomberg A, Sherman F: **Identification and**
1317 **specificities of N-terminal acetyltransferases from Saccharomyces cerevisiae.** *EMBO J*
1318 1999, **18:**6155-6168.
1319 93. Varland S, Osberg C, Arnesen T: **N-terminal modifications of cellular proteins: The**
1320 **enzymes involved, their substrate specificities and biological effects.** *Proteomics* 2015,
1321 **15:**2385-2401.
1322 94. Arnesen T, Van Damme P, Polevoda B, Helsens K, Evjenth R, Colaert N, Varhaug JE,
1323 Vandekerckhove J, Lillehaug JR, Sherman F, Gevaert K: **Proteomics analyses reveal the**
1324 **evolutionary conservation and divergence of N-terminal acetyltransferases from yeast**
1325 **and humans.** *Proc Natl Acad Sci U S A* 2009, **106:**8157-8162.
1326 95. Setty SR, Strochlic TI, Tong AH, Boone C, Burd CG: **Golgi targeting of ARF-like GTPase**
1327 **Arl3p requires its Nalpha-acetylation and the integral membrane protein Sys1p.** *Nat*
1328 *Cell Biol* 2004, **6:**414-419.
1329 96. Behnia R, Panic B, Whyte JR, Munro S: **Targeting of the Arf-like GTPase Arl3p to the**
1330 **Golgi requires N-terminal acetylation and the membrane protein Sys1p.** *Nat Cell Biol*
1331 2004, **6:**405-413.
1332 97. Behnia R, Barr FA, Flanagan JJ, Barlowe C, Munro S: **The yeast orthologue of GRASP65**
1333 **forms a complex with a coiled-coil protein that contributes to ER to Golgi traffic.** *J Cell*
1334 *Biol* 2007, **176:**255-261.
1335 98. Murthi A, Hopper AK: **Genome-wide screen for inner nuclear membrane protein**
1336 **targeting in Saccharomyces cerevisiae: roles for N-acetylation and an integral**
1337 **membrane protein.** *Genetics* 2005, **170:**1553-1560.
1338 99. Aksnes H, Osberg C, Arnesen T: **N-terminal acetylation by NatC is not a general**
1339 **determinant for substrate subcellular localization in Saccharomyces cerevisiae.** *PLoS*
1340 *One* 2013, **8:**e61012.
1341 100. Garinther WI, Schultz MC: **Topoisomerase function during replication-independent**
1342 **chromatin assembly in yeast.** *Mol Cell Biol* 1997, **17:**3520-3526.
1343 101. Champoux JJ: **DNA topoisomerases: structure, function, and mechanism.** *Annu Rev*
1344 *Biochem* 2001, **70:**369-413.

1345 102. Goto T, Wang JC: **Cloning of yeast TOP1, the gene encoding DNA topoisomerase I, and**
1346 **construction of mutants defective in both DNA topoisomerase I and DNA**
1347 **topoisomerase II.** *Proc Natl Acad Sci U S A* 1985, **82:**7178-7182.
1348 103. Thrash C, Bankier AT, Barrell BG, Sternglanz R: **Cloning, characterization, and sequence**
1349 **of the yeast DNA topoisomerase I gene.** *Proc Natl Acad Sci U S A* 1985, **82:**4374-4378.
1350 104. Wang JC: **DNA topoisomerases.** *Annu Rev Biochem* 1996, **65:**635-692.
1351 105. Kaliraman V, Mullen JR, Fricke WM, Bastin-Shanower SA, Brill SJ: **Functional overlap**
1352 **between Sgs1-Top3 and the Mms4-Mus81 endonuclease.** *Genes Dev* 2001, **15:**2730-
1353 2740.
1354 106. Cejka P, Plank JL, Dombrowski CC, Kowalczykowski SC: **Decatenation of DNA by the S.**
1355 **cerevisiae Sgs1-Top3-Rmi1 and RPA complex: a mechanism for disentangling**
1356 **chromosomes.** *Mol Cell* 2012, **47:**886-896.
1357 107. Rottensteiner H, Kal AJ, Hamilton B, Ruis H, Tabak HF: **A heterodimer of the Zn2Cys6**
1358 **transcription factors Pip2p and Oaf1p controls induction of genes encoding**
1359 **peroxisomal proteins in Saccharomyces cerevisiae.** *Eur J Biochem* 1997, **247:**776-783.
1360 108. Karpichev IV, Luo Y, Marians RC, Small GM: **A complex containing two transcription**
1361 **factors regulates peroxisome proliferation and the coordinate induction of beta-**
1362 **oxidation enzymes in Saccharomyces cerevisiae.** *Mol Cell Biol* 1997, **17:**69-80.
1363 109. Sayed-Ahmed MM, Salman TM, Gaballah HE, Abou El-Naga SA, Nicolai R, Calvani M:
1364 **Propionyl-L-carnitine as protector against adriamycin-induced cardiomyopathy.**
1365 *Pharmacol Res* 2001, **43:**513-520.
1366 110. Gunisova S, Hronova V, Mohammad MP, Hinnebusch AG, Valasek LS: **Please do not**
1367 **recycle! Translation reinitiation in microbes and higher eukaryotes.** *FEMS Microbiol*
1368 *Rev* 2018, **42:**165-192.
1369 111. Cvijovic M, Dalevi D, Bilsland E, Kemp GJ, Sunnerhagen P: **Identification of putative**
1370 **regulatory upstream ORFs in the yeast genome using heuristics and evolutionary**
1371 **conservation.** *BMC Bioinformatics* 2007, **8:**295.
1372 112. Murray-Stewart TR, Woster PM, Casero RA, Jr.: **Targeting polyamine metabolism for**
1373 **cancer therapy and prevention.** *Biochem J* 2016, **473:**2937-2953.
1374 113. Casero RA, Jr., Celano P, Ervin SJ, Porter CW, Bergeron RJ, Libby PR: **Differential**
1375 **induction of spermidine/spermine N1-acetyltransferase in human lung cancer cells by**
1376 **the bis(ethyl)polyamine analogues.** *Cancer Res* 1989, **49:**3829-3833.
1377 114. Ulrich S, Huwiler A, Loitsch S, Schmidt H, Stein JM: **De novo ceramide biosynthesis is**
1378 **associated with resveratrol-induced inhibition of ornithine decarboxylase activity.**
1379 *Biochem Pharmacol* 2007, **74:**281-289.
1380 115. Srinivasan M, Mehta P, Yu Y, Prugar E, Koonin EV, Karzai AW, Sternglanz R: **The highly**
1381 **conserved KEOPS/EKC complex is essential for a universal tRNA modification, t6A.**
1382 *EMBO J* 2011, **30:**873-881.
1383 116. Murphy FVt, Ramakrishnan V, Malkiewicz A, Agris PF: **The role of modifications in**
1384 **codon discrimination by tRNA(Lys)UUU.** *Nat Struct Mol Biol* 2004, **11:**1186-1191.
1385 117. Downey M, Houlsworth R, Maringele L, Rollie A, Brehme M, Galicia S, Guillard S,
1386 Partington M, Zubko MK, Krogan NJ, et al: **A genome-wide screen identifies the**
1387 **evolutionarily conserved KEOPS complex as a telomere regulator.** *Cell* 2006, **124:**1155-
1388 1168.

1389 118. Kisseleva-Romanova E, Lopreiato R, Baudin-Baillieu A, Rousselle JC, Ilan L, Hofmann K,
1390 Namane A, Mann C, Libri D: **Yeast homolog of a cancer-testis antigen defines a new**
1391 **transcription complex.** *EMBO J* 2006, **25:**3576-3585.
1392 119. Gaudet P, Livstone MS, Lewis SE, Thomas PD: **Phylogenetic-based propagation of**
1393 **functional annotations within the Gene Ontology consortium.** *Brief Bioinform* 2011,
1394 **12:**449-462.
1395 120. Cao J, Hou P, Chen J, Wang P, Wang W, Liu W, Liu C, He X: **The overexpression and**
1396 **prognostic role of DCAF13 in hepatocellular carcinoma.** *Tumour Biol* 2017,
1397 **39:**1010428317705753.
1398 121. Doma MK, Parker R: **Endonucleolytic cleavage of eukaryotic mRNAs with stalls in**
1399 **translation elongation.** *Nature* 2006, **440:**561-564.
1400 122. Tsuboi T, Kuroha K, Kudo K, Makino S, Inoue E, Kashima I, Inada T: **Dom34:hbs1 plays a**
1401 **general role in quality-control systems by dissociation of a stalled ribosome at the 3'**
1402 **end of aberrant mRNA.** *Mol Cell* 2012, **46:**518-529.
1403 123. Shoemaker CJ, Eyler DE, Green R: **Dom34:Hbs1 promotes subunit dissociation and**
1404 **peptidyl-tRNA drop-off to initiate no-go decay.** *Science* 2010, **330:**369-372.
1405 124. Luo J, Emanuele MJ, Li D, Creighton CJ, Schlabach MR, Westbrook TF, Wong KK, Elledge
1406 SJ: **A genome-wide RNAi screen identifies multiple synthetic lethal interactions with**
1407 **the Ras oncogene.** *Cell* 2009, **137:**835-848.
1408 125. Cohen M, Stutz F, Belgareh N, Haguenauer-Tsapis R, Dargemont C: **Ubp3 requires a**
1409 **cofactor, Bre5, to specifically de-ubiquitinate the COPII protein, Sec23.** *Nat Cell Biol*
1410 2003, **5:**661-667.
1411 126. Cohen M, Stutz F, Dargemont C: **Deubiquitination, a new player in Golgi to**
1412 **endoplasmic reticulum retrograde transport.** *J Biol Chem* 2003, **278:**51989-51992.
1413 127. Dean N, Zhang YB, Poster JB: **The VRG4 gene is required for GDP-mannose transport**
1414 **into the lumen of the Golgi in the yeast, Saccharomyces cerevisiae.** *J Biol Chem* 1997,
1415 **272:**31908-31914.
1416 128. Ballou L, Hitzeman RA, Lewis MS, Ballou CE: **Vanadate-resistant yeast mutants are**
1417 **defective in protein glycosylation.** *Proc Natl Acad Sci U S A* 1991, **88:**3209-3212.
1418 129. Hu CM, Chang ZF: **Synthetic lethality by lentiviral short hairpin RNA silencing of**
1419 **thymidylate kinase and doxorubicin in colon cancer cells regardless of the p53 status.**
1420 *Cancer Res* 2008, **68:**2831-2840.
1421 130. Safran M, Dalah I, Alexander J, Rosen N, Iny Stein T, Shmoish M, Nativ N, Bahir I, Doniger
1422 T, Krug H, et al: **GeneCards Version 3: the human gene integrator.** *Database (Oxford)*
1423 2010, **2010:**baq020.
1424 131. Vizeacoumar FJ, Arnold R, Vizeacoumar FS, Chandrashekhar M, Buzina A, Young JT,
1425 Kwan JH, Sayad A, Mero P, Lawo S, et al: **A negative genetic interaction map in isogenic**
1426 **cancer cell lines reveals cancer cell vulnerabilities.** *Mol Syst Biol* 2013, **9:**696.
1427 132. Krastev DB, Slabicki M, Paszkowski-Rogacz M, Hubner NC, Junqueira M, Shevchenko A,
1428 Mann M, Neugebauer KM, Buchholz F: **A systematic RNAi synthetic interaction screen**
1429 **reveals a link between p53 and snoRNP assembly.** *Nat Cell Biol* 2011, **13:**809-818.
1430 133. Mouaikel J, Verheggen C, Bertrand E, Tazi J, Bordonne R: **Hypermethylation of the cap**
1431 **structure of both yeast snRNAs and snoRNAs requires a conserved methyltransferase**
1432 **that is localized to the nucleolus.** *Mol Cell* 2002, **9:**891-901.
1433 134. Boon KL, Kos M: **Deletion of Swm2p selectively impairs trimethylation of snRNAs by**
1434 **trimethylguanosine synthase (Tgs1p).** *FEBS Lett* 2010, **584:**3299-3304.

1435 135. Colau G, Thiry M, Leduc V, Bordonne R, Lafontaine DL: **The small nucle(ol)ar RNA cap**
1436 **trimethyltransferase is required for ribosome synthesis and intact nucleolar**
1437 **morphology.** *Mol Cell Biol* 2004, **24:**7976-7986.
1438 136. D'Ambrosio C, Schmidt CK, Katou Y, Kelly G, Itoh T, Shirahige K, Uhlmann F:
1439 **Identification of cis-acting sites for condensin loading onto budding yeast**
1440 **chromosomes.** *Genes Dev* 2008, **22:**2215-2227.
1441 137. Haeusler RA, Pratt-Hyatt M, Good PD, Gipson TA, Engelke DR: **Clustering of yeast tRNA**
1442 **genes is mediated by specific association of condensin with tRNA gene transcription**
1443 **complexes.** *Genes Dev* 2008, **22:**2204-2214.
1444 138. Wang HZ, Yang SH, Li GY, Cao X: **Subunits of human condensins are potential**
1445 **therapeutic targets for cancers.** *Cell Div* 2018, **13:**2.
1446 139. Kohler A, Schneider M, Cabal GG, Nehrbass U, Hurt E: **Yeast Ataxin-7 links histone**
1447 **deubiquitination with gene gating and mRNA export.** *Nat Cell Biol* 2008, **10:**707-715.
1448 140. Hurov KE, Cotta-Ramusino C, Elledge SJ: **A genetic screen identifies the Triple T complex**
1449 **required for DNA damage signaling and ATM and ATR stability.** *Genes Dev* 2010,
1450 **24:**1939-1950.
1451 141. Tay Z, Eng RJ, Sajiki K, Lim KK, Tang MY, Yanagida M, Chen ES: **Cellular robustness**
1452 **conferred by genetic crosstalk underlies resistance against chemotherapeutic drug**
1453 **doxorubicin in fission yeast.** *PLoS One* 2013, **8:**e55041.
1454 142. Nguyen TT, Lim JS, Tang RM, Zhang L, Chen ES: **Fitness profiling links topoisomerase II**
1455 **regulation of centromeric integrity to doxorubicin resistance in fission yeast.** *Sci Rep*
1456 2015, **5:**8400.
1457 143. Ding J, Yu C, Sui Y, Wang L, Yang Y, Wang F, Yao H, Xing F, Liu H, Li Y, et al: **The**
1458 **chromatin remodeling protein INO80 contributes to the removal of H2A.Z at the p53-**
1459 **binding site of the p21 gene in response to doxorubicin.** *FEBS J* 2018.
1460 144. Galanos P, Pappas G, Polyzos A, Kotsinas A, Svolaki I, Giakoumakis NN, Glytsou C,
1461 Pateras IS, Swain U, Souliotis VL, et al: **Mutational signatures reveal the role of RAD52**
1462 **in p53-independent p21-driven genomic instability.** *Genome Biol* 2018, **19:**37.
1463 145. Konstantinopoulos PA, Ceccaldi R, Shapiro GI, D'Andrea AD: **Homologous**
1464 **Recombination Deficiency: Exploiting the Fundamental Vulnerability of Ovarian**
1465 **Cancer.** *Cancer Discov* 2015, **5:**1137-1154.
1466 146. Mimura S, Yamaguchi T, Ishii S, Noro E, Katsura T, Obuse C, Kamura T: **Cul8/Rtt101**
1467 **forms a variety of protein complexes that regulate DNA damage response and**
1468 **transcriptional silencing.** *J Biol Chem* 2010, **285:**9858-9867.
1469 147. Zhang J, Shi D, Li X, Ding L, Tang J, Liu C, Shirahige K, Cao Q, Lou H: **Rtt101-Mms1-**
1470 **Mms22 coordinates replication-coupled sister chromatid cohesion and nucleosome**
1471 **assembly.** *EMBO Rep* 2017, **18:**1294-1305.
1472 148. Roberg KJ, Bickel S, Rowley N, Kaiser CA: **Control of amino acid permease sorting in the**
1473 **late secretory pathway of Saccharomyces cerevisiae by SEC13, LST4, LST7 and LST8.**
1474 *Genetics* 1997, **147:**1569-1584.
1475 149. Symeonidou IE, Taraviras S, Lygerou Z: **Control over DNA replication in time and space.**
1476 *FEBS Lett* 2012, **586:**2803-2812.
1477 150. Tran NQ, Pham XH, Tuteja R, Tuteja N: **Inhibition of unwinding and ATPase activities of**
1478 **pea MCM6 DNA helicase by actinomycin and nogalamycin.** *Plant Signal Behav* 2011,
1479 **6:**327-329.

1480 151. Frohlich F, Petit C, Kory N, Christiano R, Hannibal-Bach HK, Graham M, Liu X, Ejsing CS,
1481 Farese RV, Walther TC: **The GARP complex is required for cellular sphingolipid**
1482 **homeostasis.** *Elife* 2015, **4**.
1483 152. Oh CS, Toke DA, Mandala S, Martin CE: **ELO2 and ELO3, homologues of the**
1484 **Saccharomyces cerevisiae ELO1 gene, function in fatty acid elongation and are**
1485 **required for sphingolipid formation.** *J Biol Chem* 1997, **272:**17376-17384.
1486 153. Hwang S, Gustafsson HT, O'Sullivan C, Bisceglia G, Huang X, Klose C, Schevchenko A,
1487 Dickson RC, Cavaliere P, Dephoure N, Torres EM: **Serine-Dependent Sphingolipid**
1488 **Synthesis Is a Metabolic Liability of Aneuploid Cells.** *Cell Rep* 2017, **21:**3807-3818.
1489 154. Ponnusamy S, Meyers-Needham M, Senkal CE, Saddoughi SA, Sentelle D, Selvam SP,
1490 Salas A, Ogretmen B: **Sphingolipids and cancer: ceramide and sphingosine-1-phosphate**
1491 **in the regulation of cell death and drug resistance.** *Future Oncol* 2010, **6:**1603-1624.
1492 155. Swinnen E, Wilms T, Idkowiak-Baldys J, Smets B, De Snijder P, Accardo S, Ghillebert R,
1493 Thevissen K, Cammue B, De Vos D, et al: **The protein kinase Sch9 is a key regulator of**
1494 **sphingolipid metabolism in Saccharomyces cerevisiae.** *Mol Biol Cell* 2014, **25:**196-211.
1495 156. Kim BM, Choi YJ, Lee YH, Joe YA, Hong SH: **N,N-Dimethyl phytosphingosine sensitizes**
1496 **HL-60/MX2, a multidrug-resistant variant of HL-60 cells, to doxorubicin-induced**
1497 **cytotoxicity through ROS-mediated release of cytochrome c and AIF.** *Apoptosis* 2010,
1498 **15:**982-993.
1499 157. Liu YY, Yu JY, Yin D, Patwardhan GA, Gupta V, Hirabayashi Y, Holleran WM, Giuliano AE,
1500 Jazwinski SM, Gouaze-Andersson V, et al: **A role for ceramide in driving cancer cell**
1501 **resistance to doxorubicin.** *FASEB J* 2008, **22:**2541-2551.
1502 158. Martinez R, Navarro R, Lacort M, Ruiz-Sanz JI, Ruiz-Larrea MB: **Doxorubicin induces**
1503 **ceramide and diacylglycerol accumulation in rat hepatocytes through independent**
1504 **routes.** *Toxicol Lett* 2009, **190:**86-90.
1505 159. Ibarra A, Hetzer MW: **Nuclear pore proteins and the control of genome functions.**
1506 *Genes Dev* 2015, **29:**337-349.
1507 160. Wei L, Surma M, Gough G, Shi S, Lambert-Cheatham N, Chang J, Shi J: **Dissecting the**
1508 **Mechanisms of Doxorubicin and Oxidative Stress-Induced Cytotoxicity: The**
1509 **Involvement of Actin Cytoskeleton and ROCK1.** *PLoS One* 2015, **10:**e0131763.
1510 161. Shi J, Wu X, Surma M, Vemula S, Zhang L, Yang Y, Kapur R, Wei L: **Distinct roles for**
1511 **ROCK1 and ROCK2 in the regulation of cell detachment.** *Cell Death Dis* 2013, **4:**e483.
1512 162. Colombo R, Necco A, Vailati G, Saracco B, Milzani A, Scari G: **Doxorubicin affects actin**
1513 **assembly in vitro.** *Cell Biol Int Rep* 1984, **8:**127-135.
1514 163. Colombo R, Necco A, Vailati G, Milzani A: **Dose-dependence of doxorubicin effect on**
1515 **actin assembly in vitro.** *Exp Mol Pathol* 1988, **49:**297-304.
1516 164. Colombo R, Dalle Donne I, Milzani A: **Metal ions modulate the effect of doxorubicin on**
1517 **actin assembly.** *Cancer Biochem Biophys* 1990, **11:**217-226.
1518 165. Chen XJ, Clark-Walker GD: **The petite mutation in yeasts: 50 years on.** *Int Rev Cytol*
1519 2000, **194:**197-238.
1520 166. Courtney KD, Bezwada D, Mashimo T, Pichumani K, Vemireddy V, Funk AM, Wimberly J,
1521 McNeil SS, Kapur P, Lotan Y, et al: **Isotope Tracing of Human Clear Cell Renal Cell**
1522 **Carcinomas Demonstrates Suppressed Glucose Oxidation In Vivo.** *Cell Metab* 2018,
1523 **28:**793-800 e792.
1524 167. Sanderson SM, Locasale JW: **Revisiting the Warburg Effect: Some Tumors Hold Their**
1525 **Breath.** *Cell Metab* 2018, **28:**669-670.

1526 168. Birrell GW, Brown JA, Wu HI, Giaever G, Chu AM, Davis RW, Brown JM: **Transcriptional**
1527 **response of Saccharomyces cerevisiae to DNA-damaging agents does not identify the**
1528 **genes that protect against these agents.** *Proc Natl Acad Sci U S A* 2002, **99:**8778-8783.
1529 169. O'Neil NJ, Bailey ML, Hieter P: **Synthetic lethality and cancer.** *Nat Rev Genet* 2017,
1530 **18:**613-623.
1531 170. McGary KL, Park TJ, Woods JO, Cha HJ, Wallingford JB, Marcotte EM: **Systematic**
1532 **discovery of nonobvious human disease models through orthologous phenotypes.**
1533 *Proc Natl Acad Sci U S A* 2010, **107:**6544-6549.
1534 171. Garnett MJ, Edelman EJ, Heidorn SJ, Greenman CD, Dastur A, Lau KW, Greninger P,
1535 Thompson IR, Luo X, Soares J, et al: **Systematic identification of genomic markers of**
1536 **drug sensitivity in cancer cells.** *Nature* 2012, **483:**570-575.
1537 172. Yang W, Soares J, Greninger P, Edelman EJ, Lightfoot H, Forbes S, Bindal N, Beare D,
1538 Smith JA, Thompson IR, et al: **Genomics of Drug Sensitivity in Cancer (GDSC): a resource**
1539 **for therapeutic biomarker discovery in cancer cells.** *Nucleic Acids Res* 2013, **41:**D955-
1540 961.
1541 173. Klijn C, Durinck S, Stawiski EW, Haverty PM, Jiang Z, Liu H, Degenhardt J, Mayba O, Gnad
1542 F, Liu J, et al: **A comprehensive transcriptional portrait of human cancer cell lines.** *Nat*
1543 *Biotechnol* 2015, **33:**306-312.
1544 174. Haverty PM, Lin E, Tan J, Yu Y, Lam B, Lianoglou S, Neve RM, Martin S, Settleman J,
1545 Yauch RL, Bourgon R: **Reproducible pharmacogenomic profiling of cancer cell line**
1546 **panels.** *Nature* 2016, **533:**333-337.
1547 175. Revill K, Wang T, Lachenmayer A, Kojima K, Harrington A, Li J, Hoshida Y, Llovet JM,
1548 Powers S: **Genome-wide methylation analysis and epigenetic unmasking identify**
1549 **tumor suppressor genes in hepatocellular carcinoma.** *Gastroenterology* 2013,
1550 **145:**1424-1435 e1421-1425.
1551 176. Saito S, Matsui H, Kawano M, Kumagai K, Tomishige N, Hanada K, Echigo S, Tamura S,
1552 Kobayashi T: **Protein phosphatase 2Cepsilon is an endoplasmic reticulum integral**
1553 **membrane protein that dephosphorylates the ceramide transport protein CERT to**
1554 **enhance its association with organelle membranes.** *J Biol Chem* 2008, **283:**6584-6593.
1555 177. Thean LF, Loi C, Ho KS, Koh PK, Eu KW, Cheah PY: **Genome-wide scan identifies a copy**
1556 **number variable region at 3q26 that regulates PPM1L in APC mutation-negative**
1557 **familial colorectal cancer patients.** *Genes Chromosomes Cancer* 2010, **49:**99-106.
1558 178. Leithner K, Wohlkoenig C, Stacher E, Lindenmann J, Hofmann NA, Galle B, Guelly C,
1559 Quehenberger F, Stiegler P, Smolle-Juttner FM, et al: **Hypoxia increases membrane**
1560 **metallo-endopeptidase expression in a novel lung cancer ex vivo model - role of tumor**
1561 **stroma cells.** *BMC Cancer* 2014, **14:**40.
1562 179. Park JY, Kim SA, Chung JW, Bang S, Park SW, Paik YK, Song SY: **Proteomic analysis of**
1563 **pancreatic juice for the identification of biomarkers of pancreatic cancer.** *J Cancer Res*
1564 *Clin Oncol* 2011, **137:**1229-1238.
1565 180. Corso J, Pan KT, Walter R, Doebele C, Mohr S, Bohnenberger H, Strobel P, Lenz C,
1566 Slabicki M, Hullein J, et al: **Elucidation of tonic and activated B-cell receptor signaling in**
1567 **Burkitt's lymphoma provides insights into regulation of cell survival.** *Proc Natl Acad Sci*
1568 *U S A* 2016, **113:**5688-5693.
1569 181. Wu F, Su SC, Tan GQ, Yan L, Li TY, Zhang HL, Yu JS, Wang BL: **Mus81 knockdown**
1570 **sensitizes colon cancer cells to chemotherapeutic drugs by activating CHK1 pathway.**
1571 *Clin Res Hepatol Gastroenterol* 2017, **41:**592-601.

1572 182. Kim HJ, Jo MJ, Kim BR, Kim JL, Jeong YA, Na YJ, Park SH, Lee SY, Lee DH, Lee HS, et al:
1573 **Reactive oxygen species modulator-1 (Romo1) predicts unfavorable prognosis in**
1574 **colorectal cancer patients.** *PLoS One* 2017, **12:**e0176834.
1575 183. Kim HJ, Jo MJ, Kim BR, Kim JL, Jeong YA, Na YJ, Park SH, Lee SY, Lee DH, Kim BH, et al:
1576 **Overexpression of Romo1 is an unfavorable prognostic biomarker and a predictor of**
1577 **lymphatic metastasis in non-small cell lung cancer patients.** *Onco Targets Ther* 2018,
1578 **11:**4233-4246.
1579 184. Starheim KK, Gromyko D, Evjenth R, Ryningen A, Varhaug JE, Lillehaug JR, Arnesen T:
1580 **Knockdown of human N alpha-terminal acetyltransferase complex C leads to p53-**
1581 **dependent apoptosis and aberrant human Arl8b localization.** *Mol Cell Biol* 2009,
1582 **29:**3569-3581.
1583 185. Liao X, Huang R, Liu X, Han C, Yu L, Wang S, Sun N, Li B, Ning X, Peng T: **Distinct**
1584 **prognostic values of alcohol dehydrogenase mRNA expression in pancreatic**
1585 **adenocarcinoma.** *Onco Targets Ther* 2017, **10:**3719-3732.
1586 186. Wang P, Zhang L, Huang C, Huang P, Zhang J: **Distinct Prognostic Values of Alcohol**
1587 **Dehydrogenase Family Members for Non-Small Cell Lung Cancer.** *Med Sci Monit* 2018,
1588 **24:**3578-3590.
1589 187. Zhao L, Fan J, Xia S, Pan Y, Liu S, Qian G, Qian Z, Kang HB, Arbiser JL, Pollack BP, et al:
1590 **HMG-CoA synthase 1 is a synthetic lethal partner of BRAF(V600E) in human cancers.** *J*
1591 *Biol Chem* 2017, **292:**10142-10152.
1592 188. Chen SW, Chou CT, Chang CC, Li YJ, Chen ST, Lin IC, Kok SH, Cheng SJ, Lee JJ, Wu TS, et al:
1593 **HMGCS2 enhances invasion and metastasis via direct interaction with PPARalpha to**
1594 **activate Src signaling in colorectal cancer and oral cancer.** *Oncotarget* 2017, **8:**22460-
1595 22476.
1596 189. Castro-Giner F, Ratcliffe P, Tomlinson I: **The mini-driver model of polygenic cancer**
1597 **evolution.** *Nat Rev Cancer* 2015, **15:**680-685.
1598 190. Rauhala HE, Teppo S, Niemela S, Kallioniemi A: **Silencing of the ARP2/3 complex**
1599 **disturbs pancreatic cancer cell migration.** *Anticancer Res* 2013, **33:**45-52.
1600 191. Oji Y, Tatsumi N, Fukuda M, Nakatsuka S, Aoyagi S, Hirata E, Nanchi I, Fujiki F, Nakajima
1601 H, Yamamoto Y, et al: **The translation elongation factor eEF2 is a novel**
1602 **tumorassociated antigen overexpressed in various types of cancers.** *Int J Oncol* 2014,
1603 **44:**1461-1469.
1604 192. Patel H, Abduljabbar R, Lai CF, Periyasamy M, Harrod A, Gemma C, Steel JH, Patel N,
1605 Busonero C, Jerjees D, et al: **Expression of CDK7, Cyclin H, and MAT1 Is Elevated in**
1606 **Breast Cancer and Is Prognostic in Estrogen Receptor-Positive Breast Cancer.** *Clin*
1607 *Cancer Res* 2016, **22:**5929-5938.
1608 193. Li B, Ni Chonghaile T, Fan Y, Madden SF, Klinger R, O'Connor AE, Walsh L, O'Hurley G,
1609 Mallya Udupi G, Joseph J, et al: **Therapeutic Rationale to Target Highly Expressed CDK7**
1610 **Conferring Poor Outcomes in Triple-Negative Breast Cancer.** *Cancer Res* 2017, **77:**3834-
1611 3845.
1612 194. Wang Q, Li M, Zhang X, Huang H, Huang J, Ke J, Ding H, Xiao J, Shan X, Liu Q, et al:
1613 **Upregulation of CDK7 in gastric cancer cell promotes tumor cell proliferation and**
1614 **predicts poor prognosis.** *Exp Mol Pathol* 2016, **100:**514-521.
1615 195. Wei F, Ding L, Wei Z, Zhang Y, Li Y, Qinghua L, Ma Y, Guo L, Lv G, Liu Y: **Ribosomal**
1616 **protein L34 promotes the proliferation, invasion and metastasis of pancreatic cancer**
1617 **cells.** *Oncotarget* 2016, **7:**85259-85272.

1618 196. Yang S, Cui J, Yang Y, Liu Z, Yan H, Tang C, Wang H, Qin H, Li X, Li J, et al: **Over-expressed**
1619 **RPL34 promotes malignant proliferation of non-small cell lung cancer cells.** *Gene* 2016,
1620 **576**:421-428.
1621 197. Dai J, Wei W: **Influence of the RPL34 gene on the growth and metastasis of oral**
1622 **squamous cell carcinoma cells.** *Arch Oral Biol* 2017, **83**:40-46.
1623 198. Karan D, Kelly DL, Rizzino A, Lin MF, Batra SK: **Expression profile of differentially-**
1624 **regulated genes during progression of androgen-independent growth in human**
1625 **prostate cancer cells.** *Carcinogenesis* 2002, **23**:967-975.
1626 199. Knoll M, Macher-Goeppinger S, Kopitz J, Duensing S, Pahernik S, Hohenfellner M,
1627 Schirmacher P, Roth W: **The ribosomal protein S6 in renal cell carcinoma: functional**
1628 **relevance and potential as biomarker.** *Oncotarget* 2016, **7**:418-432.
1629 200. Chen B, Tan Z, Gao J, Wu W, Liu L, Jin W, Cao Y, Zhao S, Zhang W, Qiu Z, et al:
1630 **Hyperphosphorylation of ribosomal protein S6 predicts unfavorable clinical survival in**
1631 **non-small cell lung cancer.** *J Exp Clin Cancer Res* 2015, **34**:126.
1632 201. Hou L, Li Y, Wang Y, Xu D, Cui H, Xu X, Cong Y, Yu C: **UBE2D1 RNA Expression Was an**
1633 **Independent Unfavorable Prognostic Indicator in Lung Adenocarcinoma, but Not in**
1634 **Lung Squamous Cell Carcinoma.** *Dis Markers* 2018, **2018**:4108919.
1635 202. Zabala-Letona A, Arruabarrena-Aristorena A, Martin-Martin N, Fernandez-Ruiz S,
1636 Sutherland JD, Clasquin M, Tomas-Cortazar J, Jimenez J, Torres I, Quang P, et al:
1637 **mTORC1-dependent AMD1 regulation sustains polyamine metabolism in prostate**
1638 **cancer.** *Nature* 2017, **547**:109-113.
1639 203. Zhao X, Li J, He Y, Lan F, Fu L, Guo J, Zhao R, Ye Y, He M, Chong W, et al: **A novel growth**
1640 **suppressor gene on chromosome 17p13.3 with a high frequency of mutation in human**
1641 **hepatocellular carcinoma.** *Cancer Res* 2001, **61**:7383-7387.
1642 204. Xu HN, Huang WD, Cai Y, Ding M, Gu JF, Wei N, Sun LY, Cao X, Li HG, Zhang KJ, et al:
1643 **HCCS1-armed, quadruple-regulated oncolytic adenovirus specific for liver cancer as a**
1644 **cancer targeting gene-viro-therapy strategy.** *Mol Cancer* 2011, **10**:133.
1645 205. Gan Y, Gu J, Cai X, Hu J, Liu XY, Zhao X: **Adenovirus-mediated HCCS1 overexpression**
1646 **elicits a potent antitumor efficacy on human colorectal cancer and hepatoma cells**
1647 **both in vitro and in vivo.** *Cancer Gene Ther* 2008, **15**:808-816.
1648 206. Su YC, Feng YH, Wu HT, Huang YS, Tung CL, Wu P, Chang CJ, Shiau AL, Wu CL: **Elovl6 is a**
1649 **negative clinical predictor for liver cancer and knockdown of Elovl6 reduces murine**
1650 **liver cancer progression.** *Sci Rep* 2018, **8**:6586.
1651 207. Tzatsos A, Paskaleva P, Ferrari F, Deshpande V, Stoykova S, Contino G, Wong KK, Lan F,
1652 Trojer P, Park PJ, Bardeesy N: **KDM2B promotes pancreatic cancer via Polycomb-**
1653 **dependent and -independent transcriptional programs.** *J Clin Invest* 2013, **123**:727-739.
1654 208. Wang Y, Zang J, Zhang D, Sun Z, Qiu B, Wang X: **KDM2B overexpression correlates with**
1655 **poor prognosis and regulates glioma cell growth.** *Onco Targets Ther* 2018, **11**:201-209.
1656 209. Zheng Q, Fan H, Meng Z, Yuan L, Liu C, Peng Y, Zhao W, Wang L, Li J, Feng J: **Histone**
1657 **demethylase KDM2B promotes triple negative breast cancer proliferation by**
1658 **suppressing p15INK4B, p16INK4A, and p57KIP2 transcription.** *Acta Biochim Biophys Sin*
1659 *(Shanghai)* 2018, **50**:897-904.
1660 210. Zhu XX, Yan YW, Ai CZ, Jiang S, Xu SS, Niu M, Wang XZ, Zhong GS, Lu XF, Xue Y, et al:
1661 **Jarid2 is essential for the maintenance of tumor initiating cells in bladder cancer.**
1662 *Oncotarget* 2017, **8**:24483-24490.

1663 211. Schleich S, Strassburger K, Janiesch PC, Koledachkina T, Miller KK, Haneke K, Cheng YS,
1664 Kuechler K, Stoecklin G, Duncan KE, Teleman AA: **DENR-MCT-1 promotes translation re-**
1665 **initiation downstream of uORFs to control tissue growth.** *Nature* 2014, **512:**208-212.
1666 212. Wang YW, Lin KT, Chen SC, Gu DL, Chen CF, Tu PH, Jou YS: **Overexpressed-eIF3I**
1667 **interacted and activated oncogenic Akt1 is a theranostic target in human**
1668 **hepatocellular carcinoma.** *Hepatology* 2013, **58:**239-250.
1669 213. Qi J, Dong Z, Liu J, Zhang JT: **EIF3i promotes colon oncogenesis by regulating COX-2**
1670 **protein synthesis and beta-catenin activation.** *Oncogene* 2014, **33:**4156-4163.
1671 214. Wang C, Jin G, Jin H, Wang N, Luo Q, Zhang Y, Gao D, Jiang K, Gu D, Shen Q, et al:
1672 **Clusterin facilitates metastasis by EIF3I/Akt/MMP13 signaling in hepatocellular**
1673 **carcinoma.** *Oncotarget* 2015, **6:**2903-2916.
1674 215. Torrance V, Lydall D: **Overlapping open reading frames strongly reduce human and**
1675 **yeast STN1 gene expression and affect telomere function.** *PLoS Genet* 2018,
1676 **14:**e1007523.
1677 216. Widschwendter M, Apostolidou S, Raum E, Rothenbacher D, Fiegl H, Menon U,
1678 Stegmaier C, Jacobs IJ, Brenner H: **Epigenotyping in peripheral blood cell DNA and**
1679 **breast cancer risk: a proof of principle study.** *PLoS One* 2008, **3:**e2656.
1680 217. Khakpour G, Pooladi A, Izadi P, Noruzinia M, Tavakkoly Bazzaz J: **DNA methylation as a**
1681 **promising landscape: A simple blood test for breast cancer prediction.** *Tumour Biol*
1682 2015, **36:**4905-4912.
1683 218. Savci-Heijink CD, Halfwerk H, Koster J, van de Vijver MJ: **A novel gene expression**
1684 **signature for bone metastasis in breast carcinomas.** *Breast Cancer Res Treat* 2016,
1685 **156:**249-259.
1686 219. Kornberg RD: **The molecular basis of eucaryotic transcription.** *Cell Death Differ* 2007,
1687 **14:**1989-1997.
1688 220. Hartwell LH: **Nobel Lecture. Yeast and cancer.** *Biosci Rep* 2002, **22:**373-394.
1689 221. Blackburn EH: **Telomeres and telomerase: the means to the end (Nobel lecture).**
1690 *Angew Chem Int Ed Engl* 2010, **49:**7405-7421.
1691 222. Schekman R, Sudhof T: **An interview with Randy Schekman and Thomas Sudhof.** *Trends*
1692 *Cell Biol* 2014, **24:**6-8.
1693 223. Mizushima N: **The exponential growth of autophagy-related research: from the**
1694 **humble yeast to the Nobel Prize.** *FEBS Lett* 2017, **591:**681-689.
1695 224. Bhattacharya B, Mohd Omar MF, Soong R: **The Warburg effect and drug resistance.** *Br J*
1696 *Pharmacol* 2016, **173:**970-979.
1697 225. Yang F, Kemp CJ, Henikoff S: **Anthracyclines induce double-strand DNA breaks at active**
1698 **gene promoters.** *Mutat Res* 2015, **773:**9-15.
1699 226. Flavahan WA, Gaskell E, Bernstein BE: **Epigenetic plasticity and the hallmarks of cancer.**
1700 *Science* 2017, **357**.
1701 227. de Cubas AA, Rathmell WK: **Epigenetic modifiers: activities in renal cell carcinoma.** *Nat*
1702 *Rev Urol* 2018, **15:**599-614.
1703 228. Lopez G, Liu J, Ren W, Wei W, Wang S, Lahat G, Zhu QS, Bornmann WG, McConkey DJ,
1704 Pollock RE, Lev DC: **Combining PCI-24781, a novel histone deacetylase inhibitor, with**
1705 **chemotherapy for the treatment of soft tissue sarcoma.** *Clin Cancer Res* 2009, **15:**3472-
1706 3483.

1707 229. Yang C, Choy E, Hornicek FJ, Wood KB, Schwab JH, Liu X, Mankin H, Duan Z: **Histone**
1708 **deacetylase inhibitor (HDACI) PCI-24781 potentiates cytotoxic effects of doxorubicin in**
1709 **bone sarcoma cells.** *Cancer Chemother Pharmacol* 2011, **67:**439-446.
1710 230. Choy E, Flamand Y, Balasubramanian S, Butrynski JE, Harmon DC, George S, Cote GM,
1711 Wagner AJ, Morgan JA, Sirisawad M, et al: **Phase 1 study of oral abexinostat, a histone**
1712 **deacetylase inhibitor, in combination with doxorubicin in patients with metastatic**
1713 **sarcoma.** *Cancer* 2015, **121:**1223-1230.
1714 231. Ververis K, Rodd AL, Tang MM, El-Osta A, Karagiannis TC: **Histone deacetylase inhibitors**
1715 **augment doxorubicin-induced DNA damage in cardiomyocytes.** *Cell Mol Life Sci* 2011,
1716 **68:**4101-4114.
1717 232. Li T, Zhang C, Hassan S, Liu X, Song F, Chen K, Zhang W, Yang J: **Histone deacetylase 6 in**
1718 **cancer.** *J Hematol Oncol* 2018, **11:**111.
1719 233. Tu Y, Hershman DL, Bhalla K, Fiskus W, Pellegrino CM, Andreopoulou E, Makower D,
1720 Kalinsky K, Fehn K, Fineberg S, et al: **A phase I-II study of the histone deacetylase**
1721 **inhibitor vorinostat plus sequential weekly paclitaxel and doxorubicin-**
1722 **cyclophosphamide in locally advanced breast cancer.** *Breast Cancer Res Treat* 2014,
1723 **146:**145-152.
1724 234. Vogl DT, Raje N, Jagannath S, Richardson P, Hari P, Orlowski R, Supko JG, Tamang D,
1725 Yang M, Jones SS, et al: **Ricolinostat, the First Selective Histone Deacetylase 6 Inhibitor,**
1726 **in Combination with Bortezomib and Dexamethasone for Relapsed or Refractory**
1727 **Multiple Myeloma.** *Clin Cancer Res* 2017, **23:**3307-3315.
1728 235. Xu C, Nikolova O, Basom RS, Mitchell RM, Shaw R, Moser RD, Park H, Gurley KE, Kao MC,
1729 Green CL, et al: **Functional Precision Medicine Identifies Novel Druggable Targets and**
1730 **Therapeutic Options in Head and Neck Cancer.** *Clin Cancer Res* 2018, **24:**2828-2843.
1731 236. Grandori C, Kemp CJ: **Personalized Cancer Models for Target Discovery and Precision**
1732 **Medicine.** *Trends Cancer* 2018, **4:**634-642.
1733 237. Puca L, Bareja R, Prandi D, Shaw R, Benelli M, Karthaus WR, Hess J, Sigouros M,
1734 Donoghue A, Kossai M, et al: **Patient derived organoids to model rare prostate cancer**
1735 **phenotypes.** *Nat Commun* 2018, **9:**2404.
1736 238. Kim MM, Parolia A, Dunphy MP, Venneti S: **Non-invasive metabolic imaging of brain**
1737 **tumours in the era of precision medicine.** *Nat Rev Clin Oncol* 2016, **13:**725-739.
1738 239. Costanzo M, VanderSluis B, Koch EN, Baryshnikova A, Pons C, Tan G, Wang W, Usaj M,
1739 Hanchard J, Lee SD, et al: **A global genetic interaction network maps a wiring diagram**
1740 **of cellular function.** *Science* 2016, **353**.
1741 240. Ihmels J, Collins SR, Schuldiner M, Krogan NJ, Weissman JS: **Backup without**
1742 **redundancy: genetic interactions reveal the cost of duplicate gene loss.** *Mol Syst Biol*
1743 2007, **3:**86.
1744 241. Phillips PC: **Epistasis--the essential role of gene interactions in the structure and**
1745 **evolution of genetic systems.** *Nat Rev Genet* 2008, **9:**855-867.

1746

1747

1748

Figures, Tables, and Additional Files

Figures:

Figure 1. Experimental strategy to characterize differential doxorubicin-gene interaction, with respect to the Warburg metabolic transition. (A) The phenomic model incorporates treatment of individually grown cultures of the YKO/KD collection with increasing doxorubicin (0, 2.5, 5, 7.5, and 15 ug/mL) in "fermentable/glycolytic" (HLD) or "non-fermentable/respiratory" (HLEG) media. **(B)** Representative cell array images, treated and untreated with 15 ug/mL doxorubicin. **(C)** Time series of individual culture images, exemplifying gene deletion suppression (*vps54-Δ0*) and gene deletion enhancement (*mms1-Δ0*), relative to parental control ('RF1') in HLEG media with indicated concentrations (0, 5, and 15 ug/mL) of doxorubicin. **(D)** After image analysis, data time series are fit to a logistic growth function, G(*t*), to obtain the cell proliferation parameters (CPPs), *K* (carrying capacity), *L* (time at which K/2 is reached) and *r* (maximum specific rate) for each culture. 'ΔL' (left panel) indicates K_i (see methods). **(E)** Interaction is quantified by linear regression of L_i (indicated 'Delta_L' and 'Delta_K' in right panels; see methods) across the entire dose range, which is converted to a z-score by dividing with the variance of the parental reference control (see methods). **(F)** Gene interaction profiles were grouped by recursive expectation-maximization clustering (REMc) to reveal deletion enhancing and deletion suppressing doxorubicin-gene interaction modules and the influence of the Warburg effect. Resulting clusters were analyzed with GOTermFinder (GTF) to identify enriched biological functions. **(G)** Gene Ontology Term Averaging (GTA) was used as a complement to REMc/GTF. **(H)** The model for genetic buffering of doxorubicin cytotoxicity incorporates primary and interaction effects involving glycolysis (green), and respiration (red), to explain the influence of Warburg context (blue) on doxorubicin-gene interaction (black).

Figure 2. Q-HTCP provides cell proliferation parameters as phenotypes to quantify gene interaction. (**A, B**) Average pixel intensity and standard deviation for 768 reference strain cultures at indicated times after exposure to escalating doxorubicin concentrations in **(A)** HLD or **(B)** HLEG media. (**C-D**) Semi-log plots after fitting the data plotted above for **(C)** HLD or **(D)** HLEG to a logistic function (see Fig. 1D). (**E-L**) CPP distributions from data depicted in panels A-D for (**E-H**) HLD and (**I-J**) HLEG, including (**E, I**) L, (**F, J**) K, (**G, K**) r, and (**H, L**) AUC. **(M, N)** Comparison of doxorubicin-gene interaction scores using the L *vs.* K CPP in the context of either **(M)** HLD or **(N)** HLEG media. Score distributions of knockout (YKO, green), knock down / DAmP (YKD, Red), and non-mutant parental (Ref, Purple) strain cultures are indicated along with thresholds for deletion enhancement and suppression (dashed lines at +/- 2). **(O)** Differential doxorubicin-gene interaction (using L as the CPP) for HLD vs. HLEG, classified with respect to Warburg metabolism as non-specific (NS), respiratory-specific (R), or glycolysis-specific (G) deletion enhancement (Enh) or deletion suppression (Sup). **(P-R)** Comparisons between genome-wide studies of doxorubicin-gene interaction: **(P)** Genes reported from Westmoreland *et al.* (green), Xia *et al.* (Red) or both studies (purple) are plotted overlying L interaction scores (gray) in HLD *vs.* HLEG. (**Q-R**) L interaction scores (gray) for genes reported by Westmoreland *et al.* (green), Xia *et al.* (red), or both studies (purple) in (**Q**) HLD or (**R**) HLEG media. (**S-T**) Doxorubicin-gene interaction from genome wide (GWS) and validation (V) studies on **(S)** HLD or **(T)** HLEG media.

Figure 3. Characterization of Warburg-differential, doxorubicin-gene interaction profiles. (A) The union of enhancers (L z-score > 2) or suppressors (L z-score < -2) from the HLD and HLEG analyses totaled 2802 gene interaction profiles that were subjected to REMc (see methods). **(B-C)** The column order is the same for all heatmaps;

'+' indicates doxorubicin-gene interaction and '-' indicates 'shift' (K_0; see methods). Interactions by K are negative (brown) if enhancing and positive (purple) if suppressing, while the signs of interaction are reversed for L (see methods). The heatmap color scale is incremented by twos; red indicates no growth curve in the absence of doxorubicin. **(B)** First round cluster 1-0-7 has a gene interaction profile indicative of HLEG-specific deletion enhancement. (**C**) Second round clusters (2-0.7-X) are ordered left to right by strength of influence. **(D)** The pattern of distributions for the different doxorubicin-gene interaction scores ('+' columns only from panel C) summarizes respective clusters from panel C. Deletion enhancement is considered to be qualitatively stronger if observed for K in addition to L.

Figure 4. A summary of the first and second rounds of REMc. First round clusters are at the left end of each row of heatmap thumbnails; second round clusters derived from each first round cluster are ordered to the right by relative strength. Rows are grouped into panels by similarity in their gene interaction profiles. The columns in each heatmap have the same order from left to right (see inset panel), with K to the left and L to the right. Within the K and L groups, HLD is to the left and HLEG to the right. Within each of the CPP-media groupings, 'shift' (-) is left of the doxorubicin-gene interaction (+). **(A)** Respiration-specific enhancement. **(B)** Warburg-independent enhancement. **(C)** Glycolysis-specific enhancement. **(D)** HLD and HLEG suppression modules. **(E)** Respiratory deficiency.

Figure 5. GO annotations associated with deletion enhancement or suppression of doxorubicin cytotoxicity, with respect to Warburg-dependence. Representative GO terms are listed, which were identified by REMc/GTF (orange), GTA (purple), or both methods, for HLD (left, red), HLEG (right, blue), or both media types (black), and for

enhancement (above dashed line) or suppression (below dashed line) of doxorubicin cytotoxicity. Distance above or below the horizontal dashed line indicates the GTA value for terms identified by REMc or the GTA score if identified by GTA (see methods). See Additional Files 5 and 6, respectively, for all REMc and GTA results.

Figure 6. Respiration increases the role for chromatin organization in buffering doxorubicin toxicity. **(A)** GO term-specific heatmaps for chromatin organization and its child terms (indicated by arrows) clarify related but distinct biological functions that buffer doxorubicin, with respect to Warburg status. **(B-C)** L-based doxorubicin-gene interaction scores associated with GO terms that were enriched in cluster 2-0.7-2. Dashed lines indicate z-score thresholds for enhancers (>2) and suppressors (<-2). Sub-threshold gene interaction values are plotted, but not labeled.

Figure 7. Distinct histone modifications differentially influence doxorubicin cytotoxicity. (A) Rpd3L and Rpd3S complexes exert strong HLEG-specific doxorubicin-enhancing influence relative to other Sin3-type histone deacetylases and the HDA1 complex. **(B)** In contrast to histone deacetylation (panel A), histone acetylation exhibits deletion enhancement that is Warburg-independent. **(C)** Histone H3K4 methylation by the Set1C/COMPASS complex, which requires histone mono-ubiquitination of H2B by the Bre1/Rad6 complex, is opposed by Jhd2, a histone H3K4 demethylase. The respiration-specific deletion enhancing interactions suggest the Warburg transition can protect tumors promoted by certain types of chromatin deregulation from doxorubicin.

Figure 8. Additional respiration-specific deletion-enhancing and -suppressing functions that influence doxorubicin cytotoxicity. Heatmaps depicting complete phenotypic profiles are inset, corresponding to plots of L-based doxorubicin-gene

interaction. (**A**) Protein folding in endoplasmic reticulum and the N-terminal protein-acetylating NatC complex are largely respiratory-dependent in their deletion-enhancing influence. **(B)** DNA topological change exerts deletion-enhancing interactions in both respiratory and glycolytic contexts. **(C)** GTA-identified terms tend to be smaller in number and display greater variability in the Warburg dependence among genes sharing the same functional annotation. **(D)** Functions implicated in respiratory-dependent deletion suppression of doxorubicin toxicity.

Figure 9. Glycolysis-specific enhancement and suppression of doxorubicin cytotoxicity. Doxorubicin-gene interaction profiles for HLD-specific GO terms identified by GTA are depicted for **(A)** deletion enhancement and **(B)** deletion suppression.

Figure 10. Warburg-independent deletion enhancement of doxorubicin cytotoxicity. Gene interaction profiles showing deletion enhancement in both respiratory and glycolytic context included: **(A)** *double-strand break repair via homologous recombination*, and its child terms (indicated by arrows), and **(B)** the *Cul8-RING ubiquitin ligase*, *Ino80 complex*, *Lst4-7 complex*, and *MCM complex*.

Figure 11. Warburg-independent deletion suppression of doxorubicin cytotoxicity. Doxorubicin-gene interaction profiles and L-interaction plots for genes associated with deletion suppression in HLEG or HLD media, including: (**A**) *Cellular sphingolipid homeostasis*, along with its parent term, *lipid homeostasis*, and related term *sphingolipid metabolism*; and **(B)** *actin cortical patch localization* and *telomere tethering at nuclear periphery*.

Figure 12. Use of the yeast phenomic model to predict doxorubicin-gene interaction in cancer cells. (A) *BiomaRt* was used to assign yeast-human gene

homology for the GDSC and gCSI datasets. (**B**) *PharmacoGx* was used to retrieve differential gene expression for doxorubicin sensitive cell lines from the gCSI and GDSC databases, searching data from individual tissues or across data aggregated from all tissues. Human genes that are underexpressed in doxorubicin sensitive cell lines (UES) with yeast homologs that are deletion enhancers are predicted to be causal in their phenotypic association. Similarly, human genes that are overexpressed in doxorubicin sensitive cancer cell lines (OES) would be predicted to be causal if the yeast homolog was a deletion suppressor in the phenomic dataset. (**C-D**) Boxes inside of Venn diagrams indicate the genes for which gene interaction profiles are shown in the heatmaps below. Gene names are to the right of heatmaps, with **blue** labels indicating genes identified in both the GDSC and gCSI databases and **black** labels indicating genes found only in the gCSI dataset. The category of homology (see panel A) is indicated in the left column of each heatmap. **(C)** Deletion enhancement by yeast genes predicts human functions that buffer doxorubicin cytotoxicity, and thus, reduced expression of homologs in cancer cell lines is predicted to increase doxorubicin sensitivity. (**D**) Deletion suppression by yeast genes predicts functions that mediate cytotoxicity and is shown for human homologs having significant association of overexpression in cancer cell lines with increased doxorubicin sensitivity. (**E-F**) Genes representing enhancing or suppressing modules from REMc or GTA that are **(E)** UES or **(F)** OES in at least one of the two databases. **Red** labels indicate genes found only in the GDSC database. **Additional File 13** reports all results from the analysis described above, including assessment of individual tissues.

Figure 13. Yeast phenomic model for the influence of Warburg metabolism on doxorubicin-gene interaction. Shaded areas indicate influences that are relatively

Warburg-dependent, being red or green if their effects are relatively specific to a respiratory or glycolytic context, respectively. Processes that influence doxorubicin cytotoxicity in a more Warburg-independent manner are unshaded. Arrowheads indicate processes for which genes predominantly transduce doxorubicin toxicity, based on their loss of function suppressing its growth inhibitory effects. Conversely, a perpendicular bar at the line head indicates a process that buffers doxorubicin toxicity, as genetic compromise of its function enhances the growth inhibitory effects of doxorubicin.

Additional Files:

Additional File 1. Supplemental figures. Figure S1. Doxorubicin dose responses of the YKO/KD parental strains, BY4741a, BY4742alpha, and BY4743a/alpha diploid. **Figure S2.** Correlation between interaction scores based on L *vs.* other CPPs (K, r, and AUC), for both HLD and HLEG media. **Figure S3.** Doxorubicin-gene interaction profiles for selected mitochondrial GO terms. **Figure S4.** Deletion of mitochondrial genes tends to influence doxorubicin-gene interaction in a respiratory (HLEG media) more so than a glycolytic (HLD media) context. **Figure S5.** Heatmaps for GO terms comprised of overlapping gene sets. **Figure S6.** Pleiotropic phenotypic influences from genetic perturbation of ribonucleoprotein complex subunit organization. **Figure S7.** HLD-specific deletion enhancement of doxorubicin toxicity by evolutionarily conserved genes. *See also Additional File 10 (Table S13).* **Figure S8.** GO term-specific heatmaps for *mRNA 3' end processing* and *mRNA cleavage* gene interaction profiles. **Figure S9.** Suppression of doxorubicin cytotoxicity by perturbation of sphingolipid and ceramide metabolism. **Figure S10.** Deletion suppressing doxorubicin-gene interaction for nuclear pore and actin cortical patch functions is relatively Warburg-independent.

Additional File 2. Doxorubicin-gene interaction data; Tables S1-S8. Tables S1-S4 are the genome-wide experiment: **Table S1.** YKO/KD strains in HLEG. **Table S2.** Reference cultures in HLEG. **Table S3.** YKO/KD strains in HLD. **Table S4.** Reference cultures in HLD. **Tables S5-S8** are the validation study: **Table S5.** YKO/KD strains in HLEG. **Table S6.** Reference cultures in HLEG. **Table S7.** YKO/KD strains in HLD. **Table S8.** Reference cultures in HLD.

Additional File 3. Interaction plots for HLEG. (A, B) Genome-wide and **(C, D)** validation analyses for **(A, C)** YKO/KD and **(B, D)** reference strains in HLEG. See also methods and Additional File 2.

Additional File 4. Interaction plots for HLD. (A, B) Genome-wide and **(C, D)** validation analyses. **(A, C)** YKO/KD and **(B, D)** reference strains in HLD media. See also methods and Additional File 2.

Additional File 5. REMc results with doxorubicin-gene interaction profile heatmaps and Gene Ontology enrichment (GO Term Finder; GTF) results. File A contains REMc results and associated gene interaction and shift data. **File B** is the heatmap representation of each REMc cluster after incorporating shift values and hierarchical clustering. **File C** contains the GTF results obtained for REMc clusters for the three ontologies – process, function, and component.

Additional File 6. Gene Ontology Term Averaging (GTA) results and interactive plots. File A contains all GTA values, cross-referenced with REMc-enriched terms. **File B** displays GTA values associated with above-threshold GTA scores (see note below) plotted for HLD *vs.* HLEG. GTA values for REMc-enriched terms are also included (regardless of whether |GTA score| >2). **File C** displays a subset of File B, containing

only GO Terms with above-threshold GTA scores and that were enriched by REMc/GTF. **File D** reports GTA value using the K parameter. **Files B-D** should be opened in an Internet web browser so that embedded information from **Additional File 6A** can be viewed by scrolling over points on the graphs. Subsets in each of the plots can be toggled off and on by clicking on the respective legend label. In the embedded information, X1 represents HLEG and X2 represents HLD information. Note: The GTA score threshold (for L) indicates that GTA-gtaSD > 2 for enhancers or GTA+gtaSD < -2 for suppressors, in at least one media.

Additional File 7. Systematic comparisons involving genome-wide studies of doxorubicin-gene interaction. Table S9. Genes with deletion-enhancing doxorubicin-gene interaction from *Xia et al. 2007* and *Westmoreland et al. 2009.* **Table S10.** Summary of experimental details associated with Table S9. **Table S11.** Test of enrichment for doxorubicin-gene interaction among genes encoding proteins predicted as substrates of the NatC complex. **Table S12.** Test of enrichment for doxorubicin-gene interaction among genes predicted to be regulated by conserved uORFs (*Cvijovic et al. 2007*).

Additional File 8. Quantitative summaries of REMc clusters. File A depicts REMc results, in terms of cluster distributions of L and K interaction ('shift' is not used for REMc and thus is not displayed), as a way to visualize cluster differences quantitatively. **File B** is organized by first round clusters and plots the change in p-value for significant terms with respect to round of clustering. Clusters derived from one another and sharing enrichment of the same GO term are connected by a line. Only GO terms with a background size of 500 or smaller are included. Scroll over a symbol to see embedded

detail about each GO term. The square root of the p-value is used on the y-axis to evenly distribute data.

Additional File 9. GO term-specific heatmaps for REMc/GTF-enriched clusters. GO term-specific heatmaps for significant GO process terms were generated as described in methods and Figures 3 and 4. Any related child terms are presented in subsequent pages of the parent file name. GO terms with more than 100 children, with 2 or fewer genes annotated to the term, or a file size over 300KB are not shown. All heatmaps are generated with the same layout (see Figures 3 and 4).

Additional File 10 (Table S13). HLD-specific gene deletion enhancement, not associated with 'shift' / growth deficiency. Data were selected for yeast-human homologs if the respective YKO/KD strains generated growth curves in both HLD and HLEG media (in the absence doxorubicin), and either of the following two sets of criteria were met: (1) HLD L interaction > 2 and HLEG L interaction < 2; these data were further filtered for *HLD L Interaction - HLD L Shift* > 4, and are presented in Fig. S7A.; or (2) *HLD L Interaction – HLEG L interaction* > 4 and HLEG K interaction > - 10; these data were further filtered for *HLD L Interaction - HLD L Shift* > 4, and are presented in Fig. S7B. Data included in Fig. S7 are indicated in the last column.

Additional File 11. Integration of yeast phenomic and cancer cell line pharmacogenomic data to predict human genes that modify doxorubicin toxicity in cancer cells. (A) Tables of UES and OES human genes and whether their yeast homologs were found to be deletion enhancing or deletion suppressing, respectively. **(B-C)** Overlap between the gCSI and GDSC1000 databases with regard to UES and OES human genes (**B**) across all tissues or (**C**) for individual tissues. Note: the intersection of

UES with OES between gCSI and GDSC was used as a negative control for assessing UES and OES overlap. **(D-E)** Yeast phenomic doxorubicin-gene interaction profiles for homologs of human UES or OES genes, sub-classified according to interaction type (deletion enhancing or suppressing) and Warburg-dependence of the interaction, for the **(D)** gCSI or **(E)** GDSC1000 databases. Similar to Figure 12, yeast-human homology relationships are shown to the left of heatmaps (blue - one to one; green - one to many; red - many to many). **(F-I)** Interactive plots for yeast-human homologs, comparing the p-value of human genes to L interaction scores for yeast counterparts in **(F, G)** HLD or **(H, I)** HLEG from **(F, H)** gCSI or **(G, I)** GDSC1000. For the standardized coefficient ('estimate'; color gradient), a negative value (purple) indicates UES, while a positive value (orange) indicates OES. Thus, the model would predict causality for a human gene if its yeast homolog has a positive L interaction (deletion enhancing) and is colored purple (UES), or a negative L interaction (deletion suppressing) and colored orange (OES). Genes are only plotted if the human homolog was significant (p-value < 0.05).

<u>Tables:</u>

Table 1. GO Terms enriched in REMc clusters.

Media	INT	GTA HLEG	GTA HLD	Clust	GO Term Name	p-value	Genes
Resp	Enh	5.0	2.8	1-0-7	nucleosome organization	1.1E-07	VPS71|RSC2|SWR1|LDB7|HHF1|RSC4|IES1|ISW1|ARP6|RTT106|HIR3|SWC3|HPC2|YAF9|HIR1|HIR2|HTB1|NHP6A|SWC5|NHP10
Resp	Enh	7.1	0.1	1-0-7	Set1C/COMPASS complex	5.5E-04	SPP1|SDC1|SWD1|SWD3|BRE2
Resp	Enh	3.9	-0.6	1-0-7	histone methylation	4.1E-03	SPP1|SDC1|LGE1|NOP1|SWD3|HHF1|SWD1|BRE2
Resp	Enh	3.4	3.0	1-0-7	protein import into mitochondrial matrix	6.4E-03	MGR2|TOM7|YME1|TOM70|PAM17|TIM17|TIM23|TOM6
Resp	Enh	0.6	0.8	2-0.7-1	ER membrane protein complex	4.6E-06	EMC6|EMC4|EMC3|EMC5
Resp	Enh	4.6	0.2	2-0.7-2	Sin3-type complex	1.5E-05	RCO1|RXT2|SAP30|PHO23|DEP1|UME1
Resp	Enh	5.2	-0.1	2-0.7-2	Rpd3L complex	7.1E-05	RXT2|SAP30|PHO23|DEP1|UME1
Resp	Enh	7.3	1.6	2-0.7-2	Swr1 complex	1.2E-06	SWC3|SWC5|VPS71|YAF9|SWR1|ARP6
Resp	Enh	5.9	2.1	2-0.7-2	histone exchange	5.7E-06	SWC3|SWC5|VPS71|YAF9|SWR1|ARP6
Resp	Enh	5.0	3.4	2-0.7-2	ATP-dependent chromatin remodeling	2.4E-04	SWC3|SWC5|VPS71|YAF9|SWR1|LDB7|ARP6
Resp	Enh	11.9	0.2	2-0.7-2	HIR complex	6.6E-06	HPC2|HIR1|HIR3|HIR2
Resp	Enh	11.4	3.2	2-0.7-2	DNA replication-independent nucleosome assembly	4.5E-04	HPC2|HIR1|HIR3|HIR2
Resp	Enh	11.0	1.7	1-0-8	respiratory chain complex III assembly	4.2E-02	QCR9|CBP4|FMP25
Resp	Enh	7.9	0.7	2-0.8-0	DNA topological change	2.6E-02	TOP3|MUS81
Resp	Enh	14.9	-0.4	2-0.8-1	NatC complex	5.6E-03	MAK31|MAK3
Resp	Sup	-2.6	-1.5	2-0.3-1	regulation of fatty acid beta-oxidation	2.1E-02	ADR1|OAF1|PIP2
Resp	Sup	-0.3	6.7	2-0.3-5	translation reinitiation	2.0E-02	TMA20|TIF34|TMA22
Glyc	Enh	1.1	0.5	2-0.2-2	ribonucleoprotein complex subunit organization	1.9E-02	RSA4|HBS1|BRR1|SDO1|RPS17A|DHH1|CLF1|RRP7|TIF6|RPS14A|RPS27B|PRP9
Glyc	Sup	-2.2	-3.0	2-0.4-0	7-methylguanosine cap hypermethylation	5.6E-03	SWM2|TGS1
Glyc	Sup	1.5	-0.4	2-0.4-2	mRNA 3'-end processing	8.6E-04	MPE1|CDC73|YSH1|KIN28|RNA14|NRD1
Glyc	Sup	1.3	0.9	2-0.4-2	mRNA cleavage	3.3E-02	MPE1|YSH1|POP8|RNA14
Glyc	Sup	-0.8	-2.9	2-0.4-2	meiotic chromosome condensation	3.4E-03	SMC2|YCG1|YCS4
Glyc	Sup	-1.0	-2.7	2-0.4-2	condensin complex	2.8E-03	SMC2|YCG1|YCS4
Both	Enh	2.9	2.3	1-0-6	cellular response to DNA damage stimulus	4.1E-08	CTK3|SIT4|RTT109|RVB1|RAD54|MMS22|CDC1|RAD55|PSF3|RAD50|BUD25|RAD51|MRE11|ARP8|ARP4|RAD57|TFB1|CDC7|RAD52|NPL6
Both	Enh	5.0	5.0	1-0-6	double-strand break repair via homologous recombination	2.9E-07	PSF3|RAD50|RAD51|MRE11|RAD54|MMS22|RAD57|CDC7|RAD52|RAD55
Both	Enh	7.7	9.7	1-0-6	double-strand break repair via synthesis-dependent strand annealing	4.3E-06	RAD54|RAD57|RAD51|RAD52|MRE11|RAD55
Both	Enh	9.2	5.0	2-0.6-1	ATP-dependent 3'-5' DNA helicase activity	1.9E-04	RVB1|ARP5|ARP8|ARP4
Both	Enh	9.0	2.5	2-0.6-1	Ino80 complex	2.1E-05	RVB1|IES6|ARP5|ARP8|ARP4
Both	Enh	3.4	1.6	2-0.6-1	histone acetylation	4.1E-02	RTT109|RVB1|NGG1|SPT20|ARP4
Resp	Enh	7.4	1.1	2-0.2-1	protein urmylation	1.1E-03	URM1|URE2|UBA4|ELP2
Both	Enh	9.9	3.9	2-0.2-1	Lst4-Lst7 complex	3.1E-02	LST7|LST4
Both	Sup	-4.5	-2.3	2-0.4-1	cellular sphingolipid homeostasis	9.6E-05	VPS53|VPS52|VPS54|VPS51
Both	Sup	-12.2	-7.0	2-0.4-1	fatty acid elongase activity	2.9E-02	ELO3|ELO2
Both	Sup	-3.0	-1.3	2-0.4-1	actin cortical patch localization	8.1E-03	RVS167|LSB3|RVS161|VRP1
Both	Sup	-9.0	-3.5	2-0.4-1	Rvs161p-Rvs167p complex	1.7E-02	RVS167|RVS161
Both	Sup	-4.4	-0.6	2-0.4-1	telomere tethering at nuclear periphery	1.8E-02	NUP60|MLP1|NUP120|NUP133

The table headers are defined as follows: For Column ‘Media’, ‘Resp’, ‘Glyc’, and ‘Both’ refer to whether the gene interaction type observed for the REMc cluster associated with the term was prominent in HLEG, HLD, or both media (see Fig. 4). For column ‘INT’, ‘Enh’ and ‘Sup’ indicate deletion enhancing or suppressing. Column ‘GTA’ refers to GO Term Average. Column ‘Clust’ refers to REMc ID.

Table 2. GO terms identified by GTA

GO Term Name	Media	INT	HLEG GTA	HLEG gtaSD	HLD GTA	HLD gtaSD	Genes	REMc related	p-value
HIR complex	Resp	Enh	11.9	1.5	0.2	0.9	HIR1 | HIR2 | HPC2 | HIR3	2-0.7-2	6.6E-06
histone monoubiquitination	Resp	Enh	11.4	7.0	0.1	1.2	RAD6 | BRE1	NA	NA
Ino80 complex	Resp	Enh	9.0	6.8	2.5	7.7	RVB1 | IES6 | ARP5 | ARP8 | ARP4 | ARP7 | IES5 | IES3 | NHP10 | IES2 | IES1 | RVB2 | IES4 | TAF14	3-0.6.1-1	1.5E-06
histone H4 acetylation	Resp	Enh	8.0	4.8	-0.8	2.1	ESA1 | NGG1 | ELP4 | EAF3 | HAT1	NA	NA
mitochondrial respiratory chain complex III assembly	Resp	Enh	11.0	6.8	1.7	2.0	QCR7 | CBP6 | CBP4 | BCS1 | QCR9 | FMP25 | FMP36 | CBP3	1-0-8	4.2E-02
mitochondrial respiratory chain supercomplex assembly	Resp	Enh	15.9	0.6	0.8	0.1	RCF1 | COX13	1-0-8	7.0E-02
mitochondrial outer membrane translocase complex	Resp	Enh	9.1	6.4	0.7	3.1	TOM22 | TOM5 | TOM6 | TOM70 | TOM7 | TOM40	NA	NA
protein urmylation	Resp	Enh	7.4	2.6	1.1	0.9	ELP2 | URM1 | NCS2 | UBA4 | ELP6 | URE2	2-0.2-1	1.1E-03
Elongator holoenzyme complex	Resp	Enh	8.9	3.6	0.0	0.9	TUP1 | IKI3 | ELP4 | ELP2 | ELP3 | IKI1 | ELP6	3-0.7.2-0	1.4E-04
NatC complex	Resp	Enh	14.9	1.7	-0.4	0.6	MAK31 | MAK10 | MAK3	2-0.8-1	5.6E-03
DNA topological change	Resp	Enh	7.9	5.7	0.7	2.6	RFA2 | TOP3 | MUS81 | RMI1 | TOP1 | SGS1 | RFA1 | RAD4 | TOP2	2-0.8-0	2.6E-02
tRNA (m1A) methyltransferase complex	Resp	Enh	17.0	0.8	9.3	17.4	GCD10 | GCD14	NA	NA
MUB1-RAD6-UBR2 ubiquitin ligase complex	Resp	Enh	12.9	3.1	0.9	0.5	RAD6 | MUB1 | UBR2	NA	NA
malonyl-CoA biosynthetic process	Resp	Enh	11.1	7.4	1.5	0.1	HFA1 | ACC1	NA	NA
pyridoxal 5'-phosphate salvage	Resp	Enh	11.1	8.7	1.5	5.3	PDX3 | BUD16 | BUD17	NA	NA
maintenance of transcriptional fidelity during DNA-templated transcription elongation from RNA polymerase II promoter	Resp	Enh	11.1	7.5	-0.4	4.2	RPB9 | DST1	NA	NA
RNA polymerase II transcription corepressor activity	Resp	Enh	11.0	7.6	2.2	1.7	SIN3 | MED8 | SRB7	NA	NA
pyruvate dehydrogenase activity	Resp	Enh	10.6	6.4	2.8	0.9	PDA1 | LPD1 | PDB1	NA	NA
eukaryotic translation initiation factor 2 complex	Resp	Enh	10.3	4.7	8.2	8.7	SUI2 | GCD11	NA	NA
L-aspartate:2-oxoglutarate aminotransferase activity	Resp	Sup	-3.9	0.5	-0.9	0.8	AAT2 | AAT1	2-0.4-3	5.9E-04
nuclear pore outer ring	Resp	Sup	-6.3	3.7	1.4	7.6	NUP145 | SEH1 | NUP84 | NUP120 | NUP133	3-0.4.1-0	9.7E-02
positive regulation of fatty acid beta-oxidation	Resp	Sup	-2.6	0.5	-1.5	0.2	OAF1 | ADR1 | PIP2	2-0.3-1	2.1E-02
EKC/KEOPS complex	Resp	Sup	-7.9	4.6	-1.8	1.1	KAE1 | CGI121 | GON7 | BUD32	NA	NA
spermine biosynthetic process	Resp	Sup	-2.6	0.3	-0.3	0.7	SPE4 | SPE2	NA	NA
Dom34-Hbs1 complex	Glyc	Enh	0.3	2.1	2.7	0.3	HBS1 | DOM34	NA	NA
Ubp3-Bre5 deubiquitination complex	Glyc	Enh	-1.1	3.2	8.8	2.2	BRE5 | UBP3	NA	NA
Cul4-RING E3 ubiquitin ligase complex	Glyc	Enh	1.8	4.1	4.6	2.3	HRT1 | PRP46 | SOF1	NA	NA
dTTP biosynthetic process	Glyc	Enh	-1.3	3.2	7.0	0.6	CDC21 | CDC8	NA	NA
GDP-mannose transport	Glyc	Enh	1.5	1.9	9.5	5.6	VRG4 | HVG1	NA	NA
7-methylguanosine cap hypermethylation	Glyc	Sup	-2.2	1.5	-3.0	0.9	SWM2 | TGS1	2-0.4-0	5.6E-03
meiotic chromosome condensation	Glyc	Sup	-0.8	0.9	-2.9	0.9	SMC2 | YCG1 | SMC4 | YCS4	2-0.4-2	3.4E-03
histone deubiquitination	Glyc	Sup	1.8	1.9	-3.4	1.1	SEM1 | UBP8 | SGF73 | SGF11	NA	NA
HDA1 complex	Both	Enh	8.9	0.3	4.0	1.1	HDA2 | HDA1 | HDA3	NA	NA
CTDK-1 complex	Both	Enh	15.6	0.7	3.8	0.9	CTK2 | CTK3 | CTK1	1-0-8	5.3E-02
Cul8-RING ubiquitin ligase complex	Both	Enh	9.1	4.5	6.1	1.1	MMS22 | MMS1 | RTT101 | HRT1 | RTT107	1-0-2	1.0E-01
Lst4-Lst7 complex	Both	Enh	9.9	1.4	3.9	0.3	LST7 | LST4	2-0.2-1	3.1E-02
MCM complex	Both	Enh	4.2	1.4	4.9	2.6	MCM7 | MCM6 | MCM5 | MCM2 | MCM3	NA	NA
histone H3-K56 acetylation	Both	Enh	10.3	7.0	8.6	4.3	RTT109 | SPT10	NA	NA
fatty acid elongase activity	Both	Sup	-12.2	2.4	-7.0	1.1	SUR4 | FEN1	2-0.4-1	2.9E-02
GARP complex	Both	Sup	-6.8	0.9	-3.5	0.8	VPS53 | VPS54 | VPS52 | VPS51	3-0.4.1-0	6.9E-07
nuclear cap binding complex	Both	Sup	-4.7	0.5	-3.4	0.5	STO1 | CBC2	3-0.4.1-0	9.9E-03
Rvs161p-Rvs167p complex	Both	Sup	-9.0	0.4	-3.5	0.2	RVS167 | RVS161	3-0.4.1-0	9.9E-03

The table headers are defined as follows: 'GTA SD' refers to the standard deviation of GTA; 'REMc cluster' refers to an REMc cluster ID if GTA-identified term was also found by REMc/GTF; 'p-value' reports results from REMc/GTF. See Table 1 for other header definitions.

Table 3. Yeast-human homologs with deletion enhancement and UES across all tissues

hGene	yGene	DB	Fig.	GO term	HLD L|K	HLEG L|K	GDSC pval	gCSI pval	Ref	H	Description hGene
ACTL6B	ARP4	Both	12E	Ino80 Complex	8.3|-10	16.4|-12.6	3.3E-02	3.8E-02	175	2	actin like 6B
HMGCS2	ERG13	Both	S7B	N/A	34.8|-21.4	3.7|-3.3	2.4E-02	7.9E-04	188	2	3-hydroxy-3-methylglutaryl-CoA synthase 2
PPM1L	PTC1	Both	12C	N/A	15.2|-4.7	14.7|-13	3.1E-04	1.6E-02	176-7	2	protein phosphatase, Mg2+/Mn2+ dependent 1L
RPS6KB2	SCH9	Both	12E	Sphingolipid Metabolic Process	6|-3.7	8.8|-9.8	3.5E-02	4.2E-03	NA	3	ribosomal protein S6 kinase B2
SEC11C	SEC11	Both	S7B	N/A	11.6|-1.3	2.8|0	3.5E-04	3.5E-04	178	2	SEC11 homolog C, signal peptidase complex subunit
ARFGEF2	SEC7	Both	12C	N/A	2.9|0	2.6|0.8	7.5E-03	1.5E-08	179-80	2	ADP ribosylation factor guanine nucleotide exchange factor 2
IQSEC3	SEC7	Both	12C	N/A	2.9|0	2.6|0.8	7.5E-03	4.9E-02	NA	2	IQ motif and Sec7 domain 3
PPCDC	SIS2	Both	12C	N/A	7.3|-3.5	12.1|-9.8	3.9E-02	4.7E-03	NA	2	phosphopantothenoylcysteine decarboxylase
CCS	CCS1	gCSI	NA	N/A	2.4|-0.4	5.6|-3.7	3.4E-01	1.2E-02	NA	2	copper chaperone for superoxide dismutase
HMGCS1	ERG13	gCSI	S7B	N/A	34.8|-21.4	3.7|-3.3	9.5E-01	1.4E-02	187	3	3-hydroxy-3-methylglutaryl-CoA synthase 1
HDAC6	HDA1	gCSI	7A	HDA1 Complex	5.2|-1	9.1|-1.8	9.1E-01	1.7E-03	NA	2	histone deacetylase 6
MUS81	MUS81	gCSI	8B	DNA Topological Change	5.2|-2.4	15.9|-11.1	6.9E-02	1.9E-04	181	2	MUS81 structure-specific endonuclease subunit
SGK2	SCH9	gCSI	12E	Sphingolipid Metabolic Process	6|-3.7	8.8|-9.8	4.6E-01	8.5E-04	NA	1	SGK2, serine/threonine kinase 2
CCS	SOD1	gCSI	12E	N/A	6.2|-0.5	8.1|-10.7	3.4E-01	1.2E-02	NA	2	copper chaperone for superoxide dismutase
SOD1	SOD1	GDSC	12E	N/A	6.2|-0.5	8.1|-10.7	4.3E-02	7.9E-01	NA	2	superoxide dismutase 1
PELO	DOM34	gCSI	9A	Dom34-Hbs1 Complex	2.5|-0.7	-1.2|1.1	NA	1.7E-02	NA	2	pelota mRNA surveillance and ribosome rescue factor
ADH1A	SFA1	gCSI	12E	N/A	4.8|0	0.9|-0.3	1.1E-01	2.9E-02	185-6	2	alcohol dehydrogenase 1A (class I), alpha polypeptide
ADH4	SFA1	gCSI	12E	N/A	4.8|0	0.9|-0.3	3.6E-01	3.6E-03	186	3	alcohol dehydrogenase 4 (class II), pi polypeptide
ADH6	SFA1	gCSI	12E	N/A	4.8|0	0.9|-0.3	8.6E-01	3.3E-03	185	1	alcohol dehydrogenase 6 (class V)
HIST1H3D	HHT1	Both	6A-B	Nucleosome Assembly	0.4|-0.2	15|-10.2	4.2E-02	2.1E-02	NA	2	histone cluster 1 H3 family member d
HIST1H2BN	HTB1	Both	6A-B	Nucleosome Assembly	0.2|-0.6	7.8|-5.8	4.0E-02	3.0E-06	NA	2	histone cluster 1 H2B family member n
HIST2H2BE	HTB1	Both	6A-B	Nucleosome Assembly	0.2|-0.6	7.8|-5.8	4.0E-02	2.3E-08	NA	2	histone cluster 2 H2B family member e
SETBP1	SET2	Both	6A,C	Histone exchange	1.3|-1.6	5.4|-2.5	7.3E-07	3.0E-04	NA	3	SET binding protein 1
RNF40	BRE1	gCSI	7C	Histone Monoubiquitination	-0.7|0.5	6.5|-4.9	7.4E-01	8.5E-03	NA	2	ring finger protein 40
HIST1H4D	HHF1	gCSI	6A-B	Nucleosome Assembly	-0.6|0.2	13.7|-3.8	NA	8.9E-03	NA	3	histone cluster 1 H4 family member d
HIST1H4H	HHF1	gCSI	6A-B	Nucleosome Assembly	-0.6|0.2	13.7|-3.8	8.6E-02	2.8E-06	NA	3	histone cluster 1 H4 family member h
HIST1H4I	HHF1	gCSI	6A-B	Nucleosome Assembly	-0.6|0.2	13.7|-3.8	NA	3.8E-02	NA	2	histone cluster 1 H4 family member i
HIST1H4K	HHF1	gCSI	6A-B	Nucleosome Assembly	-0.6|0.2	13.7|-3.8	NA	8.0E-03	NA	3	histone cluster 1 H4 family member k
HIST2H4A	HHF1	gCSI	6A-B	Nucleosome Assembly	-0.6|0.2	13.7|-3.8	NA	4.8E-02	NA	3	histone cluster 2 H4 family member a
HIST2H4B	HHF1	gCSI	6A-B	Nucleosome Assembly	-0.6|0.2	13.7|-3.8	NA	3.7E-03	NA	3	histone cluster 2 H4 family member b
HIST4H4	HHF1	gCSI	6A-B	Nucleosome Assembly	-0.6|0.2	13.7|-3.8	5.4E-02	2.4E-02	NA	3	histone cluster 4 H4
HIST1H4D	HHF2	gCSI	12E	Chromatin Assembly or Disassembly	-1.6|0.4	4.3|-0.1	NA	8.9E-03	NA	3	histone cluster 1 H4 family member d
HIST1H4H	HHF2	gCSI	12E	Chromatin Assembly or Disassembly	-1.6|0.4	4.3|-0.1	8.6E-02	2.8E-06	NA	3	histone cluster 1 H4 family member h
HIST1H4I	HHF2	gCSI	12E	Chromatin Assembly or Disassembly	-1.6|0.4	4.3|-0.1	NA	3.8E-02	NA	3	histone cluster 1 H4 family member i
HIST1H4K	HHF2	gCSI	12E	Chromatin Assembly or Disassembly	-1.6|0.4	4.3|-0.1	NA	8.0E-03	NA	3	histone cluster 1 H4 family member k
HIST2H4A	HHF2	gCSI	12E	Chromatin Assembly or Disassembly	-1.6|0.4	4.3|-0.1	NA	4.8E-02	NA	3	histone cluster 2 H4 family member a
HIST2H4B	HHF2	gCSI	12E	Chromatin Assembly or Disassembly	-1.6|0.4	4.3|-0.1	NA	3.7E-03	NA	3	histone cluster 2 H4 family member b
HIST4H4	HHF2	gCSI	12E	Chromatin Assembly or Disassembly	-1.6|0.4	4.3|-0.1	5.4E-02	2.4E-02	NA	3	histone cluster 4 H4
HIST1H2AE	HHT1	gCSI	6A-B	Nucleosome Assembly	0.4|-0.2	15|-10.2	NA	1.1E-02	NA	3	histone cluster 1 H2A family member e
HIST1H3E	HHT1	gCSI	6A-B	Nucleosome Assembly	0.4|-0.2	15|-10.2	NA	1.3E-02	NA	3	histone cluster 1 H3 family member e
HIST1H3H	HHT1	gCSI	6A-B	Nucleosome Assembly	0.4|-0.2	15|-10.2	NA	6.8E-03	NA	3	histone cluster 1 H3 family member h
HIST1H2AC	HTA1	gCSI	12E	Chromatin Assembly or Disassembly	-3.5|0.8	13.5|-5.2	7.1E-01	2.9E-05	NA	3	histone cluster 1 H2A family member c
HIST1H2AD	HTA1	gCSI	12E	Chromatin Assembly or Disassembly	-3.5|0.8	13.5|-5.2	3.7E-01	5.8E-03	NA	3	histone cluster 1 H2A family member d
HIST1H2AG	HTA1	gCSI	12E	Chromatin Assembly or Disassembly	-3.5|0.8	13.5|-5.2	5.6E-01	1.4E-02	NA	3	histone cluster 1 H2A family member g
HIST1H2AK	HTA1	gCSI	12E	Chromatin Assembly or Disassembly	-3.5|0.8	13.5|-5.2	NA	6.3E-04	NA	3	histone cluster 1 H2A family member k
HIST2H2AA3	HTA1	gCSI	12E	Chromatin Assembly or Disassembly	-3.5|0.8	13.5|-5.2	NA	2.6E-02	NA	3	histone cluster 2 H2A family member a3
HIST2H2AA4	HTA1	gCSI	12E	Chromatin Assembly or Disassembly	-3.5|0.8	13.5|-5.2	NA	5.3E-03	NA	3	histone cluster 2 H2A family member a4
H2BFM	HTB1	gCSI	6A-B	Nucleosome Assembly	0.2|-0.6	7.8|-5.8	NA	3.0E-02	NA	3	H2B histone family member M
H2BFWT	HTB1	gCSI	6A-B	Nucleosome Assembly	0.2|-0.6	7.8|-5.8	3.3E-01	6.5E-04	NA	3	H2B histone family member W, testis specific
HIST1H2BC	HTB1	gCSI	6A-B	Nucleosome Assembly	0.2|-0.6	7.8|-5.8	9.8E-01	5.3E-05	NA	3	histone cluster 1 H2B family member c
HIST1H2BD	HTB1	gCSI	6A-B	Nucleosome Assembly	0.2|-0.6	7.8|-5.8	4.7E-01	3.0E-06	NA	3	histone cluster 1 H2B family member d
HIST1H2BE	HTB1	gCSI	6A-B	Nucleosome Assembly	0.2|-0.6	7.8|-5.8	NA	2.5E-04	NA	3	histone cluster 1 H2B family member e
HIST1H2BF	HTB1	gCSI	6A-B	Nucleosome Assembly	0.2|-0.6	7.8|-5.8	NA	5.3E-03	NA	3	histone cluster 1 H2B family member f
HIST1H2BG	HTB1	gCSI	6A-B	Nucleosome Assembly	0.2|-0.6	7.8|-5.8	NA	5.8E-04	NA	3	histone cluster 1 H2B family member g
HIST1H2BJ	HTB1	gCSI	6A-B	Nucleosome Assembly	0.2|-0.6	7.8|-5.8	9.2E-02	1.5E-03	NA	3	histone cluster 1 H2B family member j
HIST1H2BK	HTB1	gCSI	6A-B	Nucleosome Assembly	0.2|-0.6	7.8|-5.8	NA	9.0E-04	NA	3	histone cluster 1 H2B family member k
HIST1H2BO	HTB1	gCSI	6A-B	Nucleosome Assembly	0.2|-0.6	7.8|-5.8	NA	2.9E-02	NA	3	histone cluster 1 H2B family member o
NAA30	MAK3	gCSI	8A	NatC Complex	0.2|-0.5	16.6|-11.6	8.5E-01	2.9E-02	184	2	N(alpha)-acetyltransferase 30, NatC catalytic subunit
ROMO1	MGR2	gCSI	S3C	Protein import into mitochondrial matrix	0|-0.2	10.3|0.1	7.1E-02	4.1E-02	182-3	2	reactive oxygen species modulator 1
AIRE	RCO1	gCSI	7A	Rpd3S Complex	0.9|-0.5	7.9|-4.4	5.5E-01	1.3E-03	NA	3	autoimmune regulator
ASH1L	SET2	gCSI	6A,C	Histone exchange	1.3|-1.6	5.4|-2.5	6.6E-01	5.5E-04	NA	3	ASH1 like histone lysine methyltransferase
RECQL4	SGS1	gCSI	8B	DNA Topological Change	-0.2|0.7	6.1|-2.5	7.3E-01	3.2E-02	NA	3	RecQ like helicase 4
RECQL5	SGS1	gCSI	8B	DNA Topological Change	-0.2|0.7	6.1|-2.5	2.7E-01	3.0E-04	NA	1	RecQ like helicase 5
SRCAP	SWR1	gCSI	7A	Swr1 complex	0.4|-0.5	7.3|-6.2	NA	5.1E-04	NA	3	Snf2 related CREBBP activator protein
UNC45B	TOM70	gCSI	S3C	Protein import into mitochondrial matrix	0.8|-0.4	12.4|-0.3	7.4E-01	1.6E-02	NA	2	unc-45 myosin chaperone B
MOCS3	UBA4	gCSI	8A	protein urmylation	1.5|-3.3	8.1|-3.4	8.0E-01	3.0E-02	NA	1	molybdenum cofactor synthesis 3
EMC3	EMC3	GDSC	8A	ER Membrane Protein Complex	1.5|-0.8	5.6|-1.8	1.1E-02	NA	NA	2	ER membrane protein complex subunit 3
EMC4	EMC4	GDSC	8A	ER Membrane Protein Complex	-0.1|-0.3	6.2|-1.6	2.6E-02	NA	NA	2	ER membrane protein complex subunit 4

For column 'DB': 'gCSI', 'GDSC', or 'Both' indicate UES in the gCSI, GDSC, or both databases. Column 'Fig.' refers to specific figures. Columns "HLD L|K" and "HLEG L|K" contain the L and K interaction scores for HLD and HLEG media, respectively. "GDSC pval" and "gCSI pval" refer to the significance of differential gene expression in the respective databases. 'Ref' refers to relevant literature citations. 'H' refers to homology type: '1', '2', and '3' indicate 1:1, 1:many, and many:many, respectively.

Table 4. Yeast-human homologs with deletion suppression and OES across all tissues

hGene	yGene	DB	Fig	GO term	HLD L|K	HLEG L|K	GDSC pval	gCSI pval	Ref	H	Description hGene
ACTR2	ARP2	Both	12D	Arp2/3 Protein Complex	-3.7|1.4	-3.3|-6.9	3.2E-02	6.0E-05	190	1	ARP2 actin related protein 2 homolog
SEPT6	CDC3	Both	12D	N/A	-2.1|0.7	-2.6|0.3	1.7E-04	2.8E-05	NA	1	septin 6
CSNK2A2	CKA2	Both	12D	N/A	-5.5|1	-4|1.2	4.3E-03	3.6E-03	NA	2	casein kinase 2 alpha 2
DBR1	DBR1	Both	12D	N/A	-2.1|0.6	-3.5|1	4.3E-02	9.8E-04	NA	1	debranching RNA lariats 1
PLAA	DOA1	Both	12D	N/A	-2.2|0.7	-7.7|1.9	2.6E-02	1.5E-04	NA	3	phospholipase A2 activating protein
EEF2	EFT2	Both	12D	N/A	-2.7|0.2	-2.1|1.1	1.9E-02	9.7E-06	191	2	eukaryotic translation elongation factor 2
HARS	HTS1	Both	12D	N/A	-2.4|0.6	-2.9|0.5	4.1E-03	1.6E-03	NA	1	histidyl-tRNA synthetase
CDK7	KIN28	Both	12D	N/A	-2.2|1.1	-2.5|-1.2	2.4E-02	2.6E-04	192-4	3	cyclin dependent kinase 7
METAP1	MAP1	Both	12D	N/A	-4.7|3.3	-4.2|-0.6	8.9E-03	2.3E-02	NA	1	methionyl aminopeptidase 1
RPL13A	RPL16B	Both	12D	N/A	-4.5|3.7	-5.8|1.4	1.5E-03	9.5E-05	NA	2	ribosomal protein L13a
RPL32	RPL32	Both	12D	N/A	-3.9|1	-11.3|1.1	6.9E-03	3.6E-03	198	2	ribosomal protein L32
RPL34	RPL34A	Both	12D	N/A	-4.8|2.3	-7.2|2.4	1.5E-02	4.4E-03	195-7	3	ribosomal protein L34
ZFAND4	RPL40B	Both	12D	N/A	-4.1|1.1	-5.7|1.1	3.7E-02	1.7E-02	NA	2	zinc finger AN1-type containing 4
RPS6	RPS6A	Both	12D	N/A	-5.7|1.8	-6|2.6	2.0E-04	2.5E-07	199-200	2	ribosomal protein S6
HSPA4	SSE1	Both	12D	N/A	-6.3|3	-13.7|4.4	1.5E-02	4.2E-07	NA	2	heat shock protein family A (Hsp70) member 4
NCBP1	STO1	Both	12D	N/A	-3|1.7	-4.3|1.3	2.3E-03	3.5E-04	NA	2	nuclear cap binding protein subunit 1
ELAC2	TRZ1	Both	12D	N/A	-2.3|0.6	-2.6|0.1	1.1E-05	1.5E-08	NA	3	elaC ribonuclease Z 2
UBE2D1	UBC4	Both	12D	N/A	-4.6|2.2	-12.3|2.6	1.0E-02	8.1E-03	201	1	ubiquitin conjugating enzyme E2 D1
TPRKB	CGI121	gCSI	12F	EKC/KEOPS Complex	-2.2|-0.8	-7.7|2.1	1.3E-01	7.6E-04	NA	1	TP53RK binding protein
ELOVL6	ELO2	gCSI	12F	Fatty Acid Elongase Activity	-7.7|1.4	-13.9|4.1	5.1E-01	2.7E-02	206	2	ELOVL fatty acid elongase 6
ELOVL6	ELO3	gCSI	12F	Fatty Acid Elongase Activity	-6.3|1.3	-10.5|1.9	5.1E-01	2.7E-02	206	1	ELOVL fatty acid elongase 6
NUP155	NUP170	gCSI	12F	Telomere tethering at the nuclear periphery	-3.7|0.6	-6.5|1.3	1.0E-01	4.4E-02	216-18	1	nucleoporin 155
SSRP1	POB3	gCSI	12F	FACT Complex	-4.1|1.2	-5.1|1.4	6.0E-02	2.2E-06	13	2	structure specific recognition protein 1
TGS1	TGS1	gCSI	12F	7-methylguanosine cap hypermethylation	-2.4|2.6	-3.3|0.7	8.5E-02	2.0E-03	NA	2	trimethylguanosine synthase 1
VPS53	VPS53	gCSI	12F	Cellular sphingolipid homeostasis	-2.4|1.8	-5.8|1.4	2.0E-01	2.4E-02	203-5	2	VPS53, GARP complex subunit
USP22	UBP8	Both	12F	histone deubiquitination	-2|0.8	0.3|0.3	2.3E-02	1.2E-02	NA	1	ubiquitin specific peptidase 22
SMC2	SMC2	gCSI	12F	meiotic chromosome condensation	-3.5|1.2	0.4|-0.9	1.1E-01	4.3E-02	138	3	structural maintenance of chromosomes 2
NCAPG	YCG1	gCSI	12F	meiotic chromosome condensation	-2|0.8	-0.8|-0.6	7.9E-01	9.2E-06	138	3	non-SMC condensin I complex subunit G
NCAPD2	YCS4	gCSI	12F	meiotic chromosome condensation	-2.4|0.8	-1.7|-0.9	2.3E-01	1.7E-03	NA	2	non-SMC condensin I complex subunit D2
USP44	UBP8	GDSC	12F	histone deubiquitination	-2|0.8	0.3|0.3	4.1E-04	6.1E-01	NA	2	ubiquitin specific peptidase 44
KDM2B	JHD1	Both	12F	Histone Demethylation	0.2|-0.2	-2.3|1.9	4.6E-02	3.5E-02	207-9	1	lysine demethylase 2B
AMD1	SPE2	Both	12F	spermine biosynthetic process	0.2|-0.2	-2.8|0.5	1.7E-02	1.5E-04	202	1	adenosylmethionine decarboxylase 1
SMS	SPE4	gCSI	12F	spermine biosynthetic process	-0.8|0.4	-2.4|1	NA	3.9E-02	NA	1	spermine synthase
EIF3I	TIF34	gCSI	12F	translation reinitiation	1.2|0	-3.9|1.4	8.2E-01	7.1E-05	NA	2	eukaryotic translation initiation factor 3 subunit I
STRAP	TIF34	gCSI	12F	translation reinitiation	1.2|0	-3.9|1.4	6.7E-01	9.1E-03	NA	2	serine/threonine kinase receptor associated protein
DENR	TMA22	gCSI	12F	translation reinitiation	-1.1|0.6	-6.4|1.9	4.0E-01	1.9E-02	211-15	1	density regulated re-initiation and release factor
PHF2	JHD1	GDSC	12F	Histone Demethylation	0.2|-0.2	-2.3|1.9	1.9E-03	6.8E-02	NA	1	PHD finger protein 2
JARID2	JHD2	GDSC	12F	Histone Demethylation	-0.2|0.1	-3.2|1	1.9E-03	2.5E-02	210	2	jumonji and AT-rich interaction domain containing 2

See Table 3 for header descriptions.

A

Experimental model

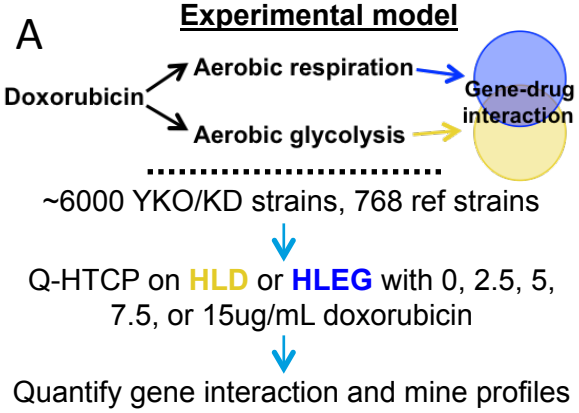

B

Imaging

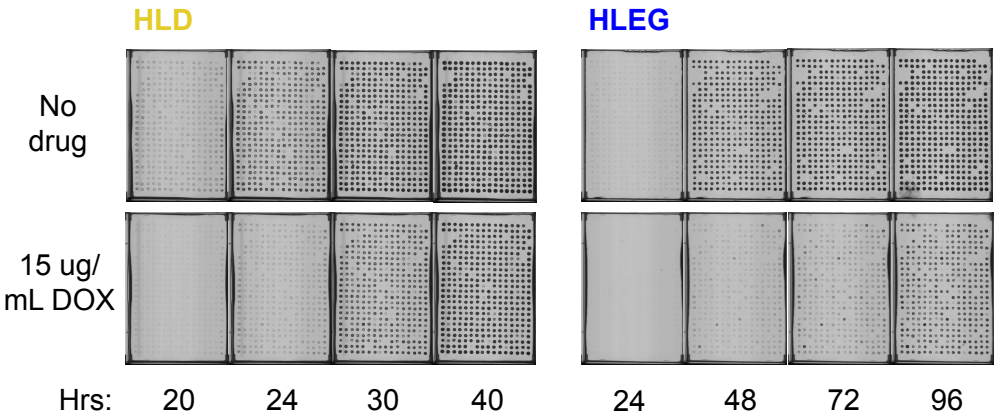

C

Image analysis

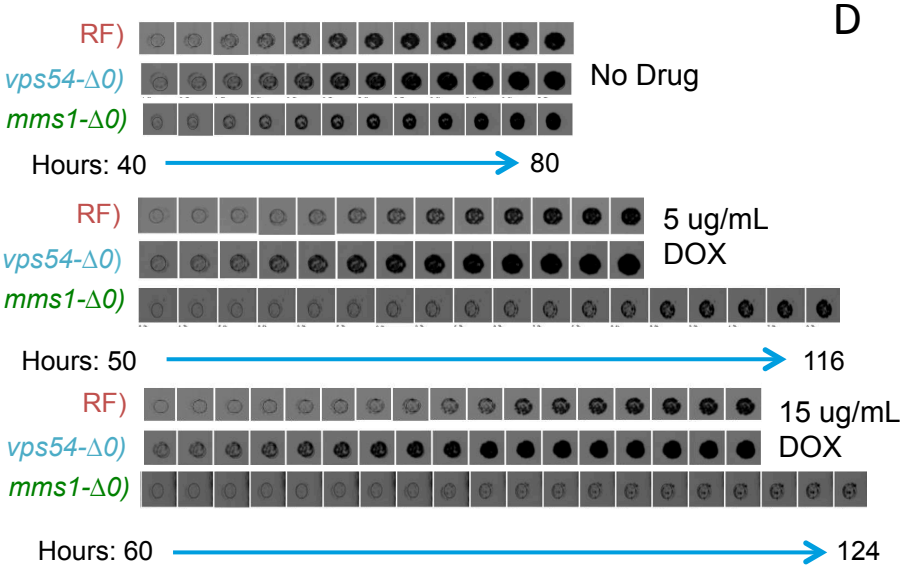

D

Growth curve fitting

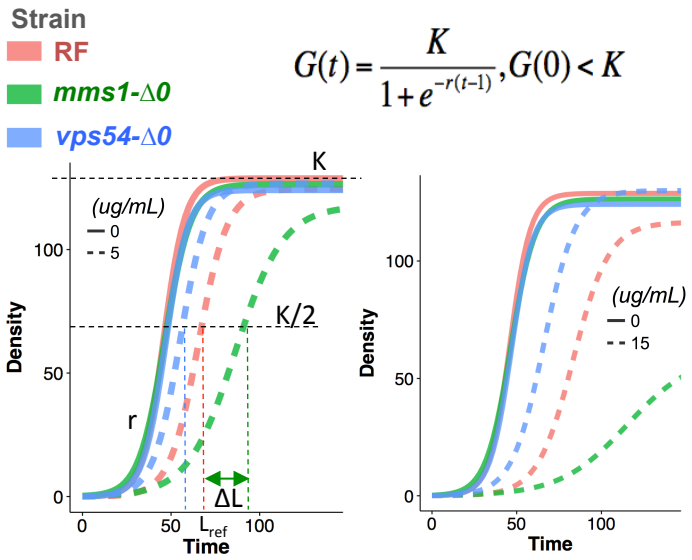

E

Quantification of Interactions

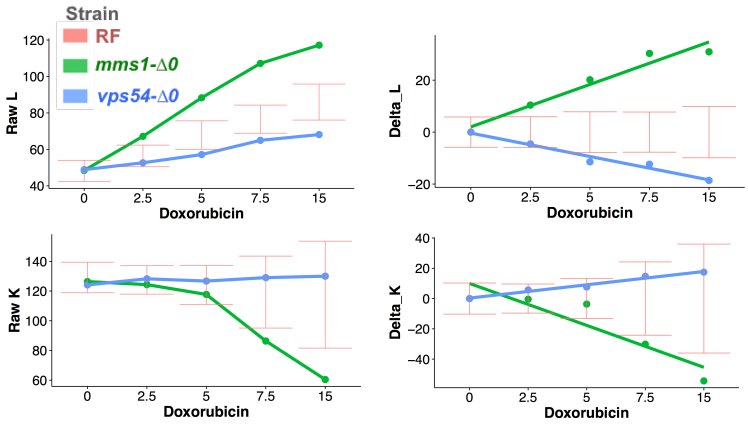

G

GTA: GO module assessment

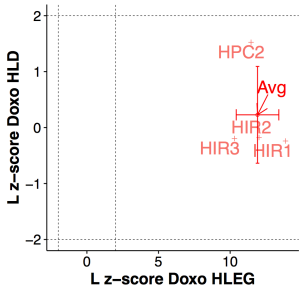

H

Warburg-dependence of doxorubicin-gene interaction

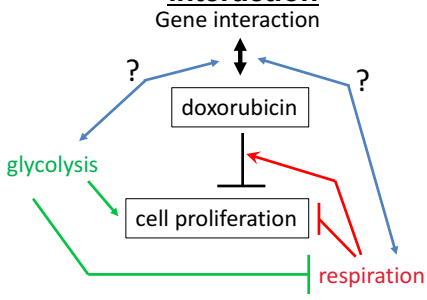

F

REMc/GTF: Gene interaction modules >> GO functional association

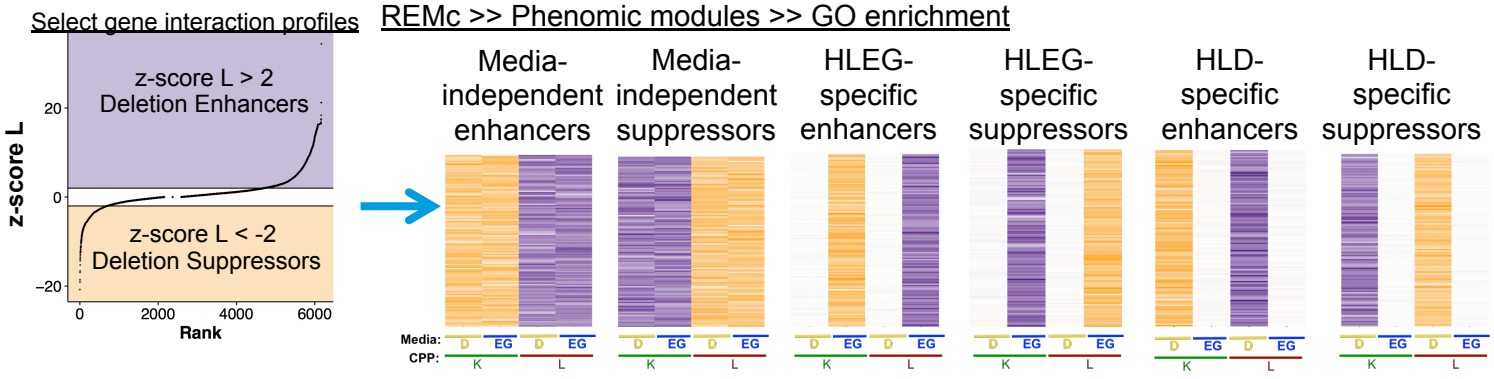

Reference strain growth curve distributions

Doxorubicin-gene interaction

Ref strain CPPs

Comparison with prior published data

Reproducibility

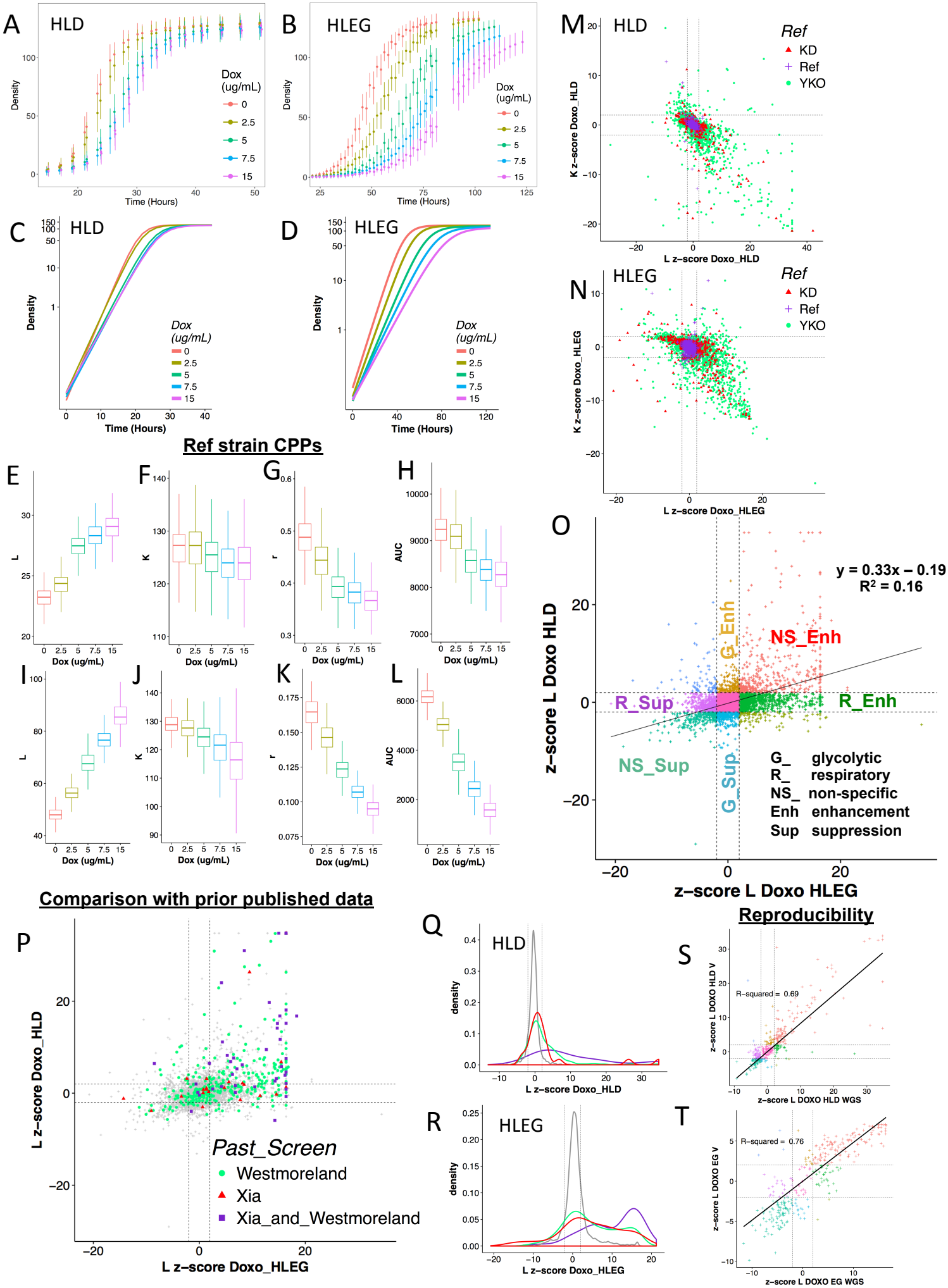

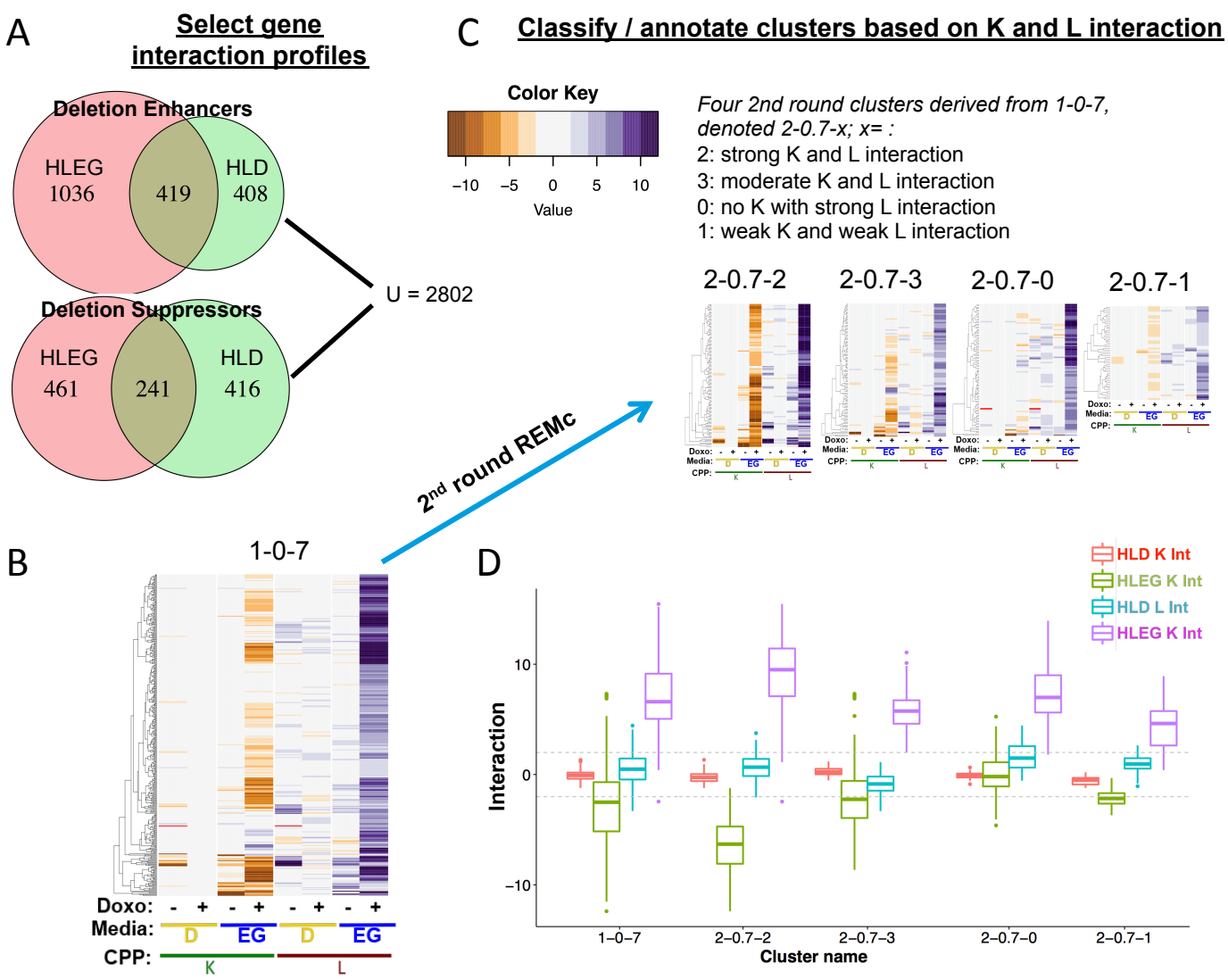
A
Select gene interaction profiles
Deletion Enhancers
HLEG 1036
419
HLD 408
Deletion Suppressors
HLEG 461
241
HLD 416
U = 2802
C
Classify / annotate clusters based on K and L interaction
Color Key
−10 −5 0 5 10
Value
Four 2nd round clusters derived from 1-0-7, denoted 2-0.7-x; x= :
2: strong K and L interaction
3: moderate K and L interaction
0: no K with strong L interaction
1: weak K and weak L interaction
2-0.7-2
2-0.7-3
2-0.7-0
2-0.7-1
2nd round REMc
B
1-0-7
Doxo: - + - + - + - +
Media: D EG D EG
CPP: K L
D
HLD K Int
HLEG K Int
HLD L Int
HLEG K Int
Interaction
10
0
−10
1−0−7
2−0.7−2
2−0.7−3
2−0.7−0
2−0.7−1
Cluster name

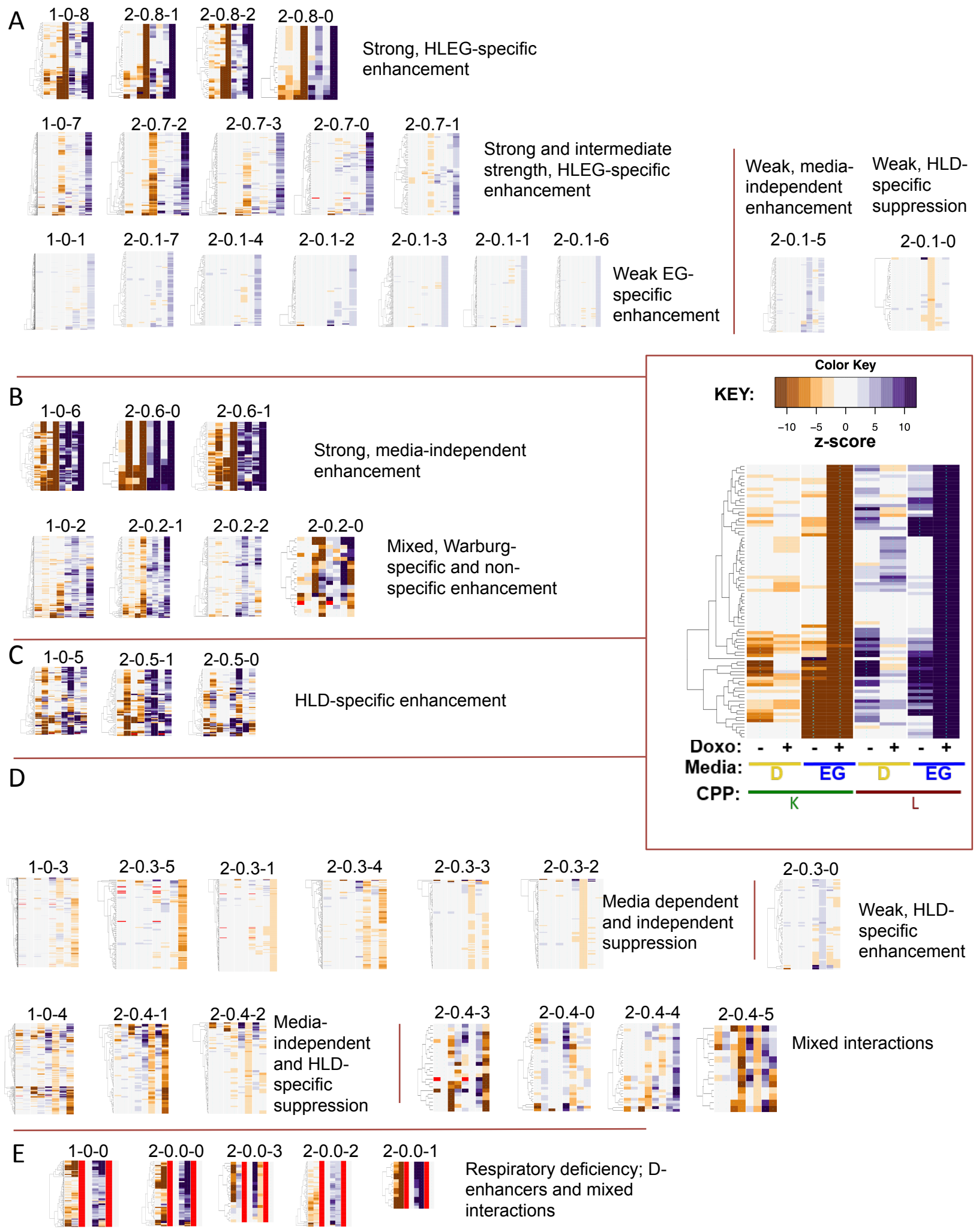
A
1-0-8
2-0.8-1
2-0.8-2
2-0.8-0
Strong, HLEG-specific enhancement
1-0-7
2-0.7-2
2-0.7-3
2-0.7-0
2-0.7-1
Strong and intermediate strength, HLEG-specific enhancement
Weak, media-independent enhancement
Weak, HLD-specific suppression
1-0-1
2-0.1-7
2-0.1-4
2-0.1-2
2-0.1-3
2-0.1-1
2-0.1-6
Weak EG-specific enhancement
2-0.1-5
2-0.1-0
B
1-0-6
2-0.6-0
2-0.6-1
Strong, media-independent enhancement
1-0-2
2-0.2-1
2-0.2-2
2-0.2-0
Mixed, Warburg-specific and non-specific enhancement
C
1-0-5
2-0.5-1
2-0.5-0
HLD-specific enhancement
Color Key
KEY:
−10 −5 0 5 10
z-score
Doxo: - + - + - + - +
Media: D EG D EG
CPP: K L
D
1-0-3
2-0.3-5
2-0.3-1
2-0.3-4
2-0.3-3
2-0.3-2
Media dependent and independent suppression
2-0.3-0
Weak, HLD-specific enhancement
1-0-4
2-0.4-1
2-0.4-2
Media-independent and HLD-specific suppression
2-0.4-3
2-0.4-0
2-0.4-4
2-0.4-5
Mixed interactions
E
1-0-0
2-0.0-0
2-0.0-3
2-0.0-2
2-0.0-1
Respiratory deficiency; D-enhancers and mixed interactions

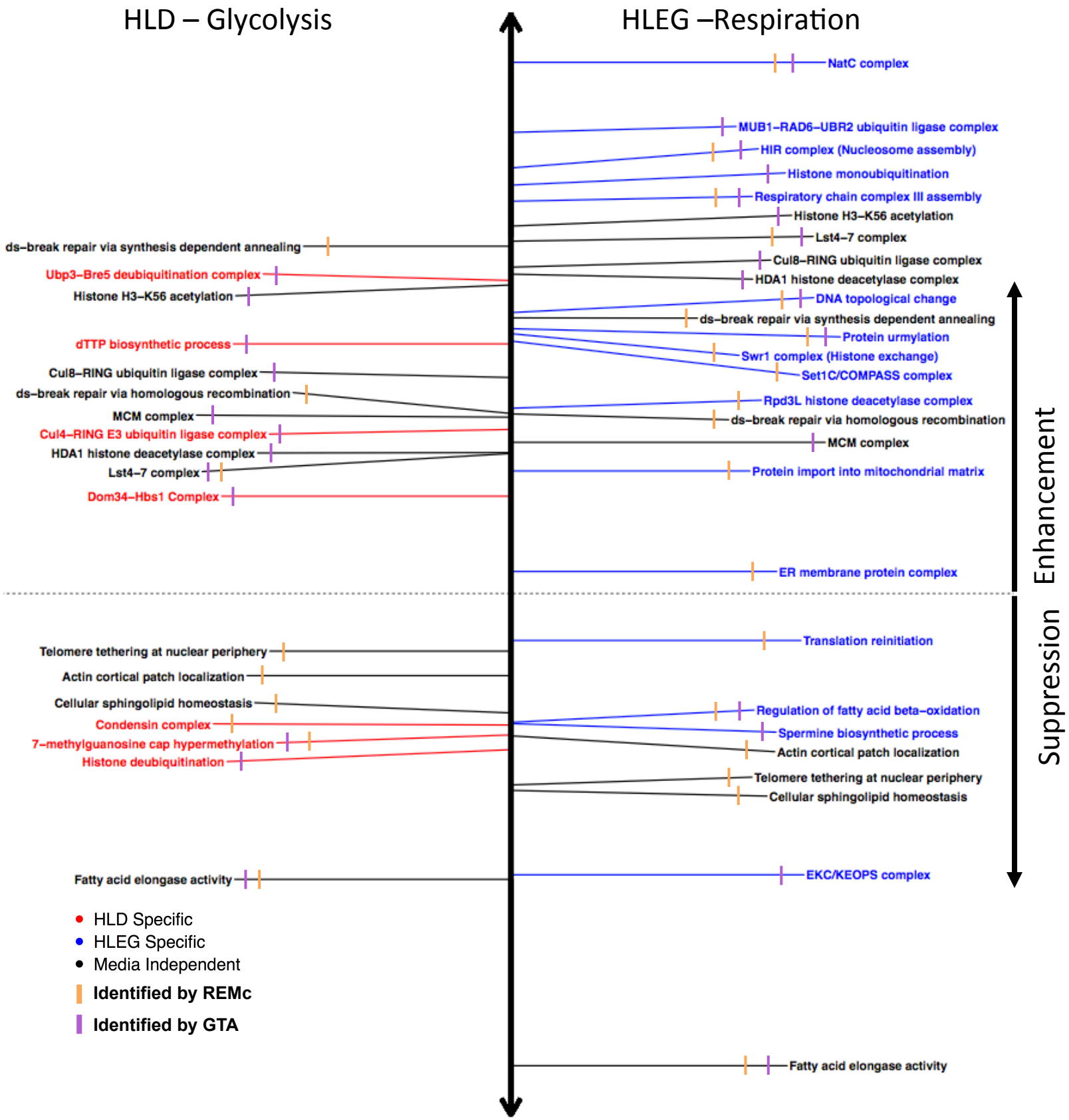
HLD – Glycolysis
HLEG –Respiration
NatC complex
MUB1–RAD6–UBR2 ubiquitin ligase complex
HIR complex (Nucleosome assembly)
Histone monoubiquitination
Respiratory chain complex III assembly
Histone H3–K56 acetylation
Lst4–7 complex
Cul8–RING ubiquitin ligase complex
HDA1 histone deacetylase complex
DNA topological change
ds–break repair via synthesis dependent annealing
Protein urmylation
Swr1 complex (Histone exchange)
Set1C/COMPASS complex
Rpd3L histone deacetylase complex
ds–break repair via homologous recombination
MCM complex
Protein import into mitochondrial matrix
ER membrane protein complex
Translation reinitiation
Regulation of fatty acid beta–oxidation
Spermine biosynthetic process
Actin cortical patch localization
Telomere tethering at nuclear periphery
Cellular sphingolipid homeostasis
EKC/KEOPS complex
Fatty acid elongase activity
ds–break repair via synthesis dependent annealing
Ubp3–Bre5 deubiquitination complex
Histone H3–K56 acetylation
dTTP biosynthetic process
Cul8–RING ubiquitin ligase complex
ds–break repair via homologous recombination
MCM complex
Cul4–RING E3 ubiquitin ligase complex
HDA1 histone deacetylase complex
Lst4–7 complex
Dom34–Hbs1 Complex
Telomere tethering at nuclear periphery
Actin cortical patch localization
Cellular sphingolipid homeostasis
Condensin complex
7–methylguanosine cap hypermethylation
Histone deubiquitination
Fatty acid elongase activity
Enhancement
Suppression
HLD Specific
HLEG Specific
Media Independent
Identified by REMc
Identified by GTA

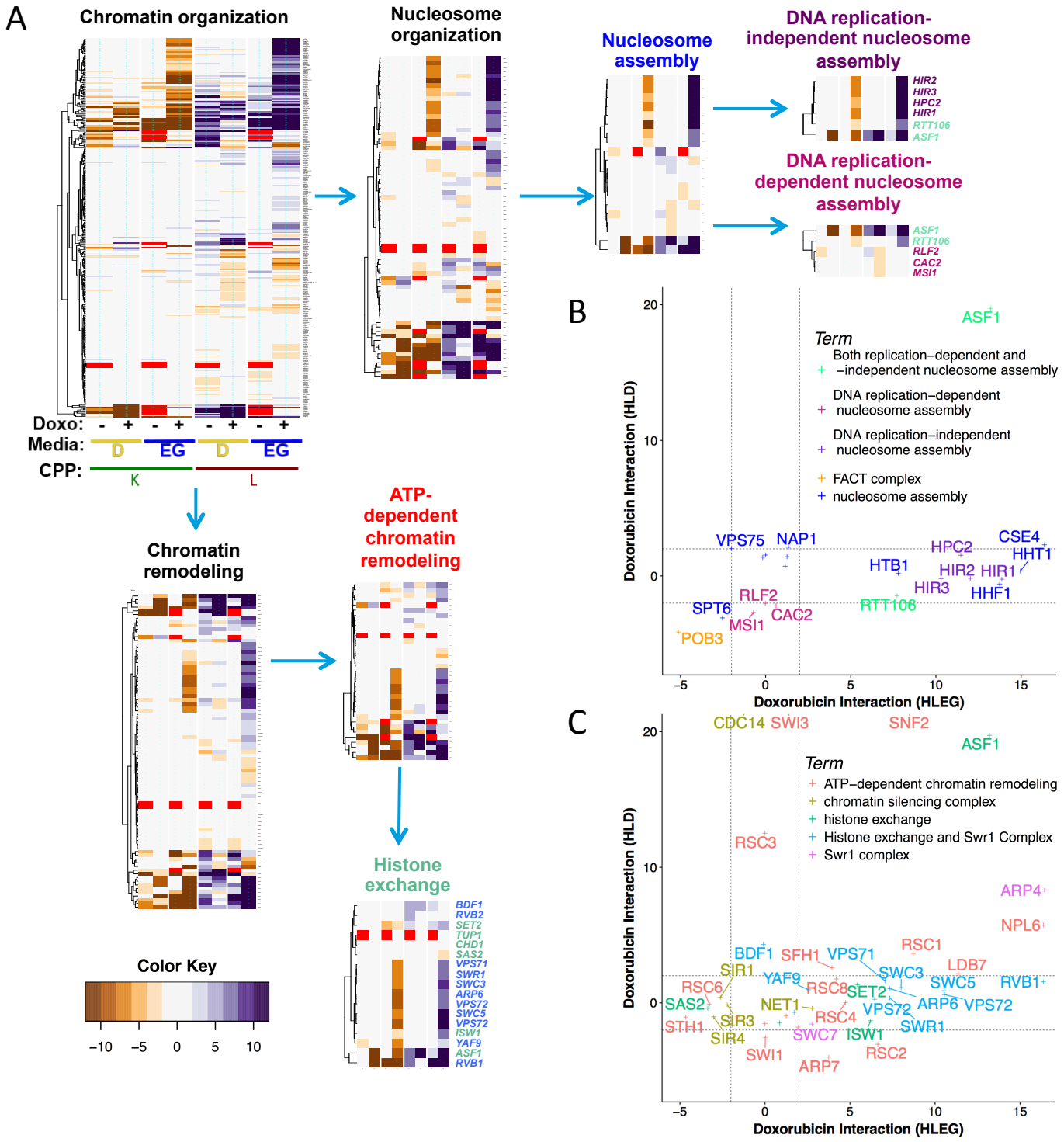
A
Chromatin organization
Nucleosome organization
Nucleosome assembly
DNA replication-independent nucleosome assembly
HIR2
HIR3
HPC2
HIR1
RTT106
ASF1
DNA replication-dependent nucleosome assembly
ASF1
RTT106
RLF2
CAC2
MSI1
Doxo: - + - + - + - +
Media: D EG D EG
CPP: K L
Chromatin remodeling
ATP-dependent chromatin remodeling
Histone exchange
BDF1
RVB2
SET2
TUP1
CHD1
SAS2
VPS71
SWR1
SWC3
ARP6
VPS72
SWC5
VPS72
ISW1
YAF9
ASF1
RVB1
Color Key
−10 −5 0 5 10
B
Doxorubicin Interaction (HLD)
Doxorubicin Interaction (HLEG)
Term
Both replication−dependent and −independent nucleosome assembly
DNA replication−dependent nucleosome assembly
DNA replication−independent nucleosome assembly
FACT complex
nucleosome assembly
ASF1
VPS75
NAP1
HPC2
CSE4
HHT1
HTB1
HIR2
HIR1
HIR3
HHF1
RLF2
SPT6
CAC2
RTT106
MSI1
POB3
C
Doxorubicin Interaction (HLD)
Doxorubicin Interaction (HLEG)
Term
ATP−dependent chromatin remodeling
chromatin silencing complex
histone exchange
Histone exchange and Swr1 Complex
Swr1 complex
CDC14
SWI3
SNF2
ASF1
RSC3
ARP4
NPL6
RSC1
BDF1
SFH1
VPS71
LDB7
SIR1
YAF9
SWC3
SWC5
RVB1
RSC6
RSC8
SET2
SAS2
NET1
VPS72
ARP6
VPS72
STH1
SIR3
RSC4
SWR1
SIR4
SWC7
ISW1
SWI1
RSC2
ARP7

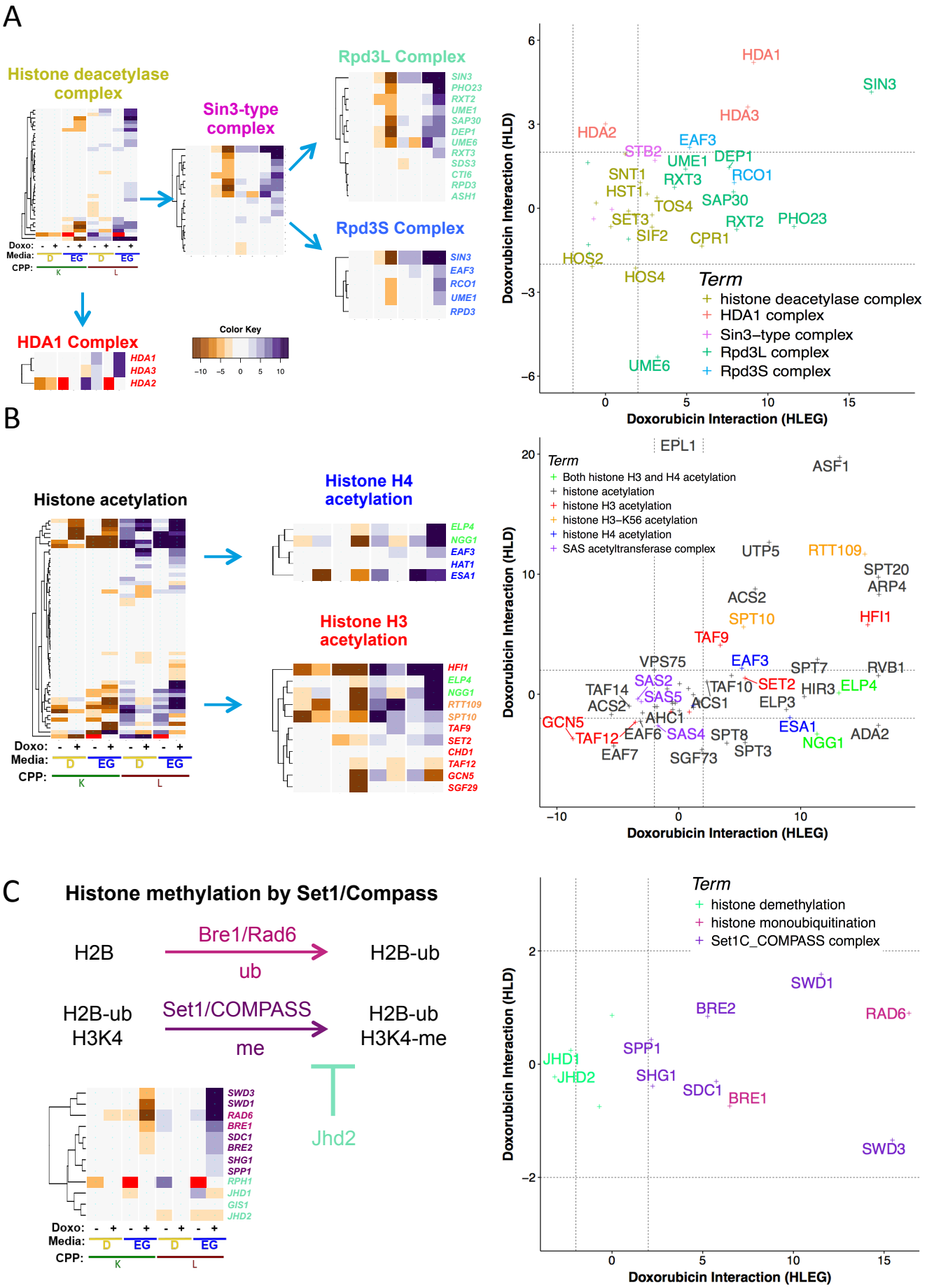
A
Histone deacetylase complex
Sin3-type complex
Rpd3L Complex
SIN3
PHO23
RXT2
UME1
SAP30
DEP1
UME6
RXT3
SDS3
CTI6
RPD3
ASH1
Rpd3S Complex
SIN3
EAF3
RCO1
UME1
RPD3
HDA1 Complex
HDA1
HDA3
HDA2
Color Key
Doxo:
Media:
CPP:
D
EG
K
L
Doxorubicin Interaction (HLD)
Doxorubicin Interaction (HLEG)
Term
histone deacetylase complex
HDA1 complex
Sin3–type complex
Rpd3L complex
Rpd3S complex
B
Histone acetylation
Histone H4 acetylation
ELP4
NGG1
EAF3
HAT1
ESA1
Histone H3 acetylation
HFI1
ELP4
NGG1
RTT109
SPT10
TAF9
SET2
CHD1
TAF12
GCN5
SGF29
Term
Both histone H3 and H4 acetylation
histone acetylation
histone H3 acetylation
histone H3–K56 acetylation
histone H4 acetylation
SAS acetyltransferase complex
C
Histone methylation by Set1/Compass
H2B
Bre1/Rad6
ub
H2B-ub
H2B-ub
H3K4
Set1/COMPASS
me
H2B-ub
H3K4-me
Jhd2
SWD3
SWD1
RAD6
BRE1
SDC1
BRE2
SHG1
SPP1
RPH1
JHD1
GIS1
JHD2
Term
histone demethylation
histone monoubiquitination
Set1C_COMPASS complex

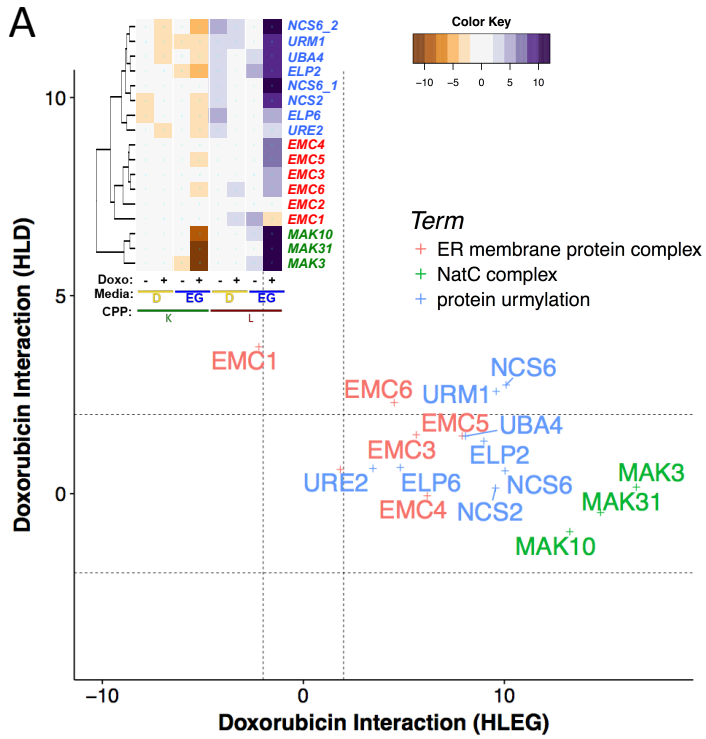

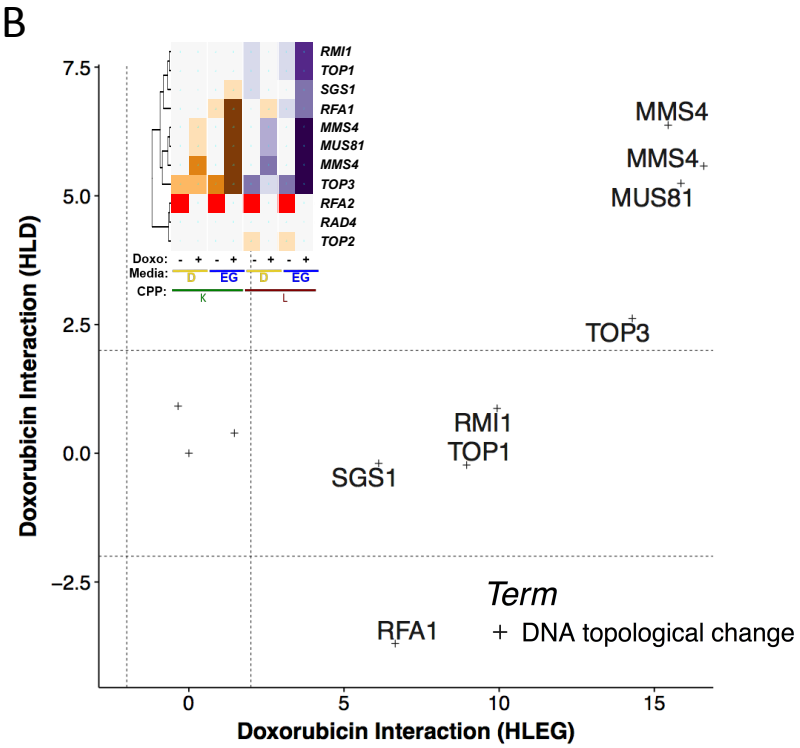

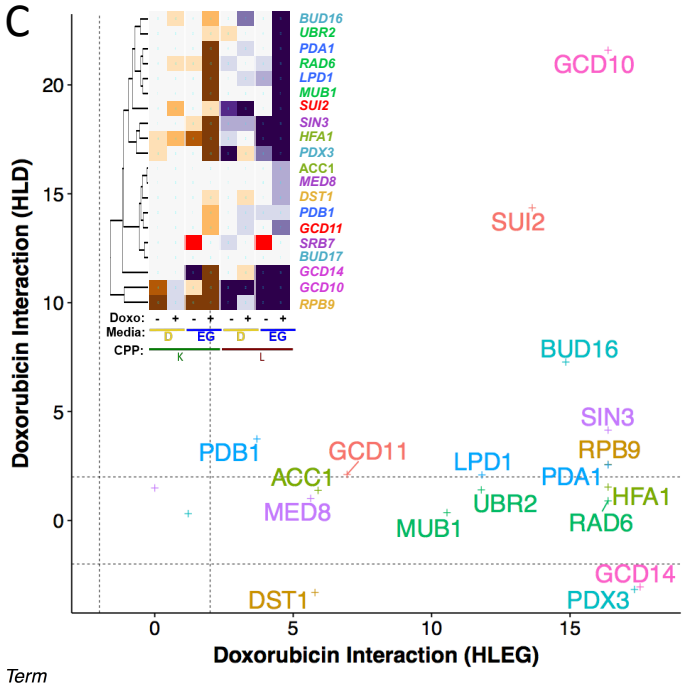

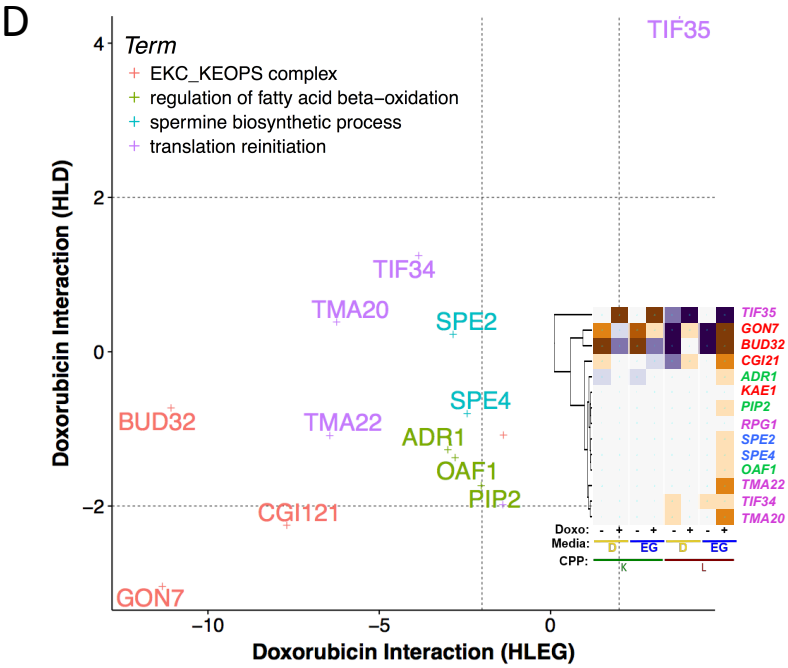

Term

- eukaryotic translation initiation factor 2 complex
- maintenance of transcriptional fidelity during DNA−templated transcription elongation from RNA polymerase II promoter
- malonyl−CoA biosynthetic process
- MUB1−RAD6−UBR2 ubiquitin ligase complex
- pyridoxal 5'−phosphate salvage
- pyruvate dehydrogenase activity
- RNA polymerase II transcription corepressor activity
- tRNA (m1A) methyltransferase complex

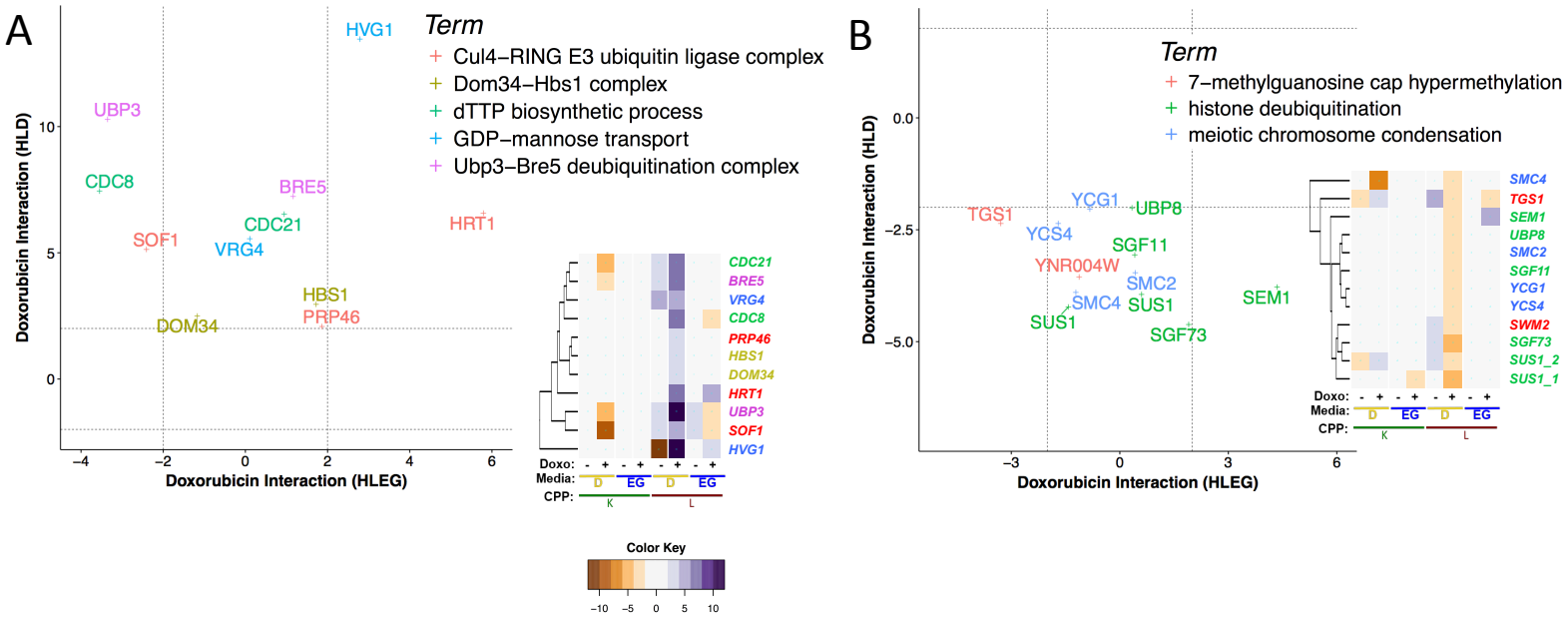
A
Term
Cul4−RING E3 ubiquitin ligase complex
Dom34−Hbs1 complex
dTTP biosynthetic process
GDP−mannose transport
Ubp3−Bre5 deubiquitination complex
HVG1
UBP3
CDC8
BRE5
CDC21
SOF1
VRG4
HRT1
HBS1
PRP46
DOM34
Doxorubicin Interaction (HLD)
Doxorubicin Interaction (HLEG)
CDC21
BRE5
VRG4
CDC8
PRP46
HBS1
DOM34
HRT1
UBP3
SOF1
HVG1
Doxo:
Media:
CPP:
D
EG
K
L
Color Key
B
Term
7−methylguanosine cap hypermethylation
histone deubiquitination
meiotic chromosome condensation
TGS1
YCG1
UBP8
YCS4
SGF11
YNR004W
SMC2
SMC4
SUS1
SEM1
SGF73
SMC4
TGS1
SEM1
UBP8
SMC2
SGF11
YCG1
YCS4
SWM2
SGF73
SUS1_2
SUS1_1

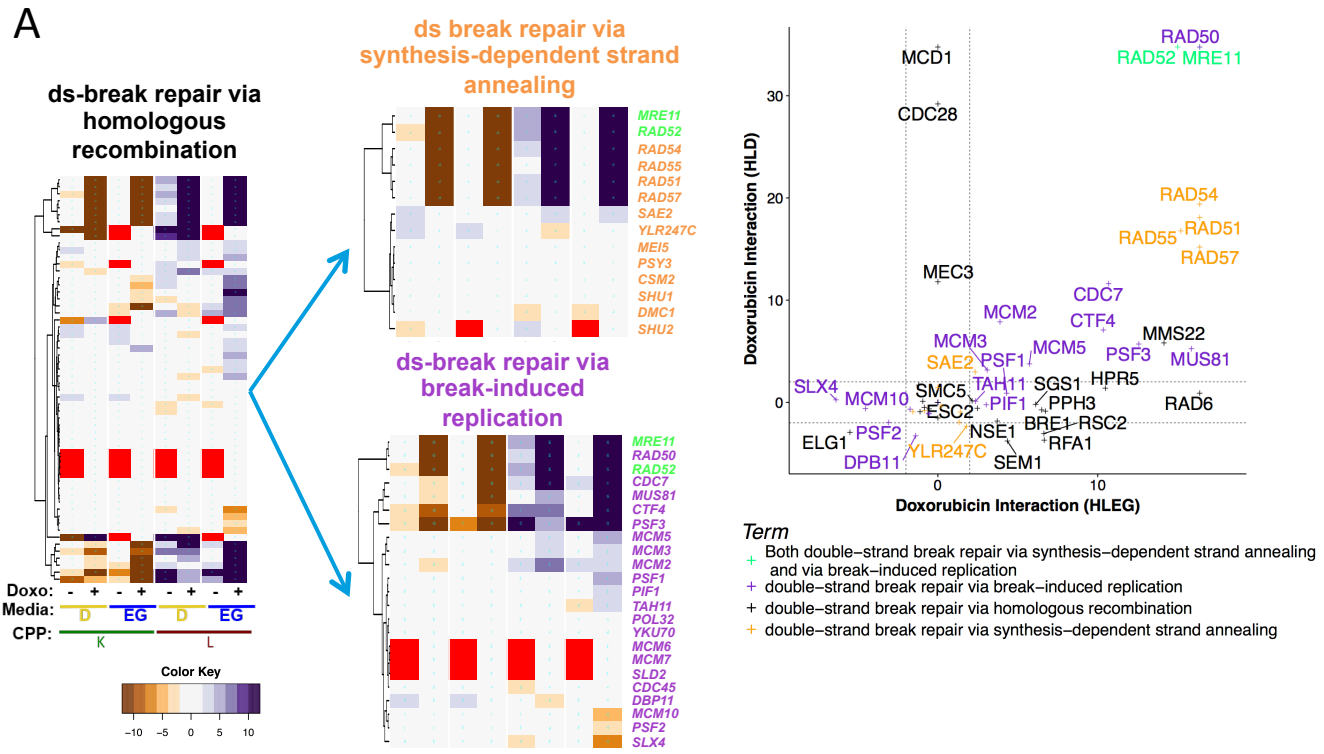
A
ds-break repair via homologous recombination
ds break repair via synthesis-dependent strand annealing
ds-break repair via break-induced replication
MRE11
RAD52
RAD54
RAD55
RAD51
RAD57
SAE2
YLR247C
MEI5
PSY3
CSM2
SHU1
DMC1
SHU2
RAD50
CDC7
MUS81
CTF4
PSF3
MCM5
MCM3
MCM2
PSF1
PIF1
TAH11
POL32
YKU70
MCM6
MCM7
SLD2
CDC45
DBP11
MCM10
PSF2
SLX4
Doxo:
Media:
CPP:
D
EG
K
L
Color Key
Doxorubicin Interaction (HLD)
Doxorubicin Interaction (HLEG)
MCD1
CDC28
MEC3
MCM2
MCM3
SAE2
PSF1
MCM5
CDC7
CTF4
MMS22
PSF3
MUS81
SLX4
MCM10
SMC5
TAH11
SGS1
HPR5
ESC2
PIF1
PPH3
RAD6
BRE1
RSC2
ELG1
PSF2
NSE1
RFA1
DPB11
YLR247C
SEM1
Term
Both double−strand break repair via synthesis−dependent strand annealing and via break−induced replication
double−strand break repair via break−induced replication
double−strand break repair via homologous recombination
double−strand break repair via synthesis−dependent strand annealing

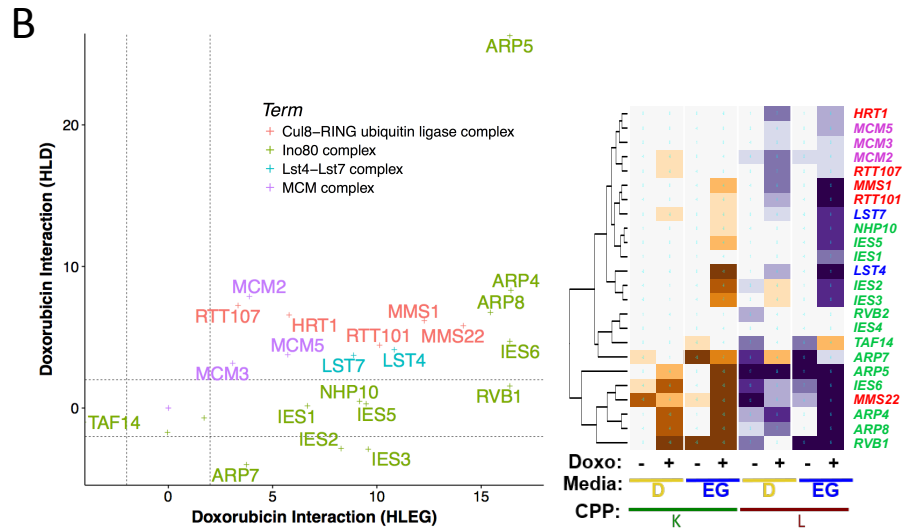
B
Doxorubicin Interaction (HLD)
Doxorubicin Interaction (HLEG)
Term
Cul8−RING ubiquitin ligase complex
Ino80 complex
Lst4−Lst7 complex
MCM complex
ARP5
MCM2
RTT107
HRT1
MCM5
MCM3
MMS1
RTT101
MMS22
LST7
LST4
ARP4
ARP8
IES6
RVB1
NHP10
IES5
IES1
IES2
IES3
TAF14
ARP7
HRT1
MCM5
MCM3
MCM2
RTT107
MMS1
RTT101
LST7
NHP10
IES5
IES1
LST4
IES2
IES3
RVB2
IES4
TAF14
ARP7
ARP5
IES6
MMS22
ARP4
ARP8
RVB1
Doxo:
Media:
CPP:
D
EG
K
L

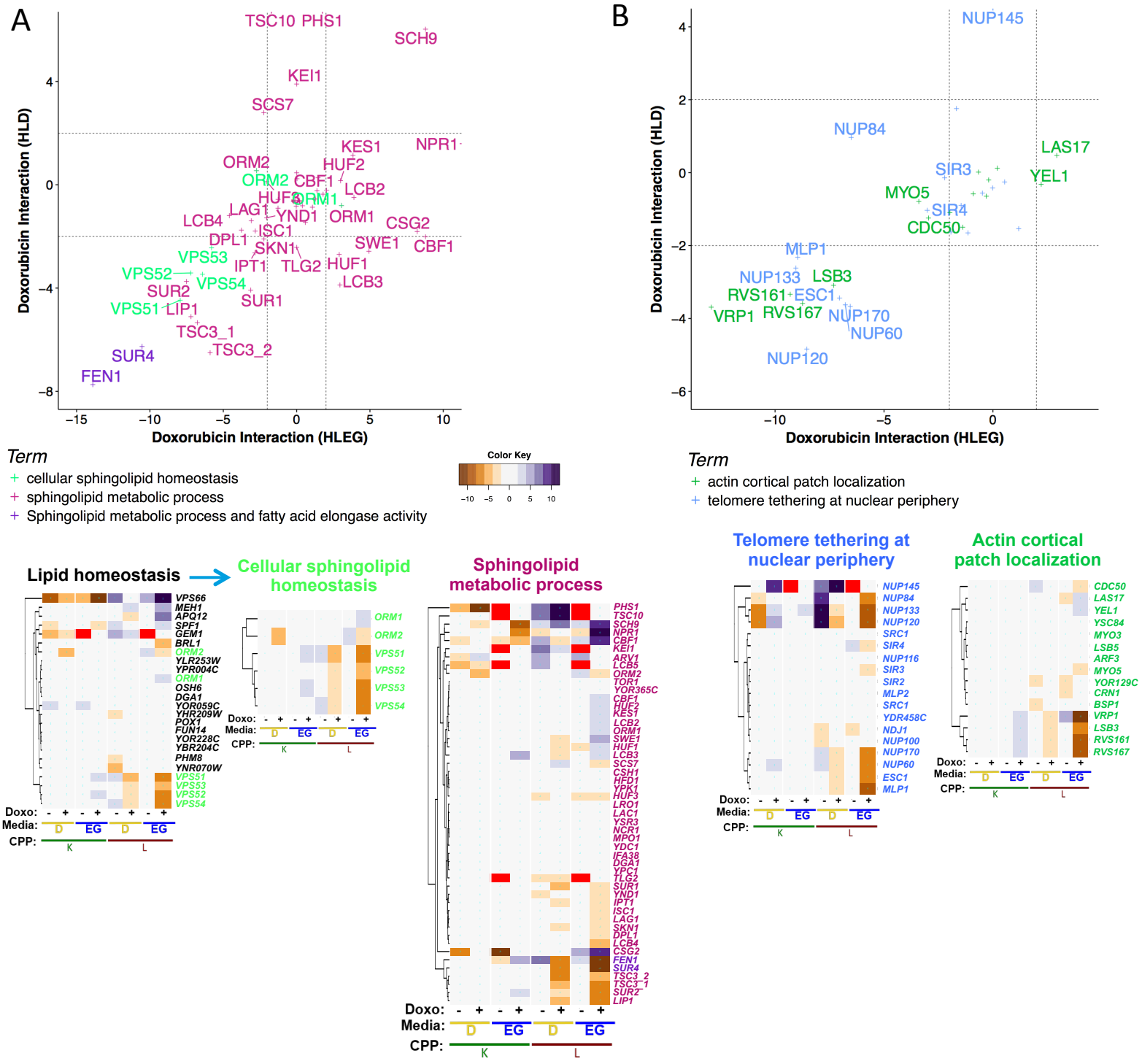
A
Doxorubicin Interaction (HLD)
Doxorubicin Interaction (HLEG)
TSC10 PHS1
SCH9
KEI1
SCS7
KES1
NPR1
ORM2
HUF2
ORM2 CBF1
LCB2
HUF2 ORM1
LAG1 YND1 ORM1
LCB4
ISC1
CSG2
DPL1
SWE1
CBF1
VPS53
SKN1
IPT1 TLG2 HUF1
VPS52
VPS54
LCB3
SUR2
SUR1
VPS51 LIP1
TSC3_1
TSC3_2
SUR4
FEN1
Term
cellular sphingolipid homeostasis
sphingolipid metabolic process
Sphingolipid metabolic process and fatty acid elongase activity
Color Key
B
NUP145
NUP84
LAS17
SIR3
YEL1
MYO5
SIR4
CDC50
MLP1
NUP133 LSB3
RVS161 ESC1
VRP1 RVS167 NUP170
NUP60
NUP120
Term
actin cortical patch localization
telomere tethering at nuclear periphery
Lipid homeostasis
Cellular sphingolipid homeostasis
Sphingolipid metabolic process
Telomere tethering at nuclear periphery
Actin cortical patch localization
Doxo:
Media:
CPP:
D
EG
K
L

A

Yeast-Human Homology

One:One (orthologs)

One:Many (human paralogs)

Many:Many (yeast and human paralogs)

Relationship	y ORF	*h homolog*	*y GDSC*	*h GDSC*	*y gCSI*	*h gCSI*
One to One	925	925	823	823	870	870
One to Many	897	2738	828	2299	877	2489
Many to Many	363	874	350	693	359	812
Total	2165	4537	2001	3815	2106	4171

B

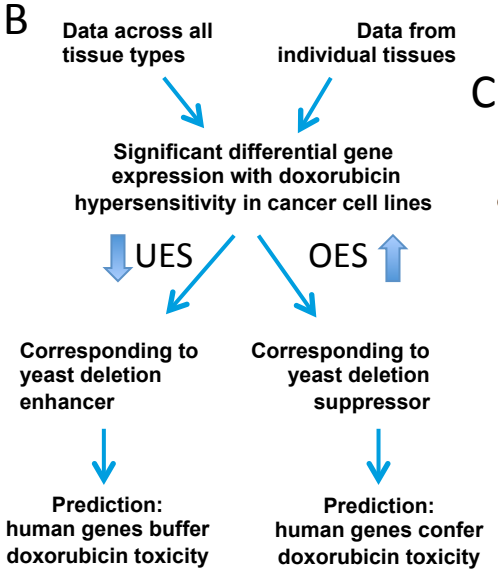

C Yeast deletion enhancer / human UES

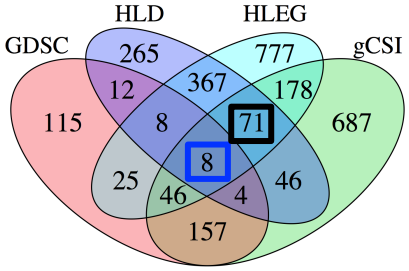

D Yeast deletion suppressor/ human OES

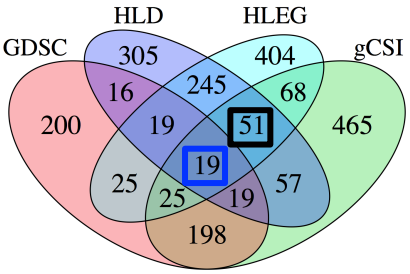

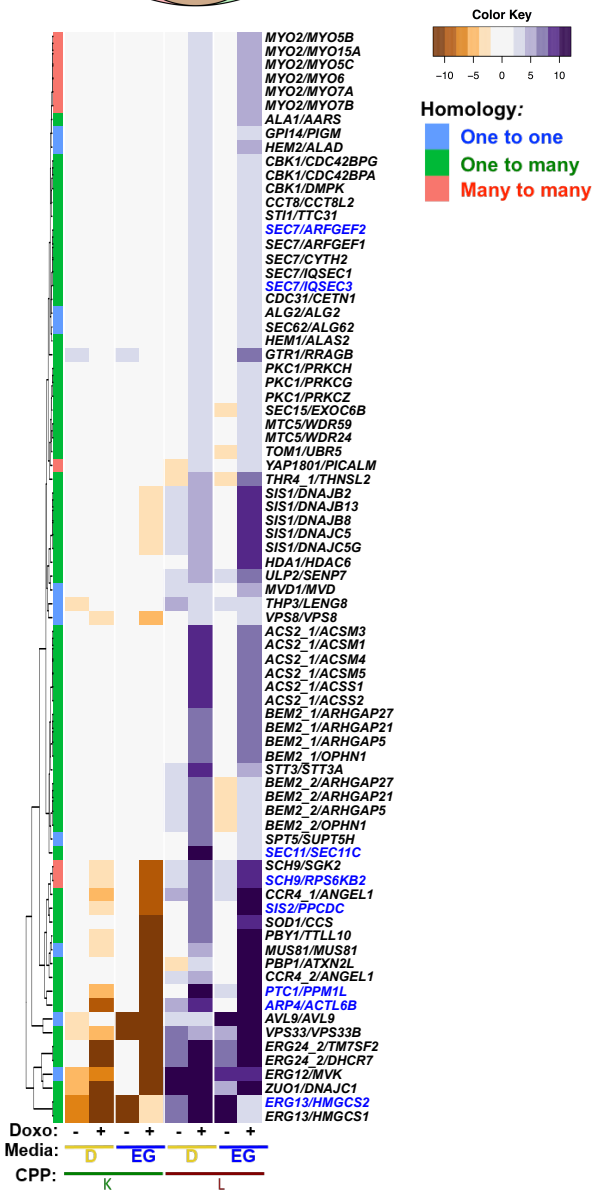

E Selected yeast and human UES

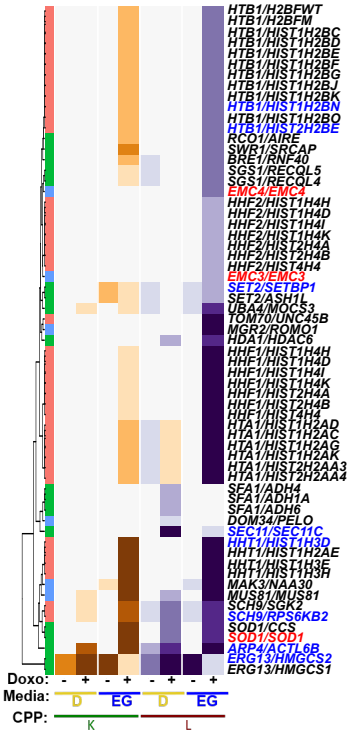

F Selected yeast and human OES

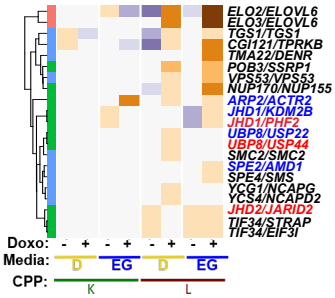

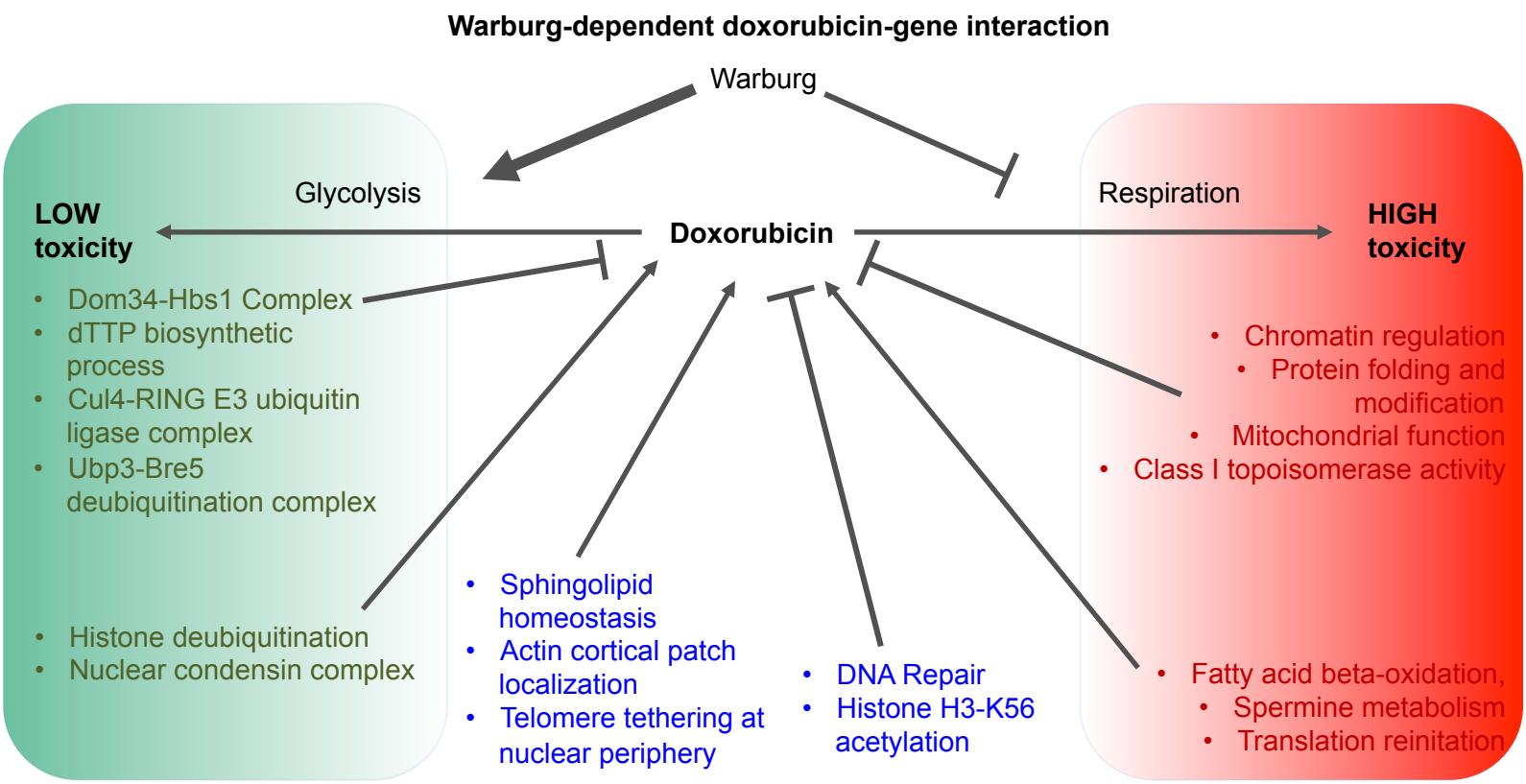
Warburg-dependent doxorubicin-gene interaction
Warburg
Glycolysis
Respiration
LOW toxicity
Doxorubicin
HIGH toxicity
• Dom34-Hbs1 Complex
• dTTP biosynthetic process
• Cul4-RING E3 ubiquitin ligase complex
• Ubp3-Bre5 deubiquitination complex
• Histone deubiquitination
• Nuclear condensin complex
• Sphingolipid homeostasis
• Actin cortical patch localization
• Telomere tethering at nuclear periphery
• DNA Repair
• Histone H3-K56 acetylation
• Chromatin regulation
• Protein folding and modification
• Mitochondrial function
• Class I topoisomerase activity
• Fatty acid beta-oxidation,
• Spermine metabolism
• Translation reinitation